Aalto-yliopisto
Aalto-universitetet
Aalto University

Master's Programme in Geoengineering

Use of Leca lightweight Aggregate in Railway Structures

Ying-Ching Lin

Master's Thesis
2021

Author Ying-Ching Lin

Title of thesis Use of Leca lightweight Aggregate in Railway Structures

Programme Geoengineering

Major Geotechnical Engineering

Thesis supervisor Prof. Solowski Wojciech

Thesis advisor(s) Lauri Savolainen and Taavi Dettenborn (Ramboll Finland Oy)

Collaborative partner Mikko Poysti (Leca Finland Oy)

Date 14.05.2021 Number of pages 87+12 **Language** English

Abstract

Railway embankment design plays an important role in ensuring comfort, safety and timely operation of railways, which are the three greatest concerns for railway passengers and operators. When adopting a material for railway embankments, it is necessary to evaluate the material in terms of its geotechnical design.

To demonstrate the use of Leca LWA in railway structures, this thesis determined a suitable cover depth and an optimal location for Leca LWA in railway embankments, as well as evaluated the effect of high-cycle loads on Leca LWA. These aims were achieved by analyzing and simulating key aspects in railway geotechnical design, such as bearing capacity, embankment stability and the displacement induced by cyclic loading.

Simulation results demonstrated that the optimal location for Leca LWA is below a 300-mm thick extra subballast layer. Such a setting could significantly improve not only the bearing capacity at the top of the subballast layer but also the stability of railway embankments. When the thickness of the extra subballast layer exceeded 300 mm, no clear improvement was observed in these two aspects of railway geotechnical design. Regarding the effect of cyclic loading on Leca LWA, it was found that the material could sufficiently bear such loading regardless of the cover depth. However, these findings are limited to the cross section studied in this work, which consisted of a 550-mm thick ballast layer followed by a 300-mm thick subballast layer, with a maximum embankment height of 2.5 m, onto which was applied a maximum axle load of 25 tons. The suitable cover depth of 1150 mm, consisting of a 550-mm thick ballast layer, followed by a 300-mm thick subballast layer and a 300-mm thick extra subballast layer, is recommended to be constructed above a Leca LWA layer.

These results could provide guidelines for geotechnical designers in effectively using Leca LWA as a railway embankment material. Additionally, this thesis has established the feasibility of using the HCA model and the Plaxis SSC model to simulate the accumulated plastic strain resulting from high-cycle loads caused by moving trains.

Keywords lightweight aggregate, railway embankment design, cyclic loading, high-cycle accumulation model

Acknowledgement

I would like to expression my gratitude towards the following people who went through the journey with me.

Professor Wojciech Solowski from Aalto University – thank you for supervising my master's thesis and always being interested in my research topic. Your advice is very much appreciated, and I have learnt a lot from you throughout my graduate studies.

Mr. Lauri Savolainen from Ramboll Finland Oy – thank you for advising me with lots of patience. It was nice that you walked me through the development of railways in Finland. You've also helped me a lot in translating Finnish literature and I really appreciate that.

Mr. Mikko Pöysti from Leca Finland Oy – thank you for providing substantial amount of Leca test data and being responsive for my questions concerning Leca LWA materials. It was also very nice of you to arrange a factory visit and that brought good memories to me.

Mr. Taavi Dettenborn and Mr. Juha Forsman from Ramboll Finland Oy – thank you for arranging this thesis topic and being a communication bridge between Leca Finland Oy and me.

Nikke – I am happy that you recommended me to pursue my master's degree in Finland. Things have turned out to be much better than I expected. My life wasn't completed 2 years ago when we were 13,000km apart from each other, but now it is.

My family members in Taiwan – There is no bond stronger than family. I love you all.

May 2021
Ying-Ching Lin

Table of Contents

Table of Appendices

List of Tables

List of Figures

Notations

λ^*	Modified compression index	-
κ^*	Modified swelling index	-
μ^*	Modified creep index	-
C_c	Compression index	-
C_s	Swelling index	-
C_α	Creep index	-
e_{init}	Initial void ratio	-
c'	Effective cohesion	kPa
ϕ'	Effective friction angle	°
ψ	Dilatancy angle	°
ν'_{ur}	Poisson's ratio for unloading / reloading	-
K_0^{NC}	Coefficient of lateral stress in normal consolidation	-
M	K_0^{NC} parameter	-
p^{eq}	Equivalent pressure	kPa
p_p^{eq}	Generalized pre-consolidation pressure	kPa
$\dot{\varepsilon}_v^c$	The volumetric creep strain	-
E_{50}^{ref}	Secant stiffness in standard drained triaxial test	kPa
E_{oed}^{ref}	Tangent stiffness for primary oedometer loading	kPa
E_{ur}^{ref}	Unloading / reloading stiffness	kPa
m	Power	-
p^{ref}	Reference stress for stiffnesses	kPa
f	Failure ratio	-
$\dot{\sigma}$	Stress rate	kPa
E	Stress dependent elastic stiffness	kPa
$\dot{\varepsilon}$	Strain rate	-
$\dot{\boldsymbol{\varepsilon}}^{\mathbf{acc}}$	Accumulated strain rate	-
$\dot{\varepsilon}^{\mathrm{acc}}$	The intensity of accumulation	-
$\mathbf{m}$	The direction of accumulation	-
f_{ampl}	The function of strain amplitude	-
$\dot{f}_N$	The function of cyclic preloading	-
f_e	The function of average void ratio	-
f_p	The function of mean stress	-

f_Y	The function of average stress ratio	-
f_π	The function of polarization change	-
p	Mean stress	kPa
q	Deviatoric stress	kPa
η	Stress ratio	-
ε^{ampl}	Strain amplitude	-
ε^{max}	Maximum value of a strain loop	-
ε^{min}	Minimum value of a strain loop	-
p^{av}	Average mean pressure	kPa
$\bar{Y}^{av}$	Average stress ratio	-
C_{N1}	A material constant belongs to $\dot{f}_N$	-
C_{N2}	A material constant belongs to $\dot{f}_N$	-
C_{N3}	A material constant belongs to $\dot{f}_N$	-
C_e	A material constant belongs to f_e	-
C_p	A material constant belongs to f_p	-
C_Y	A material constant belongs to f_Y	-
$\Delta\, e$	The change in void ratio	-
e_{min}	Minimum void ratio	-
e_{max}	Maximum void ratio	

1 Introduction

This chapter is divided into five sections: background and motivation, goals and methods, scope, research questions and the structure of the thesis.

1.1 Background and motivation

Over the centuries, trains have been used for long-distance travel, daily commuting, and transporting goods. In recent years, European governments have increased investments in railway construction in order to meet European Union carbon-reduction targets. Railways are commonly built on embankments, as shown in Figure 1. Railway Embankment design plays an important role in ensuring comfort, safety, and timely operation of railways, which are the three greatest concerns for railway passengers and operators. From a geotechnical perspective, key embankment designs include bearing capacity, stability, settlement and possibly frost heave in cold regions, such as Nordic and Baltic countries. Bearing capacity is defined as the capacity of the embankment and subsoil to sustain applied loads. Embankment stability refers to the ability of an embankment to withstand movement due to loads applied onto embankments. Settlement or soil displacement is caused by changes in loading and consolidation of the soil. Frost heave results from the uplift movement of the ground caused by the expanding volume of freezing ground water.

Figure 1. Picture of a railway embankment (Rail Technology Magazine, 2018)

In the Nordic countries, Railway tracks must often be built on soft clay and peat areas. In the past, this was due to limited construction techniques, but more recently due to the demanding vertical geometry required for planning railway connections. Furthermore, railway infrastructure upgrades or renovation work commonly occur near existing tracks, thus requiring large, steep spaces between existing structures. However, designing railway tracks built on soft clay and peat areas are especially challenging because such soil conditions can lead to excessive or differential settlement due to train loads and, in turn, railway operators need to lower the train speed before remediation works. In extreme circumstances, the soils

may not sustain loading caused by trains, thus leading to embankment failure. Therefore, ground improvement, foundation structures or a combination of both is required to modify or strengthen soil properties.

One common method for improving soil properties is to use lightweight aggregates (LWA) to replace subsoil or to form part of embankment materials. Since LWA lightens embankment structures by decreasing the incremental vertical stress in the subsoil, thus reducing the subsoil settlement and increasing the stability of embankment. This method can also be combined with other ground improvement methods, such as preloading and column stabilization (Pahkakangas et al., 2020).

In recent years, much progress has been achieved in the development of models for predicting displacement in subsoil (Sivasithamparam & Karstunen, 2015; Koskinen et al., 2002) and the overall stability of railway embankments (Savolainen et al., 2017; Mansikkamäki, 2015) under static loads. However, little work has been devoted to embankments under cyclic loading (low amplitude), as is typical for railway structures. Such loading is characterized by the shape, duration and magnitude of loading pulse, time interval between consecutive pulses, as well as the total number of loading pulses (Li et al., 2015). The plastic deformation accumulated due to cyclic loading and, in turn, results in differential settlement, which can limit the railway speed or make the train ride experience less comfortable.

A number of studies (Suiker & Borst, 2003; Wichtmann et al., 2005; François et al., 2009) have developed numerical models for natural granular materials, such as ballast and sand, under small amplitude cyclic loading. Yet, less attention has focused on the effect of cyclic loading on lightweight aggregates.

1.2 Goals and methods

To demonstrate the use of Leca® light weight aggregates (Leca LWA) in railway structures, this thesis aims to determine a suitable cover depth and an optimal location for Leca LWA in railway embankments, as well as to evaluate the effect of high cycle train loads on Leca LWA. These goals will be achieved by analyzing and simulating key aspects in railway geotechnical design, such as bearing capacity, embankment stability and the displacement induced by cyclic loading.

To evaluate the effect of cyclic loading on Leca LWA, this thesis uses the Plaxis Soft Soil Creep (SSC) model for analyzing the displacement induced by moving trains. The SSC model computes the accumulation of strain or displacement as function of time. The simulation results will be used to validate the high-cycle accumulation (HCA) model established by Wichtmann et al., (2005). The HCA model will resemble the results of laboratory cyclic compression tests on Leca LWA. Since the laboratory test results present the accumulated strain due to number of cycles instead of time, it is necessary to determine the correlation between these two phenomena. Some conditions, such as the strain amplitude and the stress, in the laboratory tests are different than in construction sites, and therefore few adjustments are required for the replicated strain curve in the HCA model.

1.3 Scope

The railway embankment experiences two stresses. The static stresses, which are induced by loads (e.g., earth pressure at rest and static traffic loads), as well as are caused by long-term environmental and soil effects (e.g., soil consolidation). The cyclic stresses, which are induced by loads (e.g., moving traffic loads), as well as are generated by seasonal environmental and soil effects (e.g., thermal stresses, frost-heaving stresses and changes of porewater pressures). This thesis focuses on the effect of static traffic loads and moving traffic loads on railway embankments. Additionally, the scope of this thesis will be limited to a maximum railway speed of 160 km/h. Different approaches will be required for the even higher speed of railways.

1.4 Research questions

The research questions are listed as follows.

Q1. What are the allowable limits for uniform and differential displacement in railways?
Q2. What are the load models used in geotechnical railway design?
Q3. How is it possible to verify sufficient bearing capacity on the top of sub-ballast layer when using Leca LWA with different cover depths (suitable cover depths in railway embankment)?
Q4. What is the optimal location for Leca LWA in railway embankments?
Q5. How does Leca LWA bear cyclic loading with different cover depths (suitable cover depths in railway embankment)?
Q6. What parameters are required for design?
Q7. What are the requirements for validating the design parameters of superstructure and embankment materials?
Q8. Are all, of the required parameters defined for Leca LWA?
Q9. What additional laboratory analyses shall be performed in the future?

1.5 Structure of the thesis

The rest of this thesis is organized as follows. Chapter 2 reviews common railway embankment materials, Leca LWA, and geotechnical railway design elements. This chapter also introduces the studied railway cross section and the material properties that are adopted for Plaxis modelling. Chapter 3 presents the Plaxis soil models used in this thesis. Chapter 4 outlines the laboratory test results of Leca LWA, the theory of the HCA model and the application of Plaxis SSC model to high-cycle train loads. Furthermore, this chapter also evaluates the proposed methodology. Chapter 5 provides the analysis results for the studied embankment cross section, including bearing capacity, embankment stability and displacements in Leca LWA layers. Chapter 6 concludes the thesis by evaluating the contribution, recommending further work, and answering research questions.

2 Railway embankments

In order to model geotechnical problems for railway structures, it is first necessary to understand the materials used for constructing railway embankments, with a focus on the Leca LWA. Furthermore, this chapter presents various geotechnical design elements, including load models, bearing capacity, stability, settlement and cyclic loading. A typical cross section of railway embankments is studied and presented in Section 2.5. Finally, Section 2.6 answers the research questions which are relevant to the literature review.

2.1 Common railway embankment materials

The purpose of a railway embankment structure is to support track superstructures, such as rails and sleepers, and to bear the loading caused by passing trains. A typical railway embankment structure consists of ballast, subballast and subgrade layers, as shown in Figure 2. Depending on the climate of the designed railway route, a frost protection layer can be added under the subballast layer.

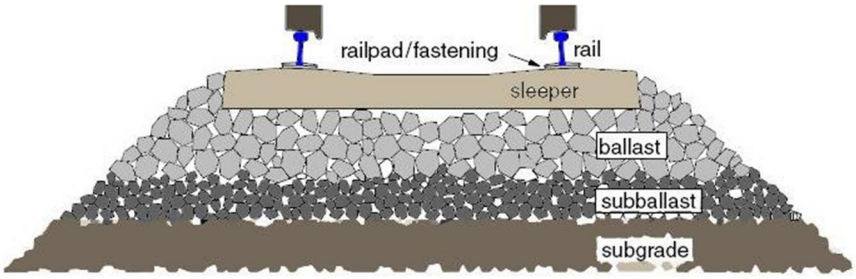

Figure 2. Railway track structure (Martinez-Soto et al., 2017)

The ballast layer, into which are embedded sleepers, is the top layer of the railway structure. The ballast layer typically consists of crushed stone, which can resist combinations of applied loads and environmental exposure. The subballast layer is located below the ballast and distributes the applied load to the subgrade as well as separates the ballast from the subgrade. Additionally, the subballast layer is also important because it allows water to drain either from the ballast, the side of the tracks or the subgrade. Thus, the subballast layer commonly contains a well-graded mixture of crushed stone or gravel and sand. (Li et al., 2015)

The embankment structure can be adversely affected by frost actions. Frost action is caused by a seasonal cold climate, which can affect the performance of railway embankments. This results from water, flowing upwards from unfrozen soil into the freezing zone, thus forming ice lenses and in turn increasing the volume of the frozen soil. This situation will further deteriorate if the subgrade is frost susceptible. (Nurmikolu & Silvas, 2013)

To prevent water infiltrating upwards from frost susceptible subgrade, a frost protection layer is required to provide sufficient thickness of the non-frost susceptible material. For railway

embankments, this frost protection layer can be formed using several different types of materials (Bane NOR Technical Regulations, 2021):

- Well graded blasted rock and crushed stone
- Well graded materials containing sand and gravel
- Light weight aggregate
- Foam glass
- Extruded polystyrene (XPS)
- Expanded polystyrene (EPS)

2.2 Leca® lightweight aggregate

Leca® Light Expanded Clay Aggregate (Leca LWA) is a ceramic material which is manufactured at approximately 1150°C using a rotary kiln. Every cubic meter of selected clays can expand to a 5-fold larger volume during the heating process. Each expanded particle has a hard and resistant exterior shell and a porous interior. Consequently, LWA is widely used in various engineering applications due to features such as low bulk density, good water permeability, insulating, strength, durability, and recyclability. Figure 3 shows the physical properties of Leca LWA.

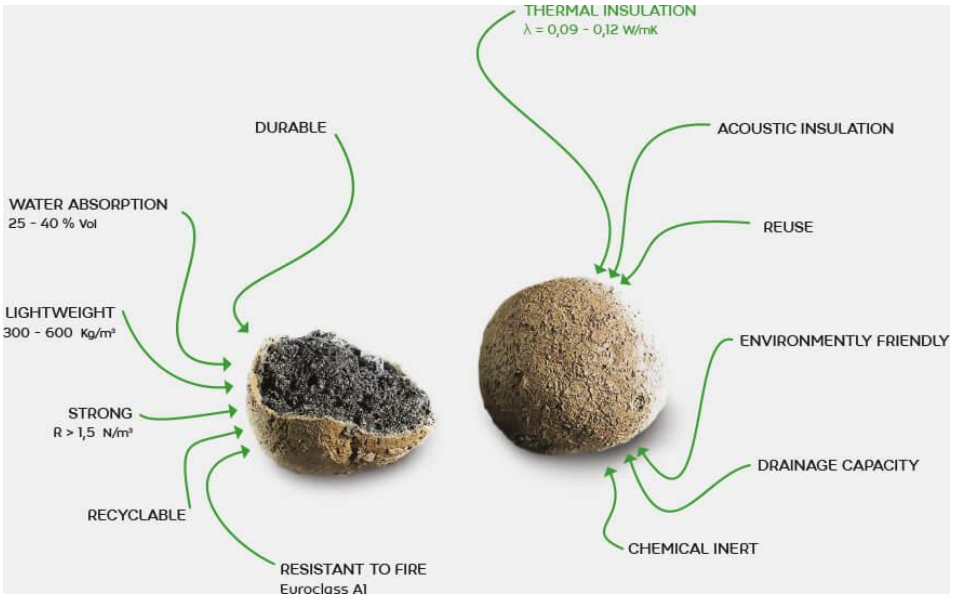

Figure 3. Leca® LWA physical properties (Leca website)

The geotechnical properties of LWA 4-32 have been presented by Pahkakangas et al. (2020), as shown in Table 1. The number followed by LWA, which is “4-32”, identifies that the grain size distribution of the material as ranging between 4 mm and 32 mm in diameter. To give a general idea of how Leca LWA differs from other natural soil types, moist unit weight and modulus of elasticity are chosen for comparison.

Table 2 shows that generally, Leca LWA is approximately more than two-thirds lighter than natural materials and can be up to 10 times larger than soft clay or nearly as equally high as that for dense sand in terms of elastic modulus. Table 1 gives Leca LWA friction angles of 33° and 40° for loose and compacted state, respectively. These values also fall between friction angles of 32° and 38° from loose to dense sand given by NCCI 7 Annex 6 (2017).

Thus, Leca LWA has good properties equivalent to that provided by medium dense sand, while having much lighter unit weight. Such characteristics can reduce earth pressure effectively without compromising strength properties. When using Leca LWA in railway embankment structures, it is expected that an increase in stability and a reduction in settlement would happen while at the same time providing good drainage and preventing frost actions from occurring in the subgrade.

Table 1. LWA 4-32 geotechnical properties (Pahkakangas et al., 2020)

Parameter	**Range of variation**	**Specific value**	**Unit**
Grain size	4–32	-	mm
Undersize/Oversize	<15 / <10	-	p-%
Density (dry density)	275 (±15 %)	-	kg/m^3
Unit weight			kN/m^3
dry density		3,0	
dry (w_{max}=30 p-%)(1)		4,0	
periodically submerged		6,0	
permanently submerged		10,0	
in buoyancy dimensioning		3,0	
Water absortion			p-%
24 h	< 20		
28 d	< 30		
300 d	< 60		
Friction angle	33–40		°
loose		34	
compacted		37	
Hydraulic permeability	10^{-3}–10^{-1}	-	m/s
Modulus of Elasticity (in bearing capacity dimensioning)	30–80 (2)	50	MPa
Thermal conductivity	0.10–0.17	0,15	W/mK
Insulation factor, a_i (3)	-	4	-
pH	9–10	-	-

1) w_{max}=30 p-%, always over water level
2) For bearing capacity dimensioning. Stress state dependent value
3) Factor describing thermal insulating properties (a_i) of Leca® LWA at 0.7 m depth, when its dry density is ≤ 400 kg/m3, and 0.15 m thick drainage layer is located below. Sand is used as a reference material (a_i=1). In challenging conditions thermal conductivity may be bigger.

Table 2. Comparison of LWA 4-32 and natural materials

Type of Soil	Moist unit weight	Compared with LWA 4-32	Modulus of elasticity	Compared with LWA 4-32
Unit	kN/m^3	%	MPa	%
LWA 4-32	6	-	50	-
Peat	8 – 16	+25 – 63	1 – 2	-4900 – 2400
Soft clay	14 – 17	+63 – 68	5 – 25	-900 – 100
Stiff clay	17 – 21	+68 – 73	25 – 75	-100 – +33
Loose sand	16 – 18	+63 – 67	10 – 24	-400 – 108
Dense sand	18 – 20	+67 – 70	48 – 81	-4 – +38
Loose gravel	17 – 19	+65 – 68	48 – 148	-4 – +66

2.3 Geotechnical railway design

This section presents key geotechnical design elements, including load models, embankment stability, allowable uniform and differential settlement and bearing capacity. The design regulations will be introduced by this section are mostly based in Finland. However, the load models used in the Scandinavian countries and Poland will be briefly discussed as well.

Two design specifications, Ratatekniset Ohjeet (RATO) Part 3 Radan rakenne and Eurokoodin soveltamisohje Geotekninen suunnittelu NCCI 7, will be frequently referred to in this section. They are widely used in Finland for railway tracks and geotechnical designs.

Ratatekniset Ohjeet (RATO) Part 3 Radan rakenne refers to the technical regulation for railway tracks. RATO 3 was published by the Finnish Transport Infrastructure Agency (Väylävirasto) which has public ownership of the Finnish railway infrastructures. (RATO 3, 2018)

Eurokoodin soveltamisohje Geotekninen suunnittelu NCCI 7 was also published by the Finnish Transport Infrastructure agency. This specification guides the application of standard SFS EN 1997-1 Geotechnical design, i.e., Eurocode 7, and Finnish National Annex (LVM) for public roads, railways, waterways, and related structures such as bridges. (NCCI 7, 2017)

2.3.1 Load models

Rail traffic actions are defined as load models in EN 1991-2: Eurocode 1: Actions on structures - Part 2: Traffic loads on bridges (2003). Five load models are provided:

- Load Model 71 and Load Model SW/0 to represent normal railway traffic on mainline railways,
- Load Model SW/2 to represent heavy rail traffic,

- Load Model HSLM to represent the loading from passenger trains at speeds exceeding 200 kN/m,
- Load Model “unloading train”. (EN 1991-2 Eurocode 1 - Part 2, 2003)

Figure 4 shows the load configuration for Load Model 71, which represents the static effect of vertical loading due to normal rail traffic. The characteristic values shall be multiplied by a factor α depending on the carrying traffic is lighter or heavier than the normal one. The value of α is ranged between 0.75 and 1.46.

Figure 5 shows the load configuration for Load Models SW/0 and SW/2 and Table 3 presents their characteristic values. Load Model SW/0 represents the static vertical loading due to normal rail traffic on continuous span bridges, while Load Model SW/2 stands for the characteristic values of vertical loading due to heavy traffic load.

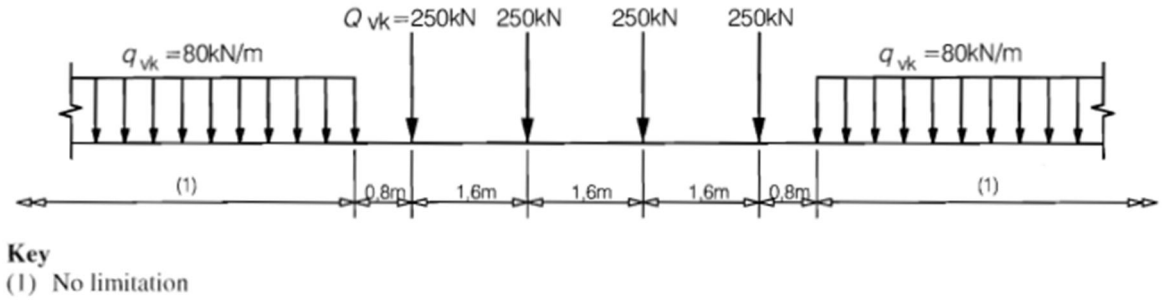

Figure 4. Load Model 71 and charateristic values for vertical loads due to normal rail traffic (EN 1991-2: Eurocode 1 - Part 2, 2003)

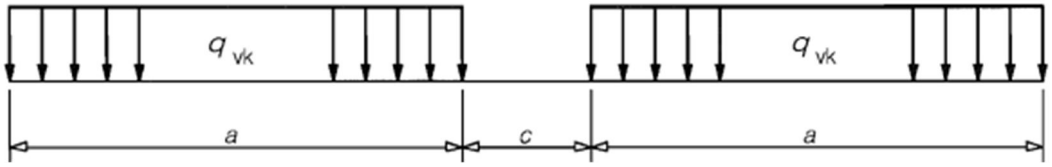

Figure 5. Load Models SW/0 and SW/2 (EN 1991-2: Eurocode 1 - Part 2, 2003)

Table 3. Characteristic values for vertical loads for Load Models SW/0 and SW/2

Load Model	q_{vk} [kN/m]	a [m]	c [m]
SW/0	133	15,0	5,3
SW/2	150	25,0	7,0

The load models used in Finland are documented in RATO 3 (2018). Figure 6 shows LM71 load diagram, which is conforming to SFS-EN-1991-2/17/, for the case of static load applying on rail tracks. The load model has four axle loads (Q_{vk}) and line loads (q_{vk}) on both ends. There is a span of 1.6 m between two axle loads, while a distance of 0.8 m is given between an axle load and the edge of one line load. Table 4 presents the different axle loads, ranged

from 17 tons to 35 tons, with their corresponding characteristic line loads (q_{stab}) for two-dimensional slope stability analysis.

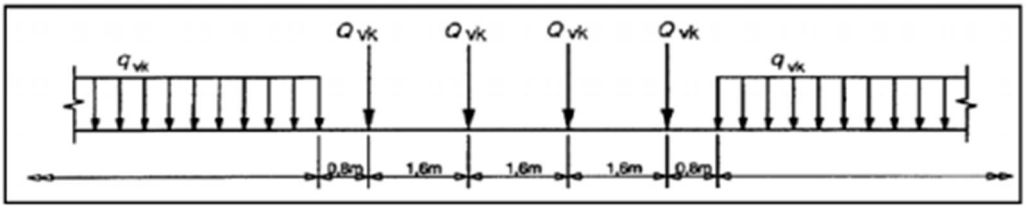

Figure 6. LM71 load diagram conforming to SFS-EN-1991-2/17/ (RATO 3 Kuva 5, 2018)

Table 4. The characteristics values for LM71 2D stability calculation. q_{stab}=line loads (q_{stab}) for two-dimensional slope stability analysis. (RATO 3 Taulukko 7, 2018)

Mitoituskuorma-kaavion tunnus	α –kerroin (1)	2D-stabiliteettilaskennassa käytettävä nauhakuorman ominaisarvo q_{stab} [kN/m]
LM71-17	0,90	92
LM71-22,5	1,0	103
LM71-25	1,10	111
LM71-27,5	1,21	119
LM71-30	1,33	129
LM71-35	1,46	142

(1) α-kertoimen arvo, joka sisältyy taulukossa esitettyihin arvoihin

When the scope of an analysis, i.e., foundation, sheet pile walls, is 0.8 m deeper than the elevation of railway tracks, LM 71 load model can be treated as presented in Figure 7. The reason is that the influence of one axle is relatively small; as a result, the load model can be simplified as one line load (q_{vk}) with an additional load increment (Δq_{vk}). Table 5 presents the different axle loads, ranged from 17 tons to 35 tons, with their corresponding line loads (q_{vk}) with additional pressure increment (Δq_{vk}). This modified load model is applicable for designing earth pressure structures and other structures where the local influence of loads is determinative. Additionally, an impulse factor (sysäyskerroin, ϕ_v) of 1.25 has to apply for this case when designing new tracks.

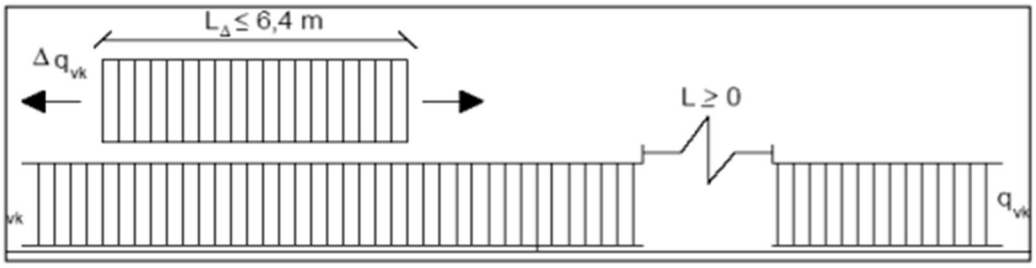

Figure 7. Treating the load model LM71 as two line loads (RATO 3 Kuva 6, 2018)

Table 5. The LM71 dimensioning axle loads and corresponding characteristic static values for equally distributed line loads. Q_{vk}=axle loads, q_{vk}=line loads, Δq_{vk}=additional pressure increment. (RATO 3 Taulukko 6, 2018)

Mitoitus-kuorma-kaavion tunnus	α-kerroin (1)	Akselikuorman ominaisarvo Q_{vk} [kN]	Nauhakuorman ominaisarvo q_{vk} [kN/m]	Δq_{vk} [kN/m]
LM71-17	0,90	188	60	58
LM71-22,5	1,0	250	80	76
LM71-25	1,10	275	88	84
LM71-27,5	1,21	300	96	92
LM71-30	1,33	333	106	102
LM71-35	1,46	370	120	111

(1) α-kertoimen arvo, joka sisältyy taulukossa esitettyihin arvoihin

Table 6 summarizes the railway regulations and local authorities for Finland, the Scandinavian countries and Poland.

Bane NORs Book 520 documented railway technical regulations for designing substructures in Norway. When analyzing the stability or load bearing capacity of a railway embankment, a characteristics line load 110 kN/m shall be adopted (Figure 8). This line load typically meets the requirements of using LM71 as the traffic load. (Christiansen, 2018)

TK Geo 13 guides the construction of roads and railways in Sweden. Three load types are offered, and Train Load 1 (Table 7) is the standard which assumes a uniform distributed load over a width of 2.5 m in the infinite longitudinal direction. (Christiansen, 2018)

BN1-59-4 regulates bridges and earthworks design under railways in Denmark. An infinite line load of 110kN/m shall be adopted when calculating 2D stability for a single-track railway. (Christiansen, 2018)

The European Standards PN-EN 15528 and PN-EN 1991 are accepted by Polish railway authorities. However, PE-EN15528 can only be used for existing railway structures. The LM71 is used for standard rail traffic on railways (Bogusz & Godlewski, 2019)

Table 6. Regulations and railway authorities in respect of countries

Country	Regulations	Railway authority in the country	Source
Finland	Ratatekniset Ohjeet (RATO) Part 3 Radan rakenne	Väylävirasto	RATO 3 (2018)
Norway	Bane NORs Book 520: Substructures (2021)	Bane NORs	Christiansen (2018)
Sweden	Trafikverkets tekniska krav för geokonstruktioner TK Geo 13 (2014)	Trafikverket	Christiansen (2018)
Denmark	BN1-59-4: Regulations for bridges and earthwork under the railway (2010)	Banedanmark	Christiansen (2018)
Poland	MTiGM (1998) PKP PLK, Technical specification concerning maintenance of railway lines Id-1 & Id-3 (2005&2009)	PKP Polskie Linie Kolejowe S.A	Bogusz & Godlewski (2019)

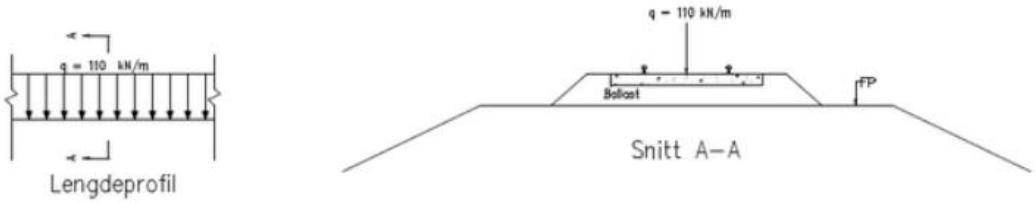

Figure 8. Characteristics line load for single-track railways (Bane NORs, 2021)

Table 7. TK Geo 13 Train Load 1 (Christiansen, 2018)

Train load [maximum weight per meter]	Train load$[kN/m^2]$	
	Dimension with characteristic values	Dimension with partial factors
6.4	34	26
8	44	32
10	53	40
12	64	48

2.3.2 Bearing capacity

The Odemark equation (Eq.(1)) is commonly used in Finland for verifying the structural capacity in geotechnical and road engineering. This method was developed by Nils Odemark in 1949 and it was based on the Boussinesq equation.

The Boussinesq method is one approach to estimate the stress distribution is a half space under a load which is normal to a surface. This method simplifies real soil behaviors to a great extent by assuming soils are linear-elastic, homogeneous and isotropic.

$$E_Y = \frac{E_A}{\left(1 - \frac{1}{\sqrt{1 + 0.81\left(\frac{h}{0.15}\right)^2}}\right)\frac{E_A}{E} + \frac{1}{\sqrt{1 + 0.81\left(\frac{h}{0.15}\right)^2\left(\frac{E}{E_A}\right)^{\frac{2}{3}}}}} \quad (1)$$

where

E_Y = bearing value on the top of the designed layer (MPa)
E_A = bearing value of the layer beneath (MPa)
h = thickness of the designed layer (m)
E = material modulus E_2 of the designed layer (MPa).

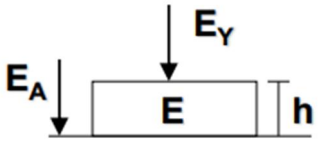

The bearing values (Kantavuus) can be defined by the plate loading test, which is an in-situ test used for determining the ultimate bearing capacity of a material. This value can be calculated by an applied load with its corresponding surface deflection. Furthermore, this test will be conducted twice (E_1, E_2) for each layer be*caus*e usually the surface deflects a lot more under a load at the first time (E_1).

InfraRYL (2020), a Finnish guideline for construction work, regulates that the average bearing value (E_2) shall be 180 MPa at the top of subballast layers when using the plate loading test. It also restricts that the ratio of E_2/E_1 according to different E_2, as shown in Table 8.

Table 8. The bearing values E_2 and their required ratio of E_2/E_1 (InfraRYL 21230.4, 2021)

E_2 (MPa)	the ratio of E_2/E_1 (MPa)
<145	≤2.5
145 – 159	≤2.6
160 – 174	≤2.7
175 – 189	≤2.8
190 – 204	≤2.9
205 – 219	≤3.0
220 –234	≤3.1
≥235	≤3.2

2.3.3 Embankment stability

Eurocode 7 Design Approach 3, which requires partial factors are applied to actions or effects of actions and to soil parameters, is used for calculating embankment stability. Partial factors are required to apply on characteristic values for taking possible undesirable deviations into account. The values of partial factors for actions or the effects of actions, for soil strength parameters and for embankment and overall embankment stability are presented in Table 9, Table 10, Table 11 and Table 12, respectively.

The overall design factor (ODF), which is a ratio of the design value for soil resistance over the design value for actions, shall be more or equal to 1.0. In general, the ultimate limit state (ULS) analysis is applicable for embankment stability problems, however, the service limit

state (SLS) analysis shall be considered if the designed structures, e.g., piled structures and bridges, are sensitive to displacements.

Table 9. Partial factors for actions or the effects of actions (STR/GEO, DA3) (NCCI 7 Taulukko A.3b, 2017)

	Permanent actions		Pre-stressed		Dominant variable load	Other simultaneous variable loads*
6.10	1.00	G	1.00	P	1.15 · (road traffic load) 1.15 · (light traffic load) 1.25 · (railway/track traffic load)	1.30 · ψ_{0i} · (other variable loads)
	or					
	1.00	G	1.00	P	1.30 · (Other permanent action)	1.15 · ψ_{0i} · (road traffic load) 1.15 · ψ_{0i} · (light traffic load) 1.25 · ψ_{0i} · (railway/track traffic load) +1.30 · ψ_{0i} · (other variable loads)

*The coefficient of ψ_{0i} is a combination factor of variable loads.

Table 10. ULS Partial factors for soil parameters (NCCI 7 Taulukko A.4, 2017)

Soil parameters**	Symbol	Values for ULS	
		M1	M2
Shearing resistance	$\gamma_{\varphi\prime}$*	1.0	1.25
Effective cohesion	$\gamma_{c\prime}$	1.0	1.25
Undrained strength	γ_{cu}	1.0	1.4
Unconfined strength	γ_{qu}	1.0	1.4
Unit weight	γ_{γ}	1.0	1.0

* This factor is applied to $tan\,\varphi'$. Moreover, a model factor of 1.15 shall be applied in addition to the partial factor when the soil is clay or silt.

** When creating a cut slope, all partial factors shall be multiplied by 1.2.

Table 11. SLS Partial factors for soil parameters (NCCI 7 Taulukko 5.1, 2017)

Soil parameters**	Symbol	Values for SLS
		M2
Shearing resistance	$g_{f\prime}$*	1.5
Effective cohesion	$g_{c\prime}$	1.8
Undrained strength	g_{cu}	1.8
Unconfined strength	g_{qu}	1.8
Unit weight	$g_{g\prime}$	1.0

* This factor is applied to $tan\,\varphi'$. Moreover, a model factor of 1.15 shall be applied in addition to the partial factor when the soil is clay or silt.

** When creating a cut slope, all partial factors shall be multiplied by 1.2.

Table 12. Partial factors for slope and overall stability (NCCI 7 Taulukko A.14, 2017)

Resistance	Symbol	R3
Earth resistance	$\gamma_{R,e}$	1.0

2.3.4 Allowable uniform and differential settlement

The design limits of uniform and differential settlement are regulated in RATO 3 (2018), as shown in Table 13. These limits vary based on different railway substructure classes, and the higher the class, the stricter the limits to follow. The classification of railway substructures is associated with speed limits, the usage of trains, and axle loads, as presented in Table 14.

Table 13. The design limits of uniform and differential settlements for different railway substructure classes (RATO 3 Taulukko 2, 2018)

Railway substructure class	100 years settlement	0-2 years settlement		2-9 years settlement	
	Uniform settlement	Max. longitudinal slope	Max. crossways slope	Max. longitudinal slope	Max. crossways slope
	mm	%	%	%	%
0	800	0.4	0.8	0.4	0.8
1	800	0.3	0.6	0.3	0.6
2	500	0.2	0.4	0.2	0.4
3	300	0.15	0.3	0.15	0.3
4	100	0.1	0.2	0.1	0.2

Table 14. Railway substructures classification (RATO 3 Taulukko 1, 2018)

Railway substructure class	Passenger traffic speed limit	Freight traffic speed limit with 225kN Raaxle load	Freight traffic speed limit with 250kN axle load
	V (km/h)	V (km/h)	V (km/h)
0	≤50	≤40	≤40
1	≤120	≤100	≤60
2	≤200	≤100	≤80
3	≤250	≤120	≤100
4	>250	>120	>100

During the railway operation, regular inspections are compulsory to ensure safety. The regulations in this regard, such as maintenance classes, the frequency of inspections and error classes, are documented in Ratatekniset Määräykset Ja Ohjeet osa 13 Radan tarkastus (2004). (RAMO 13, 2004)

Three error classes are described in Table 15. The six-pointed star indicates the severity of problems, which needs to be dealt with immediately.

The classification of maintenance is dependent on train speeds, rail types, the material of sleepers and ballast layers. The details of this classification and the frequency of inspections for each class are attached in Appendix A.

Based on maintenance classes and inspected results on vertical alignment deviation, the corresponding error class can be defined, as presented in Table 16 and Table 17.

Table 15. The classification of errors (RAMO 13, 2004)

Error class	Description	Lower the speed limit
C	Beginning error	-
D	This error is required to be include to a maintenance program or to be resolved in near future	-
✷	This error is required to be resolved immediately	The speed limit shall be lower until the error is fixed. The speed limit can resume back to normal after inspection car tests shows the error has been resolved.

Table 16. Vertical alignment deviation limits (mm) for a 5 m range (RAMO 13, 2004)

Error class	Maintenance class							
	1AA	1A	1	2	3	4	5	6
C	2	2	3	4	5	6	7	8
D	4	4	5	6	7	8	9	10
✷	7	7	8	9	10	12	13	14

Table 17. Vertical alignment deviation limits (mm) for a 70 m range (RAMO 13, 2004)

Error class	Maintenance class							
	1AA	1A	1	2	3	4	5	6
C	14	14	-	-	-	-	-	-
D	23	23	-	-	-	-	-	-
✷	33	33	-	-	-	-	-	-

2.4 Cyclic loading

Several sources cause cyclic loading, including seasonal thawing and freezing in cold region, pore water pressure variation, traffic, and nearby construction activities. Such loading may result in differential settlement, damaging structures or even cause major failure. Different sources have been studied by other researchers. Briggs et al. (2016) investigated multiple risks factors affecting highway and railway embankment failure, and two of them contribute to seasonal shrink-swell volume changes and pore water pressure variations. François et al. (2009) proposed a numerical model to predict foundation settlement under influence of repeated dynamic loading in granular soils. A case study of a building located in the vicinity of constant vehicle passage was also included in the paper.

In terms of railway traffic, it consists of smaller scale cyclic loading, repeating axel load (Do et al., 2020), and larger scale ones, trains coming and leaving (as one cycle) on an embankment. This thesis focuses on the latter one.

Deformation is developed in embankment and subgrade due to train loads. Resilient (elastic) deformation and residual (plastic) deformation compose total deformation. Resilient

deformation is reversible, while residual one is irreversible after loading removal. Furthermore, residual deformation can accumulate over time or due to number of cycles. Momoya et al. (2005) showed two types of deformation conceptually, which is presented in Figure 9. It can also be perceived that resilient deformation occurs right beneath wheels subjected to train axle load. On the contrary, residual deformation generates evenly along the rail after repetitive train passing.

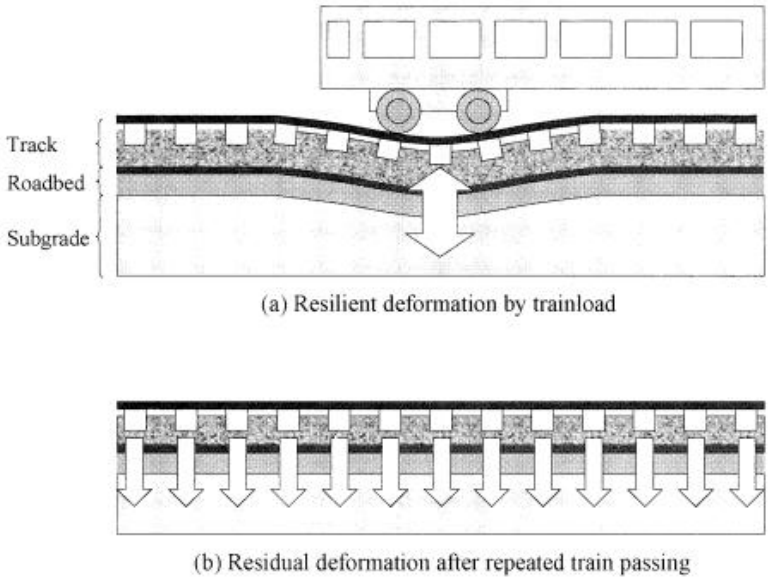

Figure 9. Diagram of (a) resilient deformation and (b) residual deformation (Momoya et al., 2005)

Momoya et al. (2005) pointed out that the deformation characteristics of subgrade are distinguishably different between applying a fixed-point cyclic loading on a sleeper and a moving wheel repeatedly passing on rails. As shown in Figure 10, it is observed that direction of principal stress rotates due to a moving-wheel load, therefore, subgrade settles uniformly. It may be concluded that modelling a dynamic fixed-point loading on a sleeper cannot replicate the deformation caused by cyclic loading realistically.

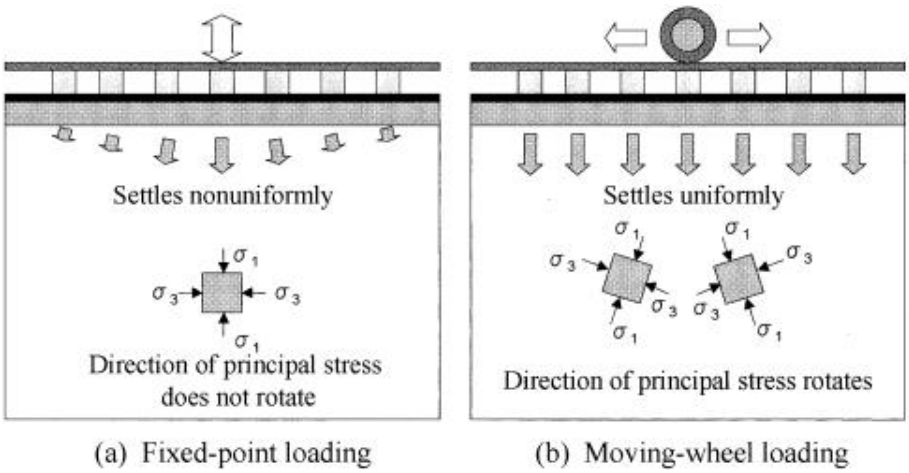

Figure 10. Stress in subgrade between (a) fixed-point loading and (b) moving-wheel loading (Momoya et al., 2005)

Figure 11 visualizes strain evolution over time under cyclic stress amplitude (σ^{ampl}). In general, the total strain (ε^{total}) can be written as following:

$$\varepsilon^{total} = \varepsilon^{N=1} + \varepsilon^{acc} \quad (2)$$

where

$\varepsilon^{N=1}$ = resilient strain developed at the first cycle
ε^{acc} = residual strain accumulation over time.

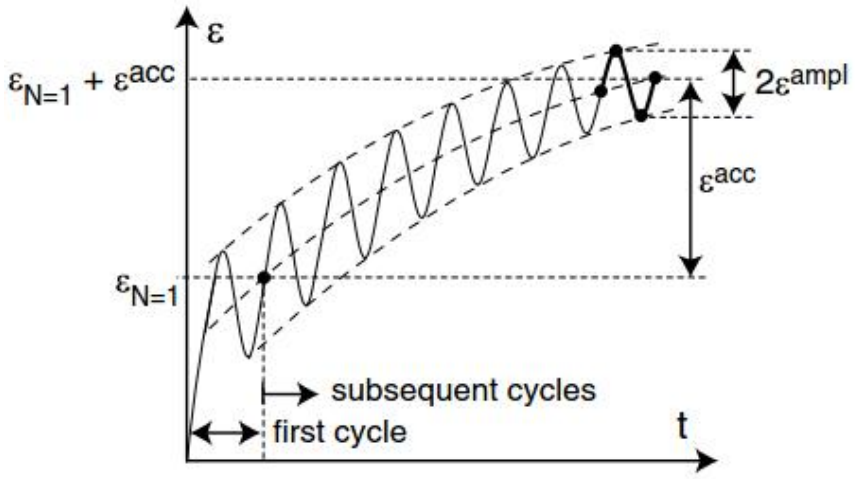

Figure 11. Development of total strain in a cyclic triaxial test (Wichtmann, 2005)

Several models (Suiker & Borst, 2003; Wichtmann et al., 2005; François et al., 2009) have been established to calibrate material behaviors under cyclic loading. This thesis chooses a high-cycle accumulation model developed by Wichtmann et al., (2005), which will be described further in Section 4.2.

2.5 Studied railway embankment profiles

This chapter presents a typical railway cross section, which will be used as the modelling geometry in every PLAXIS simulation. Section 2.5.2 and 2.5.3 show the parameters of the studied railway cross section that will be adopted in PLAXIS calculations. Section 2.5.4 presents bearing values for all the materials.

2.5.1 Typical cross section

Figure 12 presents a typical railway embankment in Finland, which consisted of ballast, subballast and frost protection layers. This cross section is documented in Ratatekniset Ohjeet (RATO) osa 3 Radan rakenne, referring as a technical regulation for railway tracks, and it is associated with the Finnish Transport Agency.

Section 2.1 shows the great variability of materials which can be used for forming a frost protection layer. This layer traditionally consists of filter sand for railways. However, this

thesis intends to use well graded crushed rock, which is closer to the material used for forming subballast layers. To avoid confusing readers, this layer is renamed as an extra subballast layer in this thesis. The detailed dimensions of the cross section are shown in Table 18.

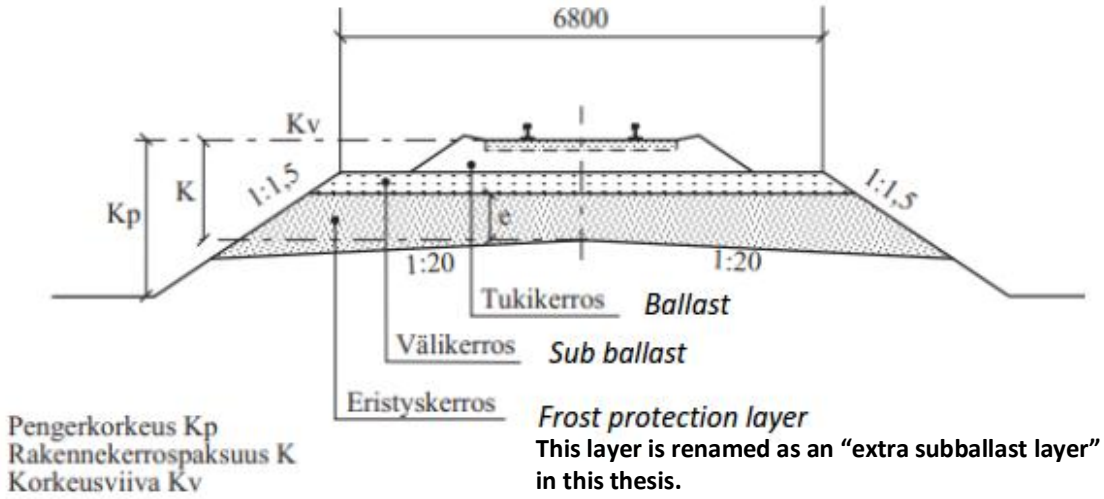

Figure 12. Selected railway cross section. Kp=embankment height, K=total thickness of structural layers, Kv=elevation (RATO 3, 2018)

Table 18. The detailed dimensions of the cross section

Components	Dimensions
Width of sleepers (single track)	2.6 m
Embankment height	1.5 m / 2.5 m
Ballast layer	0.55 m
Subballast layer	0.3 m
Extra subballast layer	0 m – 1 m (varied)
Leca LWA layer	1 m / 1.5 m / 2 m / 3 m

2.5.2 Embankment materials and their Plaxis model parameters

Kalliainen & Kolisoja, (2017) provided the HS model parameters for railway embankment structures, including ballast, subballast and extra subballast layers. The Hardening Soil (HS) model is one of the many soil models provided by PLAXIS, and the detail of this model will be discussed in section 3.1.3.

Watn et al., (2004) and Høva et al., (2009) offered various mechanical and physical properties for different type of Leca LWA. The tests were both performed by SINTEF, which is an independent research organization that conduct contract research and development projects. They provided the oedometer modulus ranges from 20 kPa to 60 kPa under 0-100 kPa vertical stress.

Table 19 summarizes HS model parameters for embankment structures. The stiffness parameters of Leca LWA are estimated based on the correlations ($E_{oed}^{ref} \approx E_{50}^{ref}, E_{ur}^{ref} \approx 3E_{50}^{ref}$) suggested by PLAXIS Material Manual, (2020).

Table 19. HS-model parameters for substructure layers (Kalliainen & Kolisoja, 2017) and Leca-LWA layer (Watn et al., 2004)

Parameters	γ_{unsat}	γ_{sat}	c'	ϕ'	ψ	E_{50}^{ref}	E_{oed}^{ref}	E_{ur}^{ref}	ν_{ur}	m	p^{ref}	K_0^{NC}
Unit	kN/m^3	kN/m^3	kPa	°	°	MPa	MPa	MPa	-	-	kPa	-
Ballast	20	20	20	45	10	250	210	500	0.2	0.5	100	0.3
Subballast	20	20	20	45	5	250	210	500	0.2	0.5	100	0.3
Frost Protection	20	20	10	45	5	160	135	320	0.2	0.5	100	0.3
Leca LWA	6	10	1	36	0	40	40	120	0.2	0.5	100	0.4

2.5.3 Subgrade and its Plaxis model parameters

Several options are used for the subgrade, which depends on the type of analysis as shown in Table 20.

Murro test embankment was set up by the Finnish Road Administration in 1993. The purpose of this test was to evaluate the hardening process of soft soil due to consolidation. This embankment was built on the subgrade which consists of 1.6 m dry crust followed by a thick layer of soft clay. The parameters of subgrade are suggested Koskinen et al., (2002) and they are presented in Table 21 and Table 22 for the Mohr-Coulomb (MC) model and the Soft Soil (SS) model, respectively. The MC model is a basic soil model included in every geotechnical engineering software, and it is also one of the options from PLAXIS. As for the SS model, it is one of the many advanced soil models provided by PLAXIS, and the detail of this model will be discussed in section 3.1.1.

Table 23 presents the HS model parameters for coarse subgrade materials, including loose silt and dense sand.

Table 20. The subgrade type used for different analyses

Analysis type	Subgrade	Plaxis soil model	Source
Embankment stability	Dry crust + soft clay	MC model	Murro test embankment (Koskinen et al., 2002)
Settlement	Dry crust + soft clay	SS model	Murro test embankment (Koskinen et al., 2002)
	Loose silt and Dense gravel	HS model	NCCI 7 Annex 6, (2017)

Table 21. MC-model parameters for soft subgrade materials (Koskinen et al., 2002)

Parameters	Depth	γ_{unsat}	γ_{sat}	c'	ϕ'	ψ	E_u	ν_{ur}	$k_x = k_y$
Unit		kN/m^3	kN/m^3	kPa	°	°	MPa	-	m/day
Dry Crust	0.0-1.6	16.2	16.2	30*	0	0	11.3	0.35	0.00055
Soft Clay	1.6-10.0	15	15	6**	0	0	2.0	0.35	0.00055

*The strength parameters are changed from drained parameter to undrained parameters. Su=30 kPa is applicable for any dry crust layer which has the thickness less than 2.0 m according to Penkereiden stabiliteetin laskentaohje (2018).

**Undrained shear strength of soft clay increased 1.77 kPa/m in depth.

Table 22. SS-model parameters for soft subgrade materials (Koskinen et al., 2002)

Para-meters	Depth	γ_{unsat}	γ_{sat}	e_{ini}	c'	ϕ'	ψ	λ^*	κ^*	ν_{ur}	K_0^{NC}	$k_x = k_y$
Unit	m	kN/m^3	kN/m^3	-	kPa	°	°	-	-	-	-	m/day
Soft clay	1.6-3.0	15.6	15.6	1.8	2	37	0	0.143	0.0107	0.35	0.7	5.5×10^{-4}

Table 23. HS-model parameters for coarse subgrade materials (NCCI Annex 6, 2017)

Para-meters	γ_{unsat}	γ_{sat}	c'	ϕ'	ψ	E_{50}^{ref}	E_{oed}^{ref}	E_{ur}^{ref}	ν_{ur}	m	p^{ref}	K_0^{NC}	$k_x = k_y$
Unit	kN/m^3	kN/m^3	kPa	°	°	MPa	MPa	MPa	-	-	kPa	-	m/day
Loose silt	15	19	1	28	0	6.5	6.5	19.5	0.2	0.7	100	0.53	0.0009
Dense sand	19	22	1	40	0	90	90	270	0.2	0.5	100	0.36	8.6400

2.5.4 The bearing values for all the materials

As mentioned in Section 2.3.2, the Odemark method is used to verify whether a subbase (e.g., subballast) layer has sufficient bearing capacity.

The recommended E-moduli for subballast and frost protection layers are documented in Finnish InfraRYL Liite 3 Kadun normaalipäällysrakenteet ja kantavuusvaatimukset kerroksittain (2015/1 asti Liite 01) (InfraRYL, 2020). Table 24 summarizes E-moduli for embankment materials.

The recommended E-moduli for different subgrades are documented in Finnish InfraRYL Liite:T1. Pohjamaan kantavuusluokitus. (Liite:T2 2017/1 julkaisussa) (InfraRYL, 2020), as shown in Table 25. In general, subgrades can be classified from A to G based on their bearing capacities.

Table 24. E-moduli for embankment materials

Layers name	Equivalent material	Odemark E-moduli	Source
Subballast	ballast crushed rock (Kanta-van kerroksen murske)	300 MPa	InfraRYL, 2020
Frost protection	Filter sand (Suodatinhiekka)	70 MPa	
Extra subballast (frost protection alternative)*	Varied, from a mixture of sand and crushed stone to ballast crushed rock	Varied (e.g., 150 – 300 MPa) depending on the selected material type	
Leca LWA	-	30 – 80 (50)**MPa	Pahkakangas et al., 2020

*When replacing a frost protection layer from sand to crushed rock, the thickness of frost protection layer is required to increase.

** This value is stress dependent.

Table 25. E-moduli for subgrades

Layers name	Classification	Odemark E-moduli	Source
Loose silt	E	20 MPa	InfraRYL, 2020
Dense gravel	B	200 MPa	
soft clay	G	5 MPa	

2.6 Summary

Review of the literature revealed answers to the following research questions.

Q1. What are the allowable limits for uniform and differential displacement in railways?

The design limits for uniform and differential displacement in Finland are specified in RATO3 (2018) and are affected by the classification of railway substructures (Table 13). These classifications of railway substructures are associated with speed limits, the usage of trains, and the designed axle loads (Table 14). In addition to the design limits, regular inspections on vertical alignment deviations during train operations are mandatory for ensuring safety. The limits for such deviations (Table 16 & Table 17) are specified in RAMO 13 (2004) and are affected by the error class (Table 15) and the maintenance class.

Q2. What are the load models used in geotechnical railway design?

Five load models, LM71, SW/0, SW/2, HSLM and LM for unloading trains, are provided by EN 1991-2: Eurocode 1: Actions on structures - Part 2: Traffic loads on bridges (2003). These load models represent railway traffic actions. The load models used in Finland are specified in RATO 3 (2018) and are conforming to EN 1991-2 as well. The regulations that define the load models or characteristic values for train loads adopted in Finland, Norway, Sweden, Denmark and Poland are summarized in Table 6.

Q3. How is it possible to verify sufficient bearing capacity on the top of sub-ballast layer when using Leca LWA with different cover depths (suitable cover depths in railway embankment)?

The bearing capacity at the top of subballast layers can be evaluated by using the Odemark method and must fulfill at least 180 MPa according to InfraRYL (2020). For verifying whether the bearing capacity of each substructure layer as per design, a series of plate loading tests shall be carried out on fields.

Q7. What are the requirements for validating the design parameters of superstructure and embankment materials?

RATO 3 (2018) specifies the load models and the design limits of uniform and differential displacements for railway designs. RAMO 13 (2004) further defines the regular inspection on operational train tracks. (Refer to the answers to the research question Q1 and Q2). InfraRYL (2020) defines the bearing capacity (i.e., Odemark E-modulus) for embankment materials (Table 24) except for Leca LWA because the application of using Leca LWA in railway embankments is relatively new. It also specifies the classification of subgrades based on their bearing capacity (Table 25). NCCI 7 (2017) regulates the partial factors for actions or the effects of actions as well as for soil parameters (Table 9, Table 10, Table 11 and Table 12).

3 Finite element analysis in PLAXIS

As all the numerical simulations in this thesis will be run by PLAXIS 2D, it is necessary to understand this program. PLAXIS 2D is a computer program that perform finite element analysis for geotechnical engineering problems, such as deformation, stability, and water flow, in two-dimensional conditions. (PLAXIS Reference Manual, 2020)

Finite Element Method (FEM) is widely used in various engineering disciplines. For geotechnical engineering applications, this involves three steps. Firstly, a modelling problem (geometry) is discretized into a huge number of small regions, called finite element. These elements have nodes defined within the elements and on the boundaries. Secondly, variables (i.e., stress, displacement) are solved by deriving element equations. as given by Eq.(3):

$$[\boldsymbol{K}_E]\{\Delta \boldsymbol{d}_E\} = \{\Delta \boldsymbol{R}_E\} \tag{3}$$

where

$\boldsymbol{K}_E$ = local element stiffness matrix
$\Delta \boldsymbol{d}_E$ = vector of all incremental nodal displacements
$\Delta \boldsymbol{R}_E$ = vector of all incremental nodal forces.

Finally in order to solve global equations with assigned boundary conditions, the global equation (Eq.(4)) can be converted from the local equation (Eq.(3)) as: (Potts and Zdravkovic, 1999)

$$[\boldsymbol{G}_E]\{\Delta \boldsymbol{G}_E\} = \{\Delta \boldsymbol{G}_E\} \tag{4}$$

where

$\boldsymbol{G}_E$ = global element stiffness matrix
$\Delta \boldsymbol{G}_E$ = vector of all incremental nodal displacements
$\Delta \boldsymbol{G}_E$ = vector of all incremental nodal forces.

PLAXIS offers a great variety of soil models, the following sections will describe those models that will be used in this thesis. Also, PLAXIS calculate types will be shortly discussed as they are essential steps for generating simulation or analysis results.

3.1 Plaxis soil models

There are four models, Mohr-coulomb (MC), Soft Soil (SS), Soft Soil Creep (SSC) and Hardening Soil (HS), used in this thesis. Since the MC-model is a basic, no detailed description will be discussed except the MC failure line which is shared in all models.

3.1.1 Soft soil model

The Soft Soil (SS) model is often used for soil materials with high degree of compressibility, and typically requires oedometer test data which provides compression index and swelling index of the tested soil specimen. These two indices enable the software to calculate elastic and plastic volumetric changes due to loading. Additionally, the SS model can distinguish primary loading and unloading-reloading based on the input of POP (initial pre-overburden pressure). Consequently, this model captures displacement / settlement of soft soil subjected to loading decently well. Table 26 provides parameters for the SS-model.

Table 26. Parameters of the SS-model

Basic stiffness		
λ^*	Modified compression index	-
κ^*	Modified swelling index	-
Basic stiffness alternative		
C_c	Compression index	-
C_s	Swelling index	-
e_{init}	Initial void ratio	-
Strength (failure criterion)		
c'	Effective cohesion	kPa
ϕ'	Friction angle	°
ψ	Dilatancy angle	°
Advanced		
ν'_{ur}	Poisson's ratio for unloading / reloading	-
K_0^{NC}	Coefficient of lateral stress in normal consolidation	-
M	K_0^{NC} parameter	-

- Yield surface

The cap yield surface which can expand due to plastic strain, along with Mohr coulomb failure line form the whole yield surface. Figure 13(a) presents a yield surface in a $p', \tilde{q}$-plane (2D), and Figure 13(b) shows a yield contour in stress principal space (3D). Furthermore, the area inside the yield surface / contour belongs to elastic regions, otherwise it pertains to plastic regions.

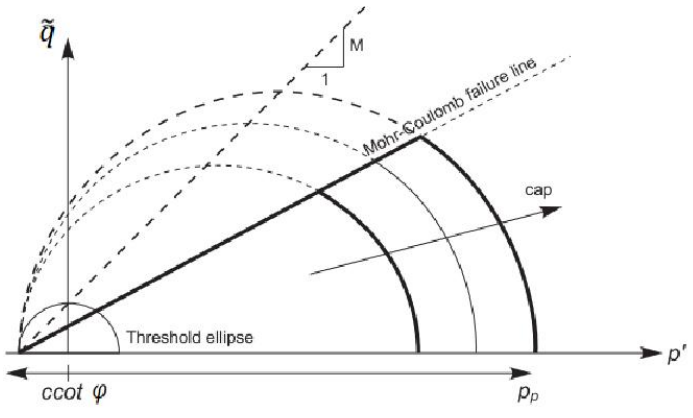

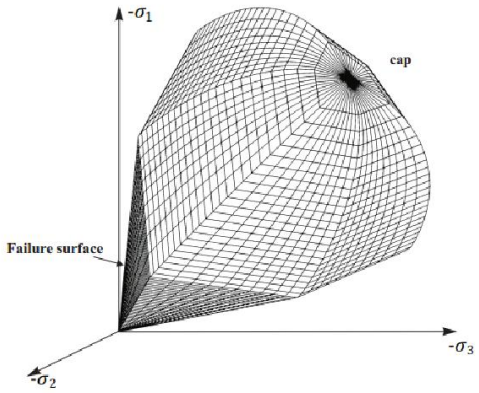

(a) Yield surface in $p', \tilde{q}$-plane (b) Yield contour in principal stress space

Figure 13. Yield surface in $p', \tilde{q}$-plane (a) and yield contour in principal stress space (b) of the SS model (PLAXIS Material Manual, 2020)

The yield function (PLAXIS Material Manual, 2020) used in the Soft Soil model is defined as:

$$f = \bar{f} - p_p \,,$$
$$\bar{f} = \frac{\tilde{q}^2}{M^2(p' + cco\,t(\varphi))} + p' \qquad (5)$$

where

$\bar{f}$ = Function of stress state $(p', \tilde{q})$
p_p = The pre-consolidation stress which is a function of plastic strain.

The soft soil model adopts Mohr coulomb failure criterion, which is defined as:

$$\tau_{ff} = c' + \sigma'_{ff}\, tan\ \phi' \qquad (6)$$

where

τ_{ff} = shear stress at failure
c' = cohesion
σ'_{ff} = normal stress on the failure plane
ϕ' = effective friction angle.

- Equations for computing soil volumetric changes

A logarithmic relation between changes in volumetric strain, ε_v, and changes in mean effective stress, p', as shown in Figure 14, is assumed in the Soft Soil model.

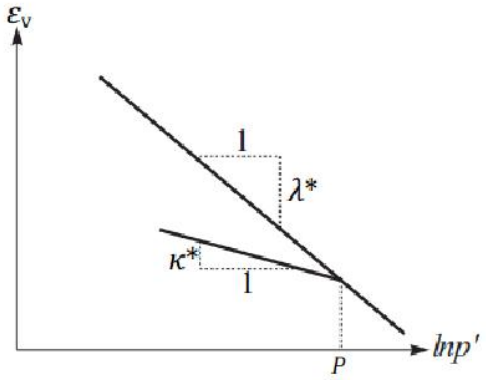

Figure 14. Logarithmic relation between volumetric strain and mean stress (PLAXIS Material Manual, 2020)

PLAXIS Material Manual (2020) gives the equations (Eq.(7), Eq.(8)) for computing the virgin compression and the unloading-reloading compression. It also provides the correlations (Eq.(9) , Eq. (10)) between C_c and λ^*, as well as, C_s and κ^*.

$$\varepsilon_v - \varepsilon_v^0 = -\lambda^* ln\left(\frac{p' + cco\,t(\varphi)}{p^0 + cco\,t(\varphi)}\right)(virgincompression) \quad (7)$$

$$\varepsilon_v^e - \varepsilon_v^{e0} = -\kappa^*\, ln\left(\frac{p' + ccot\,(\varphi)}{p^0 + cot\,(\varphi)}\right)(unloading - \ reloading\ compression) \quad (8)$$

$$\lambda^* = \frac{C_c}{2.3(1+e)} \quad (9)$$

$$\kappa^* \approx \frac{2C_s}{2.3(1+e)} \quad (10)$$

3.1.2 Soft soil creep model

The Soft Soil Creep (SSC) model can not only model the behavior of compressible soil, but also consider creep deformation (secondary compression). Basically, this model has the same basic characteristics as the SS-model. Time-dependent creep computation differs it a bit from the SS-model. Table 27 presents parameters for the SSC-model.

Table 27. Parameters of the SSC-model

Basic stiffness		
λ^*	Modified compression index	-
κ^*	Modified swelling index	-
μ^*	Modified creep index	-
Basic stiffness alternative		
C_c	Compression index	-
C_s	Swelling index	-
C_α	Creep index	-
e_{init}	Initial void ratio	-
Strength (failure criterion)		
c'	Effective cohesion	kPa
ϕ'	Friction angle	°
ψ	Dilatancy angle	°
Advanced		
ν'_{ur}	Poisson's ratio for unloading / reloading	-
K_0^{NC}	Coefficient of lateral stress in normal consolidation	-
M	K_0^{NC} parameter	-

Having received oedometer test results, stress-strain curve can be idealized as in Figure 15(a). The turning point at the intersection of slope a and slope b separates elastic and creep deformations. As in Figure 15(b), slope c gives the function increasing creep deformation in terms of time. These slopes (a, b and c) will be used for computing stress and strain in this model.

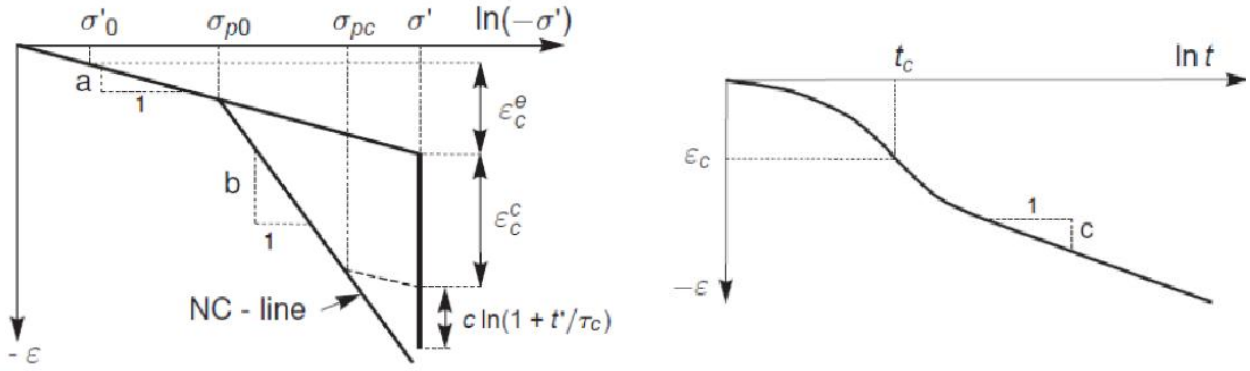

(a) Idealized stress-strain curve (b) Creep strain

Figure 15. Interpretation of oedometer test results (PLAXIS Material Manual, 2020)

The equivalent pressure (p^{eq}) in $p', \tilde{q}$-plane is defined by the following:

$$p^{eq} = p' + \frac{\tilde{q}^2}{M^2(p' + ccot\,(\varphi))}, \qquad (11)$$

$$M = \frac{6sin\,(\varphi_c)}{3 - sin\,(\varphi_c)}$$

where

p' = isotropic stress
$\tilde{q}$ = deviatoric stress
c = cohesion
φ = friction angle at failure
M = critical state line
φ_c = critical state friction angle.

Based on 1D-model (Eq.(11)), the following 3D equations can be elaborated by Eq.(12). Figure 16 shows p^{eq}-ellipse in a $p', \tilde{q}$ plane.

$$p^{eq} = \sigma_1' \left[\frac{1 + 2K_0^{nc}}{3} + \frac{3(1 - K_0^{nc})^2}{M^2(1 + 2K_0^{nc})} \right],$$
$$p_p^{eq} = \sigma_p \left[\frac{1 + 2K_0^{nc}}{3} + \frac{3(1 - K_0^{nc})^2}{M^2(1 + 2K_0^{nc})} \right] \quad (12)$$

where

K_0^{nc} = coefficient of lateral stress in normal consolidation
p_p^{eq} = generalized pre-consolidation pressure, which is proportional to 1D σ_p.

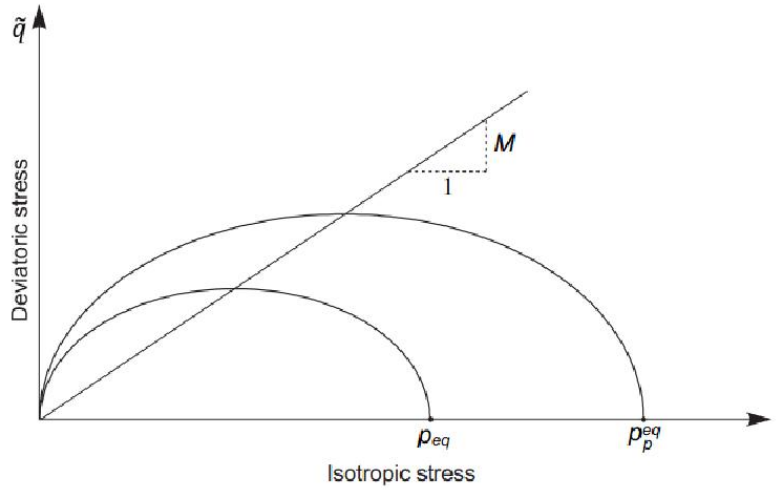

Figure 16. Diagram of p^{eq}-ellipse in a $p', \tilde{q}$ plane (PLAXIS Material Manual, 2020)

The volumetric creep strain ($\dot{\varepsilon}_v^c$) is computed by Eq.(13). The 1D creep model with slopes a, b and c can be substituted by the stiffness parameters, κ^*, $\lambda^*$and μ^* as presented in Eq.(15) by using Eq.(14).

$$-\dot{\varepsilon}_v^c = \frac{c}{\tau}\left(\frac{p^{eq}}{p_p^{eq}}\right)^{\frac{b-a}{c}},$$

$$p_p^{eq} = p_{p0}^{eq}\exp\left(\frac{-\varepsilon_v^c}{b-a}\right) \tag{13}$$

wherein p_{p0}^{eq} denotes initial conditions ($\dot{\varepsilon}_v^c$ = 0, t = 0).

$$\kappa^* \approx 2a, \qquad \lambda^* = b, \qquad \mu^* = c \tag{14}$$

$$-\dot{\varepsilon}_v^c = \frac{\mu^*}{\tau}\left(\frac{p^{eq}}{p_p^{eq}}\right)^{\frac{\lambda^*-\kappa^*}{\mu^*}},$$

$$p_p^{eq} = p_{p0}^{eq} exp\left(\frac{-\varepsilon_v^c}{\lambda^*-\kappa^*}\right) \tag{15}$$

3.1.3 Hardening soil model

One benefit of using the Hardening Soil (HS) is that this model can calibrate elastic deformation more accurately compared to the purely linear elastic model. This contributes to the more advanced stiffness parameters that is capable of computing hyperbolic stress-strain curve (Figure 17).

Also, the yield surface can expand due to plastic straining, which is similar to the two previously discussed models (SC and SSC), to the contrary of a perfectly plastic model, i.e., MC-model. Table 28 provides parameters for the HS-model.

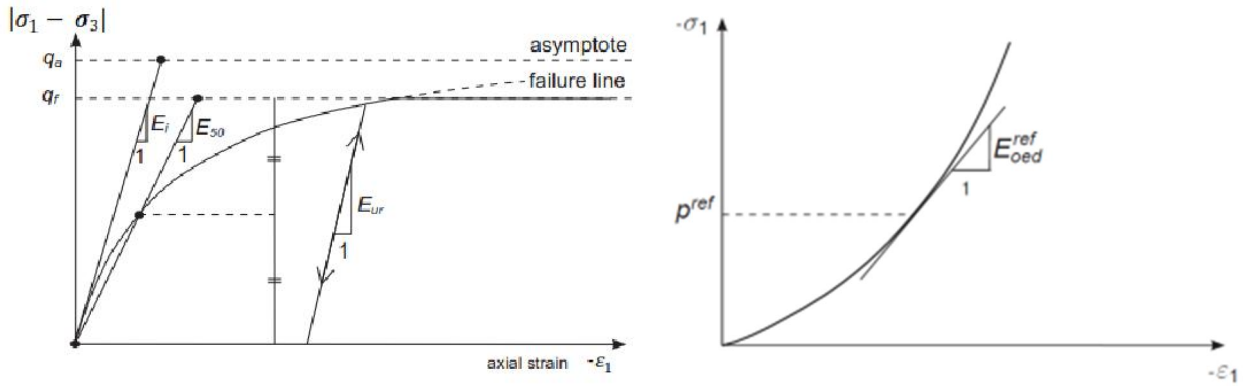

(a) Hyperbolic relation of stress- strain in primary loading for a standard drained test

(b) Oedometer test results

Figure 17. Definition of HS-stiffness modulus (PLAXIS Material Manual, 2020)

Table 28. Parameters of the HS-model

Basic stiffness		
E_{50}^{ref}	Secant stiffness in standard drained triaxial test	kPa
E_{oed}^{ref}	Tangent stiffness for primary oedometer loading	kPa
E_{ur}^{ref}	Unloading / reloading stiffness	kPa
m	Power	-
Basic stiffness alternative		
C_c	Compression index	-
C_s	Swelling index	-
e_{init}	Initial void ratio	-
Strength (failure criterion)		
c'	Effective cohesion	kPa
ϕ'	Friction angle	°
ψ	Dilatancy angle	°
Advanced		
ν'_{ur}	Poisson's ratio for unloading / reloading	-
p^{ref}	Reference stress for stiffnesses	kPa
K_0^{NC}	Coefficient of lateral stress in normal consolidation	-
f	Failure ratio	-

3.2 Calculation type

This thesis uses three calculate types offered by PLAXIS (PLAXIS Reference, 2020), which are plastic, safety, and consolidation, and they will be briefly reviewed in this section.

It is common to start the calculation steps with generating initial stresses using either gravity loading or K_0 procedure. The former one generates initial stresses by applying soil self-weight.

The safety calculation type enables PLAXIS to compute global safety factors, which is essential for embankment stability problems. The factor of safety (FoS) is linked to the total multiplier (ΣMsf), as defined in Eq.(16), at failure. It can also be seen that the shear strength parameters of the soil will be progressively reduced until the failure of the structure appears.

$$\Sigma Msf = \frac{tan\,\varphi_{\text{input}}}{tan\,\varphi_{\text{reduced}}} = \frac{c_{\text{input}}}{c_{\text{reduced}}} = \frac{s_{u,\,\text{input}}}{s_{u,\,\text{reduced}}} \tag{16}$$

The consolidation calculation type allows PLAXIS to analyze the development and dissipation of excess porewater pressure along with given time. Therefore, this calculation type will be adopted for displacement / settlement problems.

4 Methodology

Since PLAXIS is commonly used for modelling more advanced problems encountering in geotechnical engineering, it is natural to find an existing model of PLAXIS for simulating the displacement induced by railway cyclic loading as well.

As introduced in Section 3.1.2, the SSC-model enable PLAXIS to compute creep deformation as a function of time. Consequently, this model may suit the purpose of simulating cyclic loading because they both take increasing plastic strain into account.

However, Leca LWA performed cyclic compression test (Section 4.1), which gives the deformation as a function of number of cycles. Therefore, it is essential to correlate these two analysis results, which are, the deformation as a function of time in PLAXIS and the deformation as a function of number of cycles. The high-cycle accumulation model (Section 4.2) was introduced to serve this purpose. Section 4.3 shows the application of PLAXIS SSC-model to high cycle train load. The simulations of displacement induced by cyclic loading in Leca LWA layers, which were further used to validate the HCA model using Leca laboratory test data. Lastly, Section 4.4 evaluates the methodology chapter.

4.1 Leca LWA lab test data

Leca Finland Oy provided considerable amount of Leca LWA test results, however, only the relevant test methods and outcomes are included in this section. Section 4.1.2 shows the interpretation of the compression index for Leca LWA, which is an essential parameter for computing settlement in PLAXIS.

4.1.1 Cyclic compression test

According to EN15732:2012 Annex B, determination of the resistance to cyclic compression loading, the test method is summarized as following. A sample of LWA, placed in a steel, cylindrical container (200-mm height x 200-mm width), is firstly compacted by vibration, and a cyclic compressive load with constant amplitude is then applied to the sample. The applied cyclic load, with a typical range of 5 kPa to 120 kPa, has a frequency of 4 Hz. This test has a duration of 2×10^6 cycles.

- Leca LWA 4-32 materials produced by Leca Finland Oy

This thesis studies this exact type of Leca LWA. Research Institutes of Sweden (RISE) carried out the laboratory cyclic compression test for Leca LWA 4-32 materials on behalf by Leca Finland Oy.

RISE received two samples (Leca LWA 4-32) prepared by Leca Finland Oy, and then conducted the test dated May 21 – June 4, 2018. It is documented in RISE's test report that both samples were dry (0% water content) and the cyclic load of 12kPa to 120kPa were

applied during the test. Figure 18 shows the test results of deformation (%) versus the number of cycles (N).

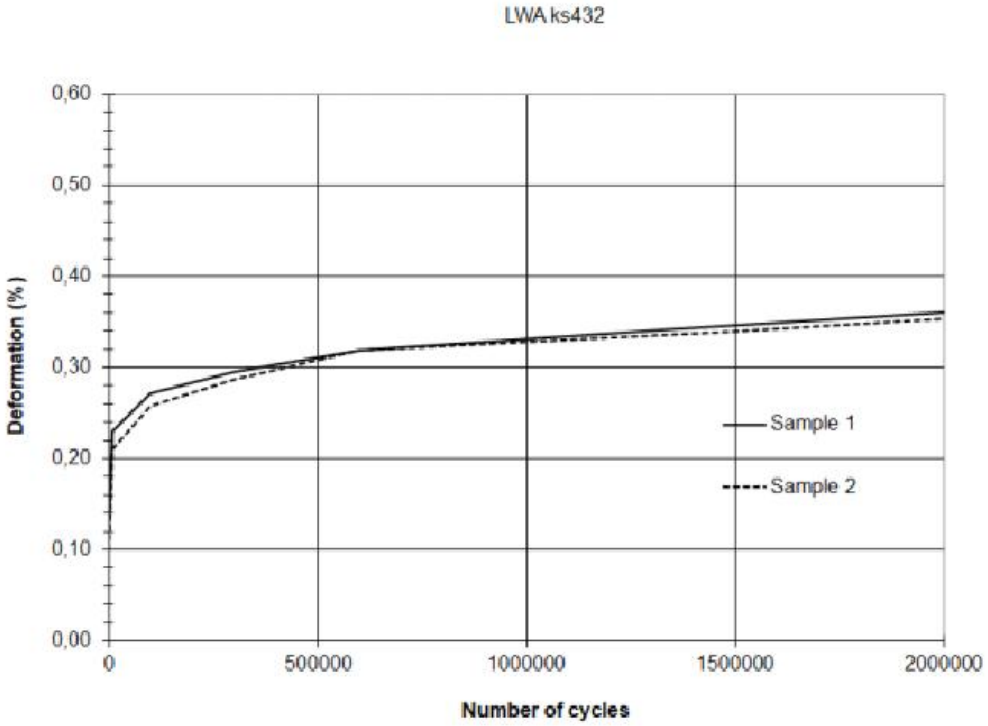

Figure 18. Leca LWA Fin 4-32 deformation versus the number of cycles (RISE, 2018)

4.1.2 Oedometer test

The main purpose of the oedometer test is to determine the relation between short term deformation of materials with increasing applied stress. A test sample was placed in a cylindrical container (150-mm width x 300-mm height), and it is then compacted by vibration or tamping. The load is applied stepwise as shown in Figure 19(a).

- Leca LWA 4-32 materials produced by Leca Finland Oy

No required data to this test can be found for this exact type of Leca LWA.

- Other tests for Leca LWA with various types produced by multiple countries

Høva et al., (2009) conducted extensive testing program for different types of Leca LWA and they were documented in a SINTEF report. This report contains oedometer test results for different types of Leca LWA. Although these products are not exact the same as the research material, they are still worthy of reference due to the similar manufacturing process of all Leca LWA products. Figure 19 shows the load steps and the oedometer modulus for Norwegian LWA 4-32 (Nor LWA 4-32) samples. This type of Leca LWA is chosen for this thesis because it has the same grain size distribution as the studied material, which is Fin LWA 4-32.

Load step [kPa]	Duration of load step [min]	Progressive time [min]
7.91	12	12
32.91	12	24
57.91	12	36
82.91	12	48
107.91	12	60
132.91	12	72
157.91	12	84
182.91	12	96
207.91	12	108
252.91	12	120
302.91	12	132
402.91	12	144

(a) Load steps

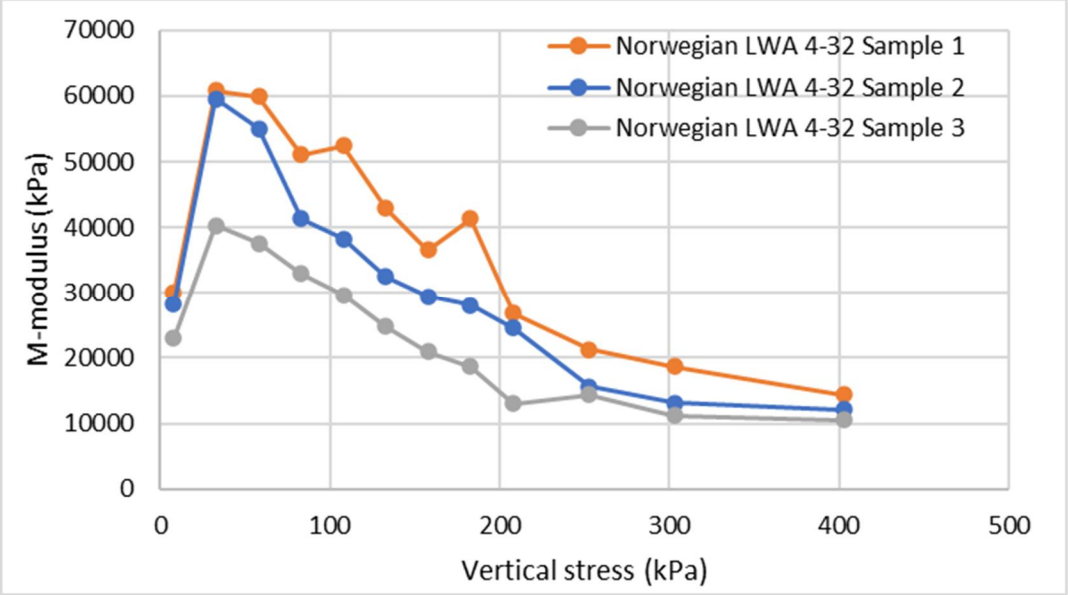

(b) M-modulus versus vertical stress

Figure 19. Oedometer test results for Norwegian LWA 4-32 samples (Høva et al., 2009)

In this SINTEF report, the oedometer modulus (M) is defined as:

$$M = \frac{d\sigma'}{d\varepsilon} \tag{17}$$

where

$d\sigma'$ = delta effective stress (kPa)
$d\varepsilon$ = delta strain (-).

Since Norwegian LWA 4-32 materials have the same grain size distribution as the studied materials, the three curves of Norwegian LWA 4-32 in Figure 19 (b) are adopted to replot a typical oedometer test results. Such results contain vertical stresses (logarithmic scale) in x-axis and changing void ratios (e) in y-axis.

By knowing the initial height of samples (h_0) is 300 mm and the initial void ratio (e_{init}) of Leca LWA is 0.5, the delta e (Δe) is plotted using a correlation as given in Eq.(18). The results are shown in Figure 20.

These samples have pre-consolidation pressures approximately 200 kPa, which will be shown using Plaxis soil test in Section 4.3.1.

$$\frac{\Delta h}{h_0} = \frac{\Delta e}{1 + e_0} \tag{18}$$

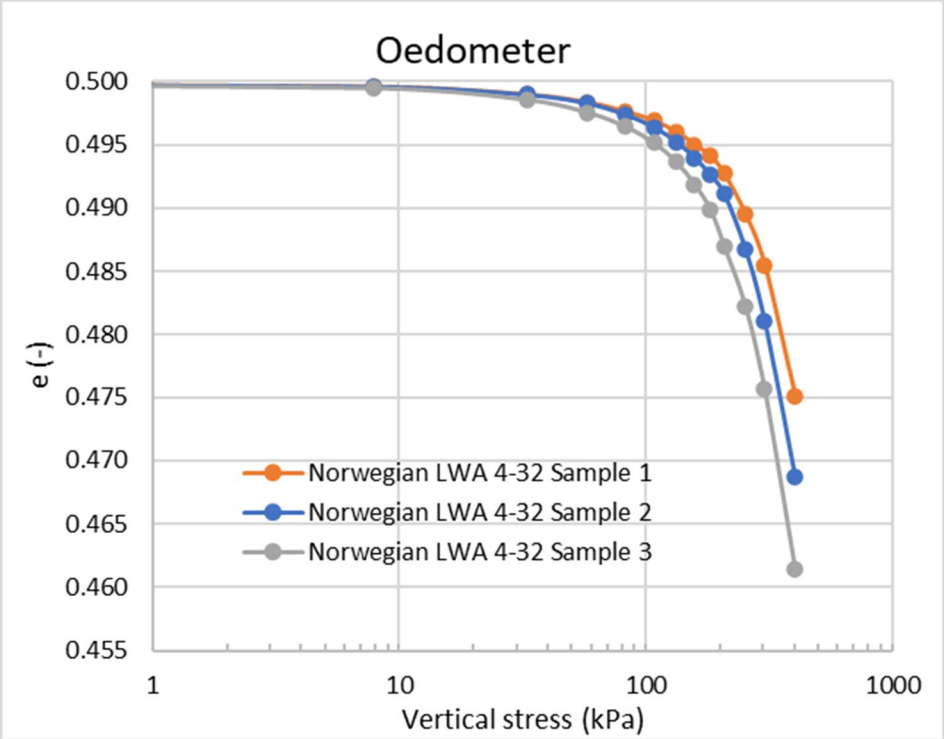

Figure 20. The oedometer test results for Norwegian LWA 4-32 materials

4.2 The High-cycle accumulation model

The high-cycle accumulation (HCA) model was established by Wichtmann et al., (2005). The purpose of using this model is to predict the accumulation of strain or stress under cyclic loading with large amount of cycles and with relatively small strain amplitude ($\varepsilon^{ampl} < 10^{-3}$). The typical applications include railways, water gates and foundations of offshore wind turbines.

The HCA model was developed based on a series of cyclic triaxial drained tests on multiple specimens of sand. The developers of this model discovered that the strain amplitude, the cyclic preloading history, the average stress, the density, and the grain size distribution have an influence on the direction and the intensity of strain accumulation (Wichtmann et al., 2005). These functions will be discussed in Section 4.2.2.

Section 4.2.4 shows the use of HCA model for replicating Leca LWA. This model will reproduce the strain accumulation under cyclic loading as in Figure 18. However, this replicated curve will be further adjusted because the given conditions, e.g., strain amplitude and stresses, of laboratory tests are different from that of on construction site which will be simulated using Plaxis. This adjustment will be presented in Section 4.3.2.

4.2.1 Constitutive relations

Wichtmann et al., (2009) proposed the relation of stress and strain as following:

$$\dot{\boldsymbol{\sigma}} = E : (\dot{\boldsymbol{\varepsilon}} - \dot{\boldsymbol{\varepsilon}}^{acc}) \qquad (19)$$

where

$\dot{\boldsymbol{\sigma}}$ = stress rate
E = stress dependent elastic stiffness
$\dot{\boldsymbol{\varepsilon}}$ = strain rate
$\dot{\boldsymbol{\varepsilon}}^{\mathrm{acc}}$ = accumulated strain rate.

Basically, this equation links the stress rate (change per cycle) over a stress-dependent elastic stiffness with strain rate, it can also be expressed in the matrix as Eq.(20) where v stands for Poisson's ratio.

$$\begin{bmatrix} \dot{\sigma}_{11} \\ \dot{\sigma}_{22} \\ \dot{\sigma}_{33} \\ \dot{\sigma}_{12} \\ \dot{\sigma}_{13} \\ \dot{\sigma}_{23} \end{bmatrix} = \frac{E}{(1+v)(1-2v)} \begin{bmatrix} 1-v & v & v & 0 & 0 & 0 \\ v & 1-v & v & 0 & 0 & 0 \\ v & v & 1-v & 0 & 0 & 0 \\ 0 & 0 & 0 & 1-2v & 0 & 0 \\ 0 & 0 & 0 & 0 & 1-2v & 0 \\ 0 & 0 & 0 & 0 & 0 & 1-2v \end{bmatrix} \begin{bmatrix} \dot{\varepsilon}_{11} - \dot{\varepsilon}_{11}^{acc} \\ \dot{\varepsilon}_{22} - \dot{\varepsilon}_{22}^{acc} \\ \dot{\varepsilon}_{33} - \dot{\varepsilon}_{33}^{acc} \\ \dot{\varepsilon}_{12} - \dot{\varepsilon}_{12}^{acc} \\ \dot{\varepsilon}_{13} - \dot{\varepsilon}_{13}^{acc} \\ \dot{\varepsilon}_{23} - \dot{\varepsilon}_{23}^{acc} \end{bmatrix} \qquad (20)$$

The accumulated strain rate is described as the project of the intensity of accumulation ($\dot{\varepsilon}^{\mathrm{acc}}$) and the direction of accumulation ($\mathbf{m}$), as shown in Eq.(21). The intensity of accumulation ($\dot{\varepsilon}^{\mathrm{acc}}$) consists of six functions, which will be described in the next section.

$$\dot{\boldsymbol{\varepsilon}}^{acc} = \dot{\varepsilon}^{acc}\boldsymbol{m} \tag{21}$$

4.2.2 Intensity of accumulation

Wichtmann et al., (2009) proposed Eq.(22) to describe the effect of different functions on the intensity of accumulation.

$$\dot{\varepsilon}^{acc} = f_{ampl}\dot{f}_N f_e f_p f_Y f_\pi \tag{22}$$

where

f_{ampl} = strain amplitude
$\dot{f}_N$ = cyclic preloading
f_e = average void ratio
f_p = average mean stress
f_Y = average stress ratio
f_π = polarization change.

As the HCA model was developed based on a series of cyclic triaxial drained tests, it is necessary to define basic stress and strain components in the test, which is shown in Figure 21. The mean stress (p) and the deviatoric stress (q) can be calculated as in Eq.(23) and Eq.(24), respectively, assuming soil is in plane-strain condition.

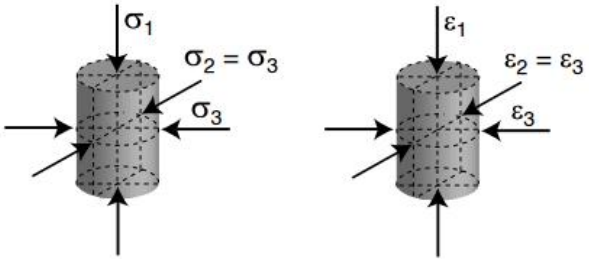

Figure 21. Definition of stress and strain components in the triaxial test (Wichtmann, 2005)

$$p = \frac{\sigma_1 + \sigma_3}{2} \tag{23}$$

$$q = \sigma_1 - \sigma_3 \tag{24}$$

Based on p and q, the stress ratio (η) can be defined as following:

$$\eta = \frac{q}{p} \tag{25}$$

- The influence of strain amplitude (f_{ampl})

The strain amplitude is defined as Eq.(26), for one-dimensional cycles. The magnitude of ε_{ampl}, as shown in Figure 22, determines f_{ampl}.

$$\varepsilon^{ampl} = \frac{\left(\varepsilon^{max} - \varepsilon^{min}\right)}{2} \tag{26}$$

where

ε^{max} = maximum value of a strain loop
ε^{min} = minimum value of a strain loop.

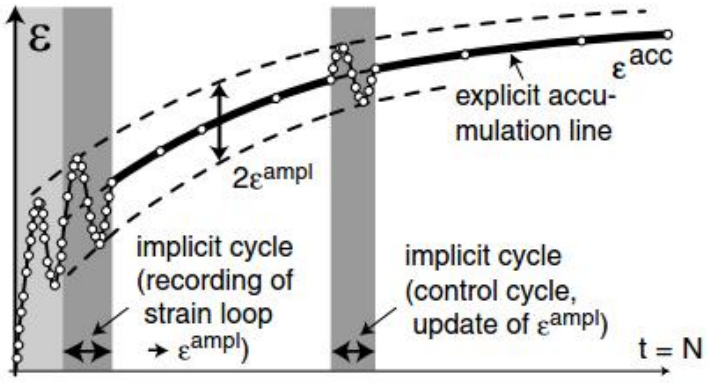

Figure 22. Definition of strain amplitude (Wichtmann, 2005)

The function of f_{ampl} is shown as Eq.(27), showing that there is a linear relation between $\dot{\varepsilon}^{acc}$ and $(\varepsilon^{ampl})^2$. Since ε^{ampl} should be smaller than 10^{-3}, f_{ampl} has the maximum value of 100.

$$f_{ampl} = min\left\{\left(\frac{\varepsilon^{ampl}}{\varepsilon_{ref}^{ampl}}\right)^2 ; 100\right\}, \varepsilon_{ref}^{ampl} = 10^{-4} \tag{27}$$

- The influence of cyclic preloading ($\dot{f}_N$)

The function of $\dot{f}_N$ is written as Eq.(28), where the $\dot{\varepsilon}^{acc}$ accumulates with the increasing number of cycles (N).

$$\dot{f}_N = \underbrace{C_{N1}C_{N2}exp\left[-\frac{g^A}{C_{N1}f_{ampl}}\right]}_{\dot{f}_N^A} + \underbrace{C_{N1}C_{N3}}_{\dot{f}_N^B} \tag{28}$$

$$g^A = \int f_{ampl}\frac{C_{N1}C_{N2}}{1 + C_{N2}N} \tag{29}$$

wherein C_{N1}, C_{N2} and C_{N3} are material constants, g^A is the preloading variable.

When a tested material experiences a constant f_{ampl}, the accumulation curve can be approximated by the logarithm function as presented in Eq.(30).

$$f_N = C_{N1}[l\,n(1 + C_{N2}N) + C_{N3}N] \tag{30}$$

- The influence of void ratio (f_e)

The function of f_e has a hyperbolic relation with void ratio, as shown in Eq.(31).

$$f_e = \frac{(C_e - e)^2}{1 + e}\frac{1 + e_{ref}}{(C_e - e_{ref})^2}, e_{ref} = e_{max} \tag{31}$$

wherein C_e is a constant.

As shown in Eq.(31), f_e is dependent on C_e, e and e_{max}. Wichtmann et al., (2005) proposed a method of determining the constant C_e. A series of triaxial drained tests with different initial void ratio ($0.58 \le e_{init} \le 0.80$) were conducted under the constant average stress ($p^{av} = 200kPa$, $\eta^{av} = 0.75$) and the constant amplitude ratio ($\xi = 0.3$) throughout the entire trials. The results were plotted in the accumulated strain $\varepsilon^{acc}/\bar{f}_{ampl}$ versus the void ratio, as presented in Figure 23. The constant C_e was adjusted to fit with the data of $\varepsilon^{acc}/\bar{f}_{ampl}$ under the varied number of cycles ($N = 20 \ldots 100000$).

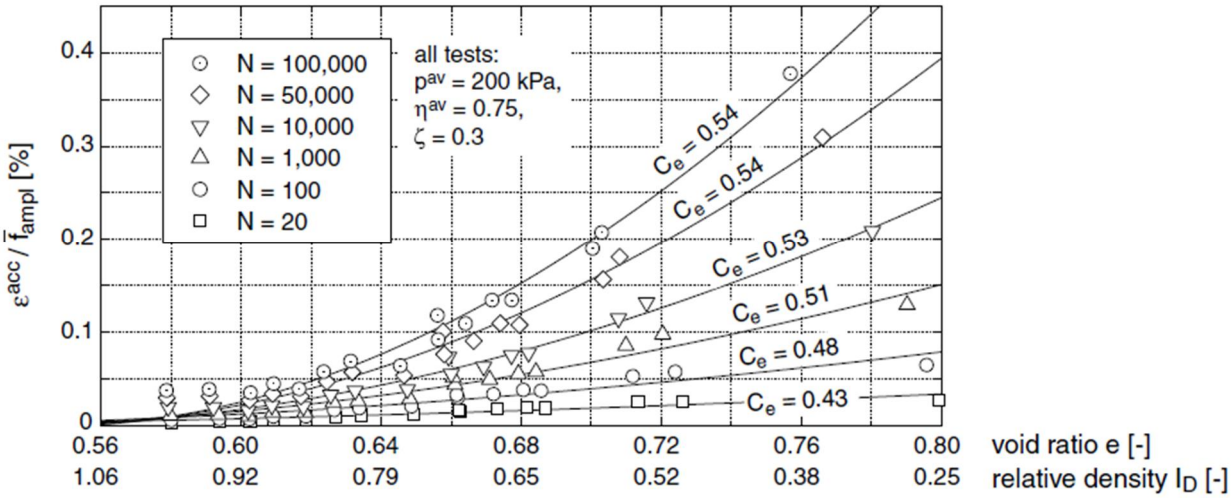

Figure 23. Determination of C_e (Wichtmann et al., 2005)

- The influence of average mean stress (f_p)

The function of f_p is expressed as Eq.(32), where the $\dot{\varepsilon}^{acc}$ decreases exponentially with increasing average mean pressure (p^{av}).

$$f_p = exp\left[-C_p\left(\frac{p^{av}}{p^{ref}} - 1\right)\right], p^{ref} = p^{atm} = 100kPa \quad (32)$$

wherein C_p is a constant.

- The influence of average stress ratio (f_Y)

The function of f_Y is written as Eq.(33), where the $\dot{\varepsilon}^{acc}$ increases exponentially with growing average stress ratio ($\bar{Y}^{av}$).

$$f_Y = ex\,p[C_Y \bar{Y}^{av}] \quad (33)$$

wherein C_Y is a constant.

The average stress ratio ($\bar{Y}^{av}$) is characterized as following:

$$\bar{Y}^{av} = \frac{Y\ -\ 9}{Y_c\ -\ 9}, \quad (34)$$

$$Y = \frac{27\ (\ 3\ +\ \eta\ )}{(\ 3\ +\ 2\,\eta\ )\ (3\ -\ 2\,\eta)}, \quad (35)$$

$$Y_c = \frac{9 - sin^2\ \varphi_c}{1 - sin^2\ \varphi_c} \quad (36)$$

wherein φ_c stands for critical friction angle.

- The influence of polarization change (f_π)

During the process of applying cyclic loading, the shape of strain loop could change. However, neither the cyclic triaxial test performed by Wichtmann et al., (2005), nor the cyclic compression test for Leca® LWA 4-32 materials (section 4.1.1) was taken these changes into consideration. As a result, f_π = 1 holds for the both cases.

4.2.3 Direction of accumulation

The direction of accumulation ($\boldsymbol{m}$), also known as cyclic flow rule, is highly dependent on the average stress ratio (η^{av}), and it can be approximated by the flow rule of the modified Cam Clay model. (Wichtmann et al., 2009)

4.2.4 Use of the HCA model for replicating Leca LWA lab tests

The purpose of this section is to reproduce the strain accumulation under cyclic loading as in Figure 18.

Since the given the maximum and minimum stresses of 120 kPa and 12 kPa for cyclic loading were not exceeded pre-consolidation pressures, approx. 200 kPa, in the oedometer tests (Section 4.3.1), ε^{ampl} can be interpreted using the swelling index (C_s).

Unloading-reloading tests were not included in the previous oedometer tests as shown in Figure 19, therefore, it is assumed that the swelling index is the slope between the first two vertical stresses points (7.91 kPa and 32.91 kPa) in Figure 20.

The change of void ratio ($\Delta\, e$) between the stresses of 120 kPa and 12 kPa can be calculated as in Eq. (37). The strain amplitude (ε^{ampl}) can be further computed using Eq. (38). Having known ε^{ampl} for each oedometer test, f_{ampl} can be calculated using Eq. (27). Table 29 summarizes the values of f_{ampl} for Norwegian LWA 4-32 materials. The median value of f_{ampl}, 11.49, is used for reproducing the strain accumulation of Leca LWA.

$$\Delta\, e = C_s \times log\frac{120}{12} \tag{37}$$

$$\varepsilon^{ampl} = \frac{\Delta\, e}{2 \times (1 + e_{init})} \tag{38}$$

Table 29. Calculated f_{ampl} for Norwegian LWA 4-32 materials

Name	Norwegian LWA 4-32 Sample 1	Norwegian LWA 4-32 Sample 2	Norwegian LWA 4-32 Sample 3	Eq.
C_{s}	0.00100	0.00102	0.00150	-
$\Delta\, e$	0.00101	0.00102	0.00150	(37)
ε^{ampl}	0.00034	0.00034	0.00050	(26) (38)
f_{ampl}	11.35	11.49	25.04	(27)

The values of 1.00, 1.47 and 1.00 are adopted for the functions of f_{e} , f_{p} and f_Y as shown in Table 30, Table 31 and Table 32, respectively. Two constants, C_{p} and C_Y, for sandy materials tested by Wichtmann et al., (2005) are used for Leca LWA because the received data is incapable of producing values for the constants. The constant C_{e} has a value of 0.54 provided by Wichtmann et al., (2005) for a sandy material which has higher e-related (e, e_{ref}, e_{min}) values. This C_{e} value was not adopted because it produced incorrect accumulation rates for Leca LWA. Therefore, a suitable value of 0.43 is adopted for at least ensuring a reasonable accumulation rate.

The accumulation rate ($\dot{\boldsymbol{\varepsilon}}^{\mathbf{acc}}$) for Leca LWA under a large number of cycles can be computed using Eq.(21). Since the oedometer test only allows vertical movements, the direction of accumulation ($\mathbf{m}$) points downward vertically for Leca LWA.

Table 33 shows C_{N1}, C_{N2} and C_{N3} values for replicating the accumulation rate of Fin LWA 4-32 samples. Table 34 presents the calculated $\dot{f}_N$ and $\dot{\boldsymbol{\varepsilon}}^{\mathbf{acc}}$ with respect of number of cycles (N) using Eq.(30) and Eq.(22). The replicated curve together with 2 samples are shown in Figure 24.

The uncertainties of these values of will be evaluated in Section 4.4.

Table 30. Calculated f_e for Leca LWA 4-32

Name	Value	Note
f_{e}	1.00	Calculated by Eq. (31)
C_{e}	0.43	A suitable value
e	0.50	e_0
e_{ref}	0.50	$e_{ref} = e_{max}$ (Wichtmann et al., 2005)

Table 31. Calculated f_p for Leca LWA 4-32

Name	Value	Note
f_p	1.47	Calculated by Eq. (32)
C_p	0.43	Wichtmann et al., (2005)
p^{av}	10	Assumed the sample was under iso-tropic stresses
p^{ref}	100	$p^{ref} = p^{atm} = 100kPa$ (Wichtmann et al., 2005)

Table 32. Calculated f_Y for Leca LWA 4-32

Name	Value	Note
f_Y	1.00	Calculated by Eq. (33)
C_Y	2.00	Wichtmann et al., (2005)
$\bar{Y}^{av}$	0	Calculated by Eq. (34)
η	0	Assumed the sample was under iso-tropic stresses

Table 33. Replicated C_{N1}, C_{N2} and C_{N3} for Leca LWA 4-32

Name	Value	Note
C_{N1}	0.00205	Replicated by Eq. (30)
C_{N2}	0.00150	
C_{N3}	0.01400	

Table 34. Calculated for $\dot{f}_N$ and $\dot{\varepsilon}^{acc}$ for Leca LWA 4-32

N	$\dot{f}_N$	$\dot{\varepsilon}^{acc}$ (%)
0	0.0000	0.0000
100	0.0019	0.0325
10000	0.0104	0.1751
30000	0.0126	0.2131
100000	0.0151	0.2548
300000	0.0173	0.2928
700000	0.0190	0.3222
1500000	0.0206	0.3486
2000000	0.0212	0.3586
3000000	0.0220	0.3727

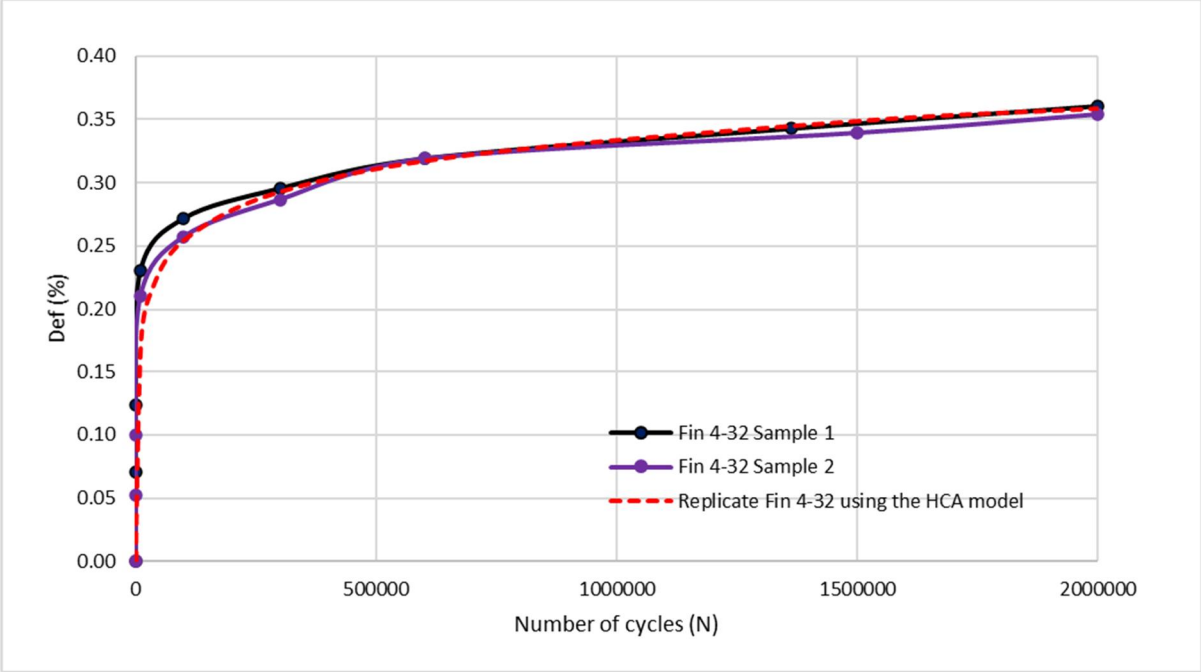

Figure 24. Replication of Fin 4-32 samples by using the HCA model

4.3 Application of PLAXIS soft soil model to high-cycle train load

Plastic (residual) strain accumulates due to cyclic loading caused by trains. On the other hand, the Plaxis SSC-model is capable of computing strain / displacement increment in terms of time with the input of creep index. Since the mechanism of increasing plastic strain is the same between these two cases, this section studies the possibility of correlating the plastic strain increment due to number of load cycles and due to time.

Since the replicated curve of Leca LWA using the HCA model in the earlier section 4.2.4 had different conditions, e.g., strain amplitude and stresses, than that of in construction sites which will be simulated using Plaxis, some adjustments in the HCA model are required for validating the Plaxis simulations.

4.3.1 PLAXIS simulations

Since the parameters of λ^*, κ^* and μ^* of Plaxis SSC model can correlate to the compression index, the swelling index and the creep index, the oedometer test results (Figure 19) are used for interpreting these indices for Leca LWA.

Unloading-reloading tests were not included in the previous oedometer tests as shown in Figure 19, therefore, it is assumed that the swelling index (C_s) is the slope between the first two vertical stresses points (7.91 kPa and 32.91 kPa) in Figure 20. The compression index (C_c) is the slope between the third last and last points (252.91 kPa and 402.91 kPa) in Figure 20. Table 35 summarized C_c and C_s for Norwegian LWA 4-32 materials.

Table 35. C_c and C_s for Norwegian LWA 4-32 materials

Name	Norwegian LWA 4-32 Sample 1	Norwegian LWA 4-32 Sample 2	Norwegian LWA 4-32 Sample 3
C_c	0.0714	0.0894	0.1032
C_s	0.00100	0.00102	0.00150

Norwegian LWA 4-32 sample 2 has the median value among the three tests, therefore, its C_c and C_s are used for calculating λ^* and κ^* as shown in Eq.(39) and Eq.(40). The value of μ^* is assumed to be half of κ^*. Table 36 presented the parameters for Leca LWA using Plaxis SSC model.

$$\lambda^* = \frac{C_c}{2.3(1+e_{init})} = \frac{0.0894}{2.3(1+0.5)} = 0.0259 \quad (39)$$

$$\kappa^* \approx \frac{2C_s}{2.3(1+e_{init})} \approx \frac{2\times 0.00102}{2.3(1+0.5)} = 0.000589 \quad (40)$$

Table 36. SSC-model parameters for Leca LWA

Parameters	γ_{unsat}	γ_{sat}	c'	ϕ'	ψ	λ^*	κ^*	μ^*	ν_{ur}	$k_x = k_y$
Unit	kN/m^3	kN/m^3	kPa	°	°	-	-	-	-	m/day
Leca® LWA	6	10	1	36	0	0.0259	5.89E-4	2.95E-4	0.2	8.64

The Plaxis SoilTest option can simulate basic soil lab tests, such as Triaxial, Oedometer, and DSS. The function of Oedometer is used for Leca LWA (Table 36) with the same load steps as given by Figure 19(a). The simulation results are presented in Figure 25, which vertical reconsolidation pressures (p') of 220 kPa, 245 kPa and 200 kPa are used for replicating the oedometer results of Norwegian LWA 4-32 sample 1, sample 2, and sample 3, respectively. The median value of p', 220 kPa, will be used as the pre-overburden pressure (POP) for Leca LWA layers.

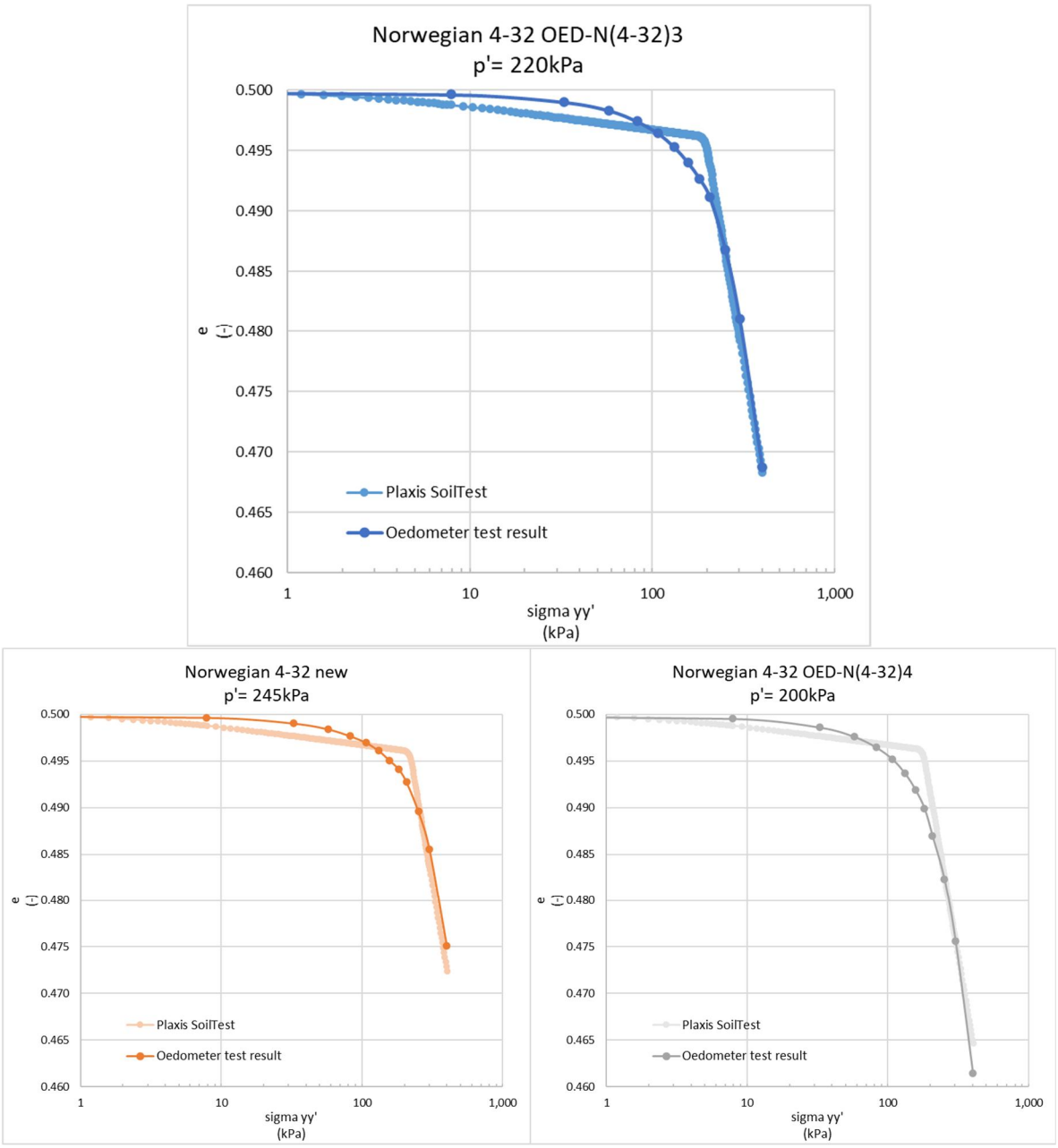

Figure 25. Simulation of the oedometer test results by using Plaxis SoilTest

Table 37 summarize the dimensions of the model for computing displacements induced by cyclic loading in Leca LWA layer, and Figure 26 presents the model in Plaxis. The ballast, subballast and extra subballast layers use the HS-model and their parameters are presented in Table 19. The Leca LWA layer use the SSC-model (Table 36) with the pre-overburden pressure (POP) of 220 kPa. The subgrade for this model adopts dense gravel, and its parameters is shown in Table 23. Dense gravel has stiff properties which make most of displacements induced by cyclic loading occur in Leca LWA layers.

Table 37. Dimensions of the model for cyclic loading

Components	Dimensions
Width of railway sleepers	2.6 m
Ballast layer	0.55 m
Subballast layer	0.3 m
Extra subballast layer	0.3 m
Leca LWA layer	3.0 m

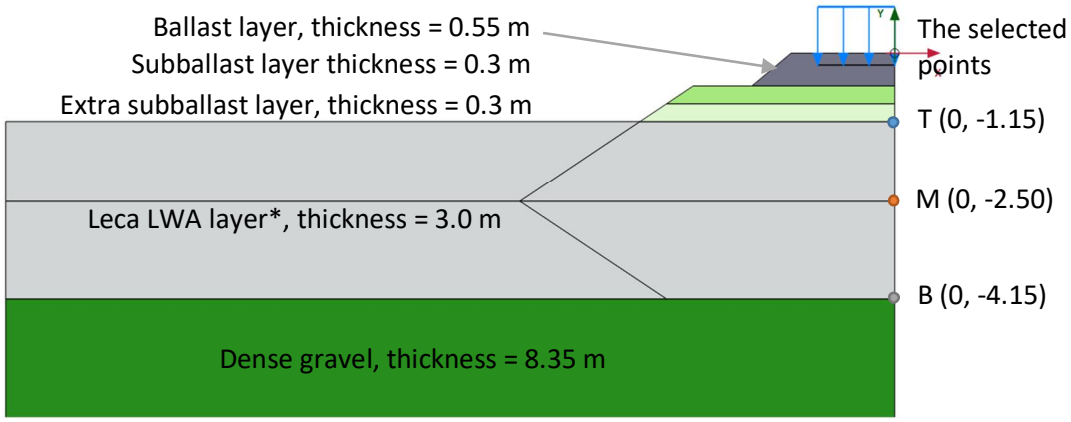

*Figure 26. The cross section for cyclic loading analysis. *This approach of modelling Leca LWA (without proper excavations) must ensure the sufficient embankment stability.*

As for loads, which are modelled for computing displacement induced by cyclic loading, they can be referred to Table 5. The line load (q_{vk}) of 80 kN/m with an additional load increment (Δq_{vk}) of 76 kN/m are corresponding to the axle loads of 22.5 tons. Since the railway sleeper has a width of 2.6 m, the uniformly distributed load of 75 kN/m^2 is modelled at the depth of 200 mm below the track in the Plaxis simulation. The calculation is shown in Eq. (41), which also includes the impulse factor (ϕ_v) of 1.25 for designing new tracks.

$$q_{LM71-22.5\,t} = \frac{(q_{vk} + \Delta q_{vk})\,\phi_v}{L} = \frac{(80+76)\times 1.25}{2.6} = 75\ kN/m^2 \qquad (41)$$

The mesh option of very fine was used, and a coarseness factor of 0.5 is applied to Leca LWA layers. A water table was assigned to be far away below the ground surface for all calculations. Five construction stages were involved as presented in Table 38 and Figure 41.

The POP of 220 kPa can only be generated in Leca LWA layers when the initial stress is calculated by using K_0 procedure at the initial phase (stage 1). Therefore, Leca LWA layers are activated together with the subgrade at the initial phase. The ballast, subballast, and extra subballast layers are then activated at the stage 2.

Table 38. Staged construction for cyclic loading analysis

	Stage	Calculation type	Note
1	Initial phase	Plastic, K_0 procedure	Leca LWA POP = 220kPa
2	Build the whole embankment	Plastic	
3	Loading	Plastic	for computing resilient strain
4	Unloading	Plastic	
5	Cyclic loading	Consolidation, t = 10000d	for computing accumulated residual strain in terms of time

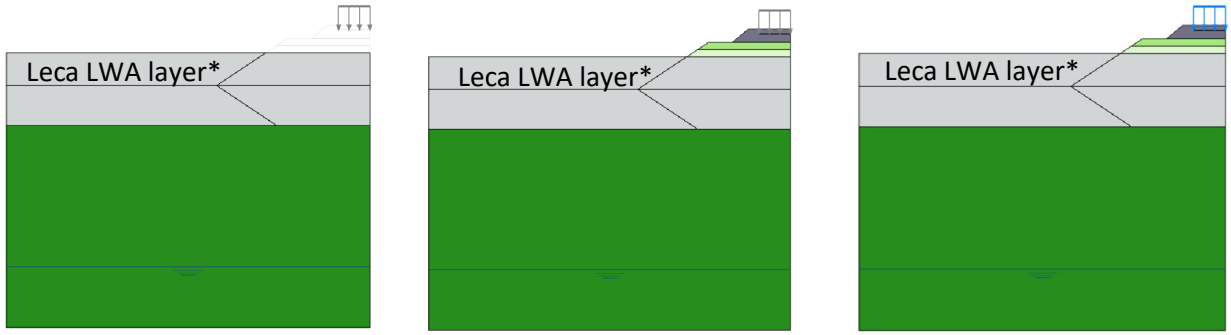

*Figure 27. Pictures of staged construction. *This approach of modelling Leca LWA (without proper excavations) must ensure the sufficient embankment stability.*

Figure 28 shows the deformed mesh at stage 6. Figure 29 and Figure 30 show the pictures of effective vertical stress distribution ($\sigma_{yy'}$) in railway embankments at stage 3 and 4. Figure 31 presents the analysis results of accumulated vertical strain in terms of time. Figure 32 presents the analysis results of vertical displacement in terms of time. Three points on the top, middle and bottom of Leca at the central line are selected for plotting this graph, which are (0, -1.15), (0. -2.50) and (0, -4.15).

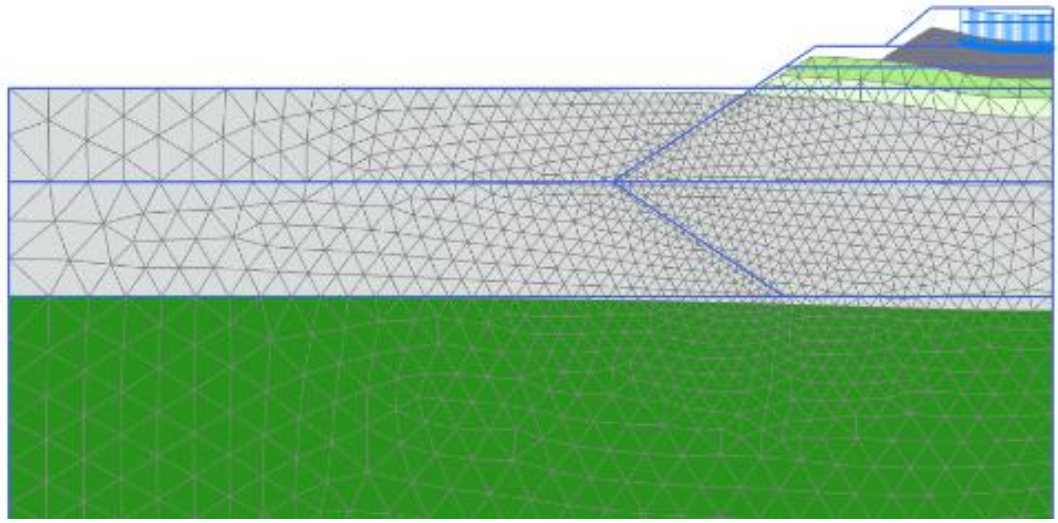

Figure 28. Deformed mesh at stage 5 cyclic loading

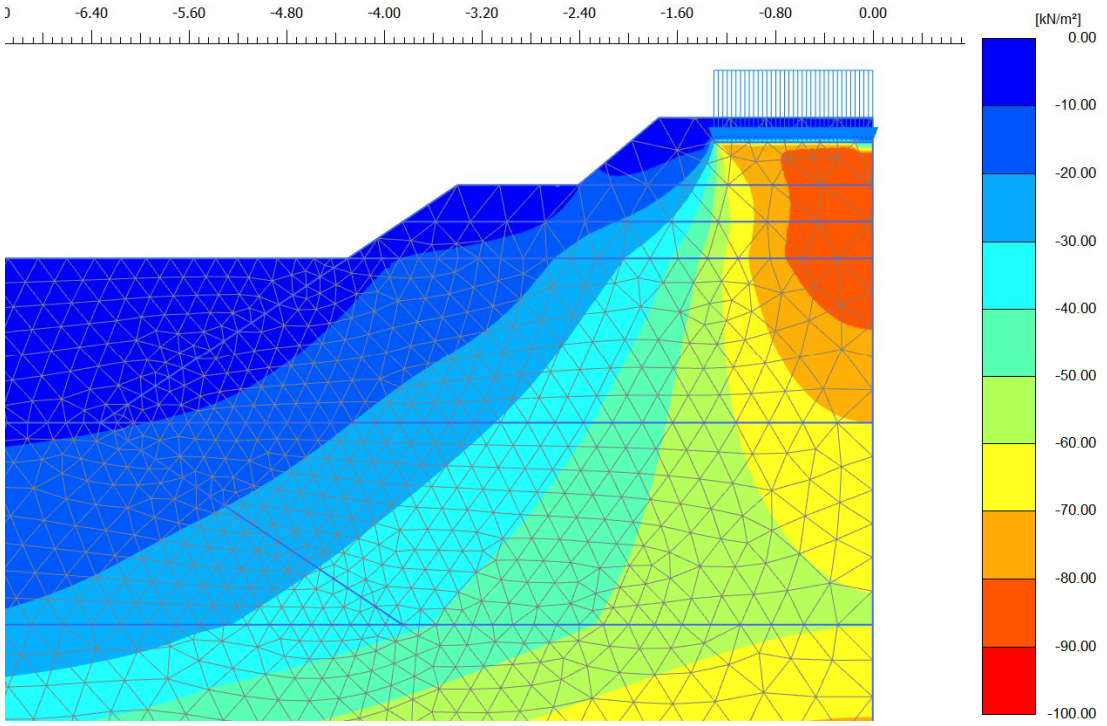

Figure 29. σ_{yy}' at stage 3 loading

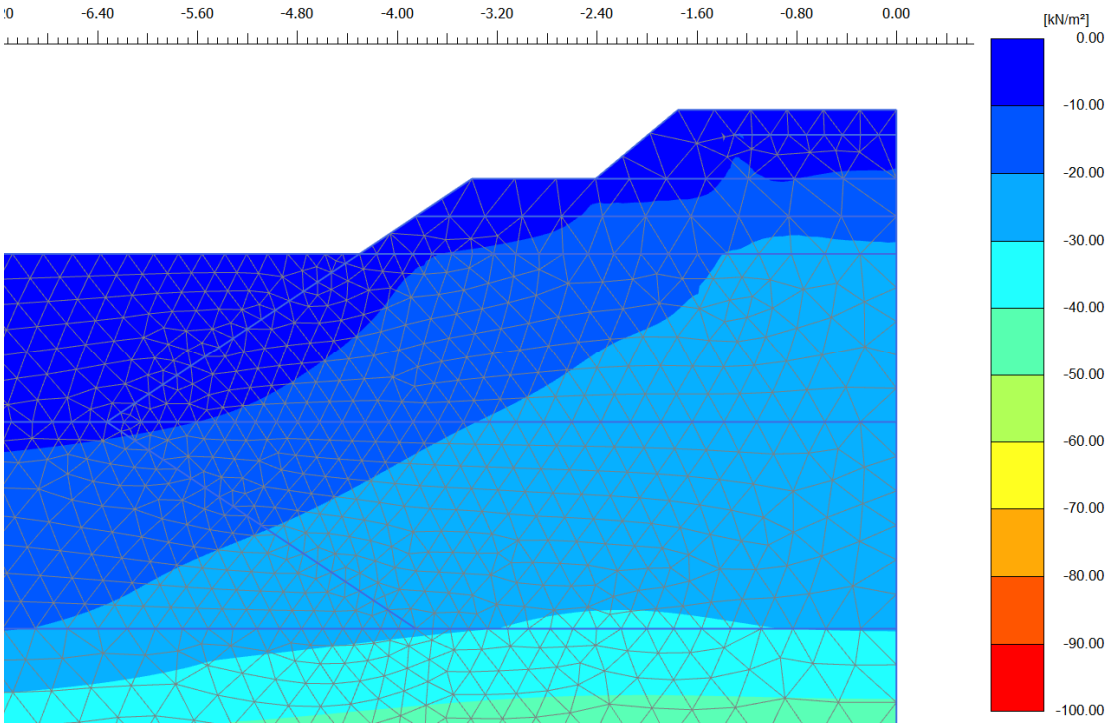

Figure 30. σ_{yy}' at stage 4 unloading

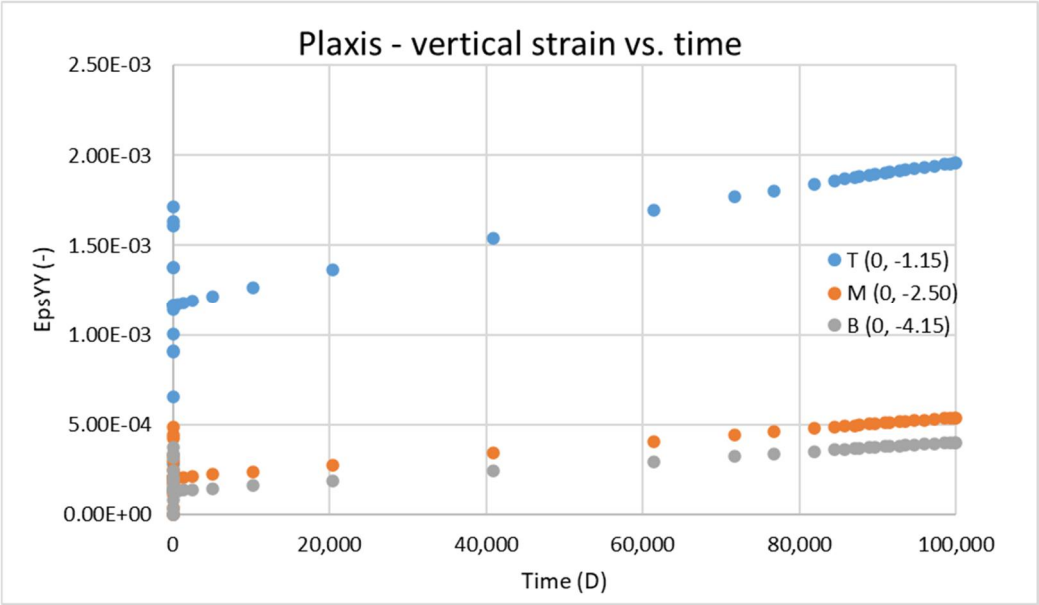

Figure 31. Leca LWA – vertical strain vs. time

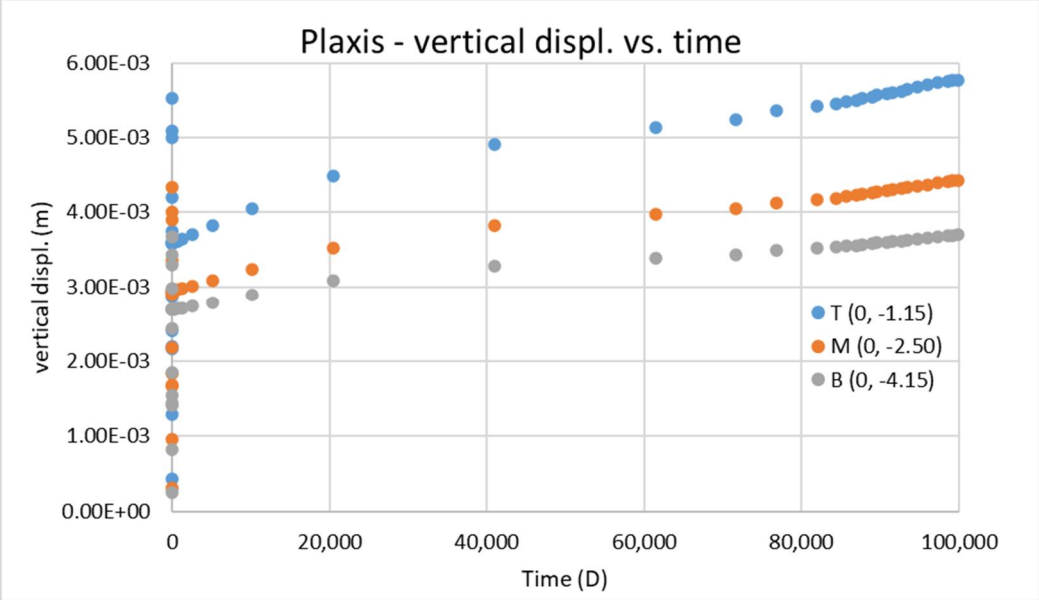

Figure 32. Leca LWA – vertical displacement vs. time

4.3.2 Validation of Plaxis simulations using the HCA model

Section 4.2.4 shows the replicated curve of accumulated strain over the number of cycles in Fin LWA 4-32 by using the HCA model. However, the given conditions, e.g., strain amplitude and stresses, of laboratory tests are different than that of in construction sites. Consequently, some adjustments in the HCA model are required for validating the Plaxis simulations.

Since Leca LWA materials experience different mean stresses and loads in the Plaxis simulations than in cyclic compression tests, the functions of f_{ampl} and f_p are recalculated as presented in Table 39 and Table 40.

The ε_{max} and ε_{min} of the three selected points are read from Plaxis outputs at the stage of loading and unloading (Table 38), respectively. The ε^{ampl} and f_{ampl} are therefore calculated by using Eq.(26) an Eq.(27). The p^{av} of the three points are read from Plaxis outputs at the stage of loading, and the function of f_p is computed using Eq.(32).

The functions of f_{e} and f_Y remain the same values of 1.0 as the cyclic compression tests (Table 30 and Table 32). The function of $\dot{f}_N$ controls $\dot{\varepsilon}^{acc}$ which accumulates with the increasing number of cycles. The values used for this function is presented in Table 34 with corresponding number of cycles.

With the values of f_{ampl} , f_p , f_{e} , f_Y and $\dot{f}_N$, the vertical strain accumulation due to number of cycles at the three selected points can therefore be estimated by using Eq.(22) as presented in Figure 33.

Table 39. f_{ampl} for the selected stress points

Name	T (0, -1.15)	M (0, -2.50)	B (0, -4.15)
ε_{max}	1.766E-3	0.492E-3	0.375E-3
ε_{min}	1.209E-3	0.206E-3	0.130E-4
ε^{ampl}	2.785E-4	1.430E-4	1.225E-4
f_{ampl}	7.76	2.04	1.50

Table 40. f_p for the selected stress points

Name	T (0, -1.15)	M (0, -2.50)	B (0, -4.15)
p^{av}	46.22kPa	53.49kPa	41.57kPa
p^{ref}	100	100	100
C_p	0.43	0.43	0.43
f_p	1.26	1.22	1.29

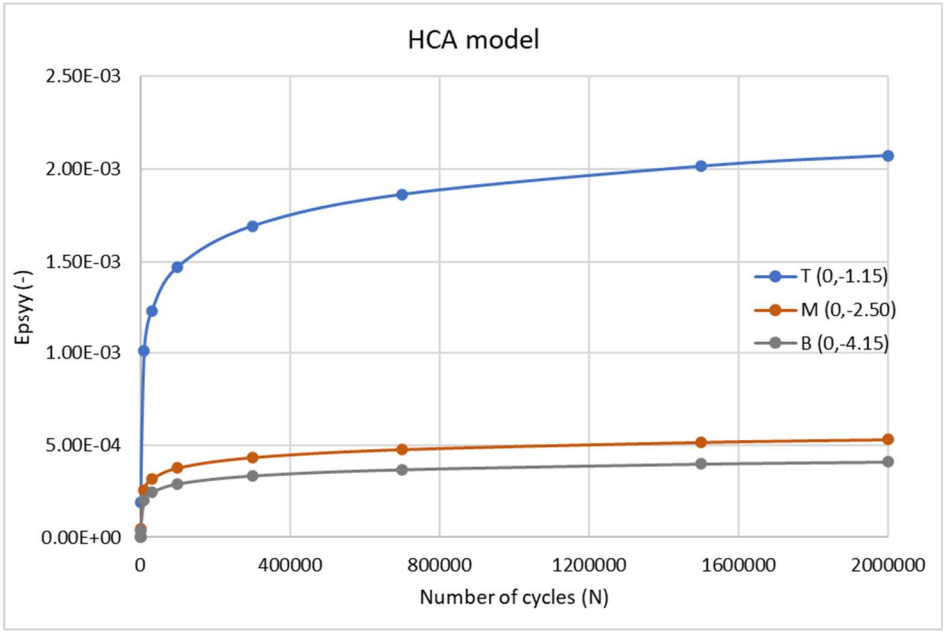

Figure 33. Leca LWA - vertical strain vs. number of cycles

Figure 34 merges Figure 31 and Figure 33 in order to show the correlation between number of cycles (N) and time (D). The magnitude of vertical strain (Epsyy) are close, however, the accumulation curve of HCA model has a more logarithmic relation than that of Plaxis simulations. The possible reasons will be further discussed in Section 4.4.

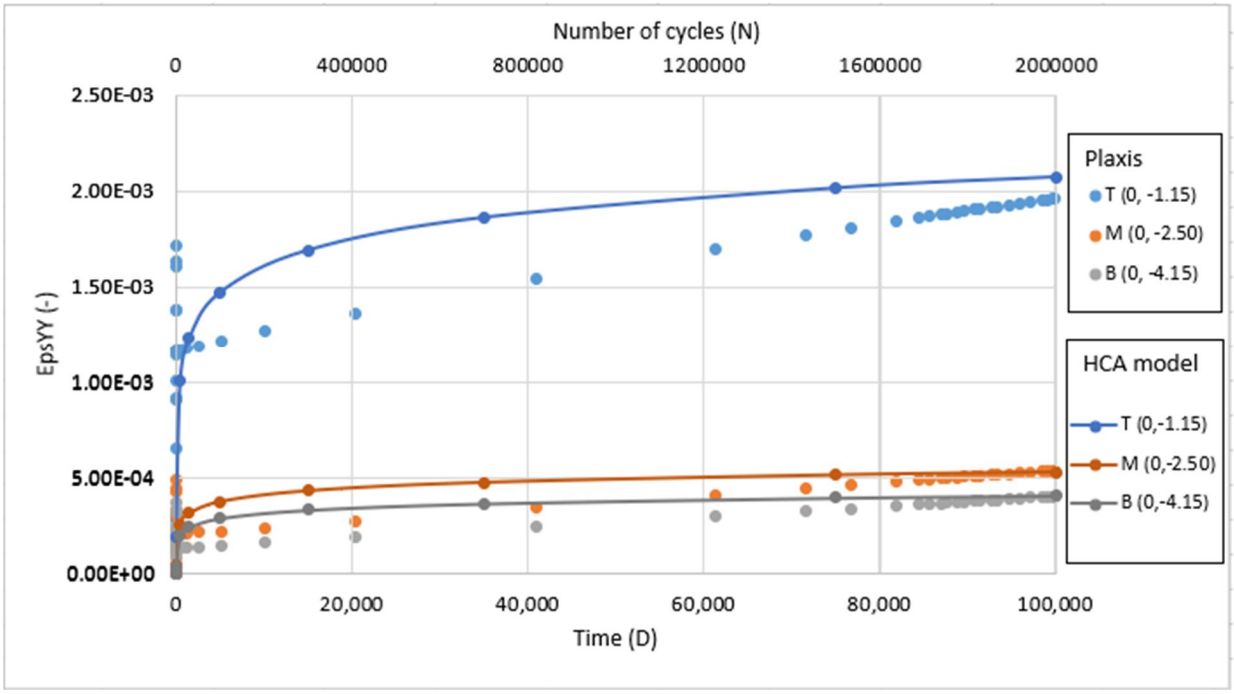

Figure 34. Leca LWA - the vertical strain correlation between number of cycles (N) and Time (D)

4.3.3 The correlation between number of cycles and time

As seen in Figure 35, subgrade response to moving loads, one cycle can be either generated by 2 or 4 axle loads depending on the spacing of adjacent axle loads. The earth pressure on the left side of Figure 35 was measure at the depth of 0.7 m.

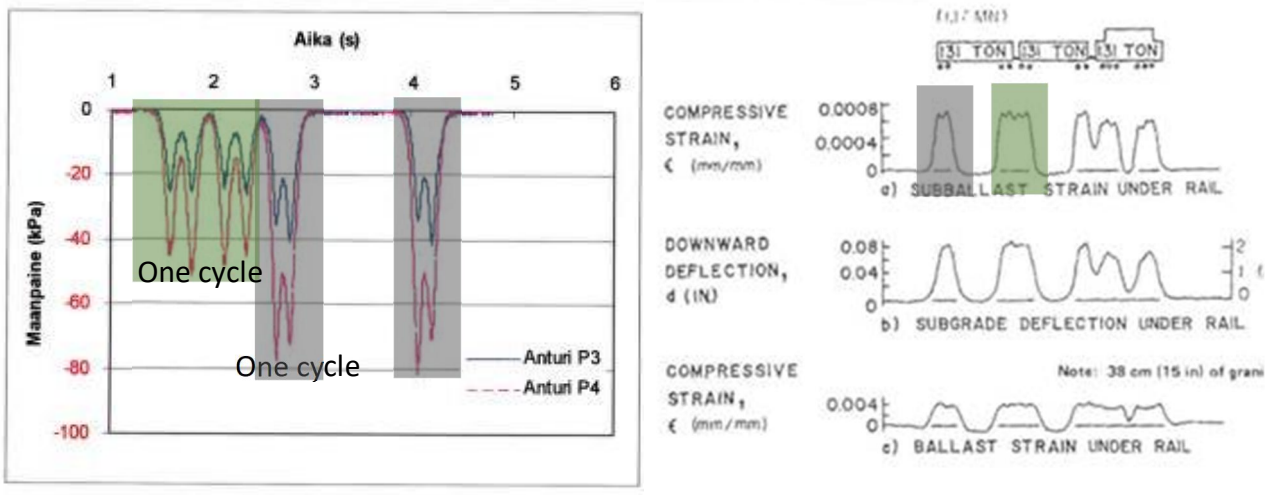

Figure 35. Subgrade response to moving loads with two examples (Nurmikolu, 2004)

Annual gross tons for different railway routes in 2019 are reported by Väylävirasto (Appendix B). Few routes are selected for studying as presented in Table 41.

Nurmikolu (2004) reported that 3 million cycles can be approximated to represent 150 million tons railway track load when using two adjacent 250 kN axle loads as one cycle. Therefore, the number of cycles per year for the selected route can be estimated by using the same approximation. The estimated number of cycles per track per year and per track per decade and the correlated time in Plaxis using Figure 34 are shown in Table 41 for each railway track section.Table 42 presents the accumulated vertical strain (Epsyy) and the accumulated vertical displacement ($|u_y|$) for each railway section at the three selected points in Leca LWA layers. These values are based on the estimated number of cycles per track per decade, and their corresponding time in Plaxis per track per decade (Table 41), and they are read from the results of Plaxis simulations (Figure 31 and Figure 32). Furthermore, these values are only counted in the construction stage of cyclic loading (Table 38). In other words, the values accumulated before the final stage (cyclic loading) are excluded.

Table 41. Railway track sections with their corresponding traffic (Väylävirasto, 2019) and estimated number of cycles

Railway track section	Gross tons per year (data from Väylävirasto)	Number of tracks	Estimated number of cycles* per track/ per year	Estimated number of cycles* per track/ per decade	Converted to time in Plaxis per track/ per decade
	million	-	million	million	day
Lahti – Kouvola	17.2	2	0.17	1.7	85000
Seinäjoki – Pännäinen	7.8	1	0.16	1.6	80000
Turku – Toijala	3.9	1	0.08	0.8	40000

*two adjacent 250 kN axle loads generate one cycle

Table 42. The values of Epsyy and |uy| at the selected points for each railway track section

Railway track section	Estimated number of cycles* per track/ per decade	The selected points					
		T (0, -1.15)		M (0, -2.5)		B (0, -4.15)	
		Epsyy	$\|u_y\|$	Epsyy	$\|u_y\|$	Epsyy	$\|u_y\|$
	million	-	mm	-	mm	-	mm
Lahti – Kouvola	1.7	1.89E-3	1.85	4.80E-4	1.23	5.00E-4	0.82
Seinäjoki – Pännäinen	1.6	1.81E-3	1.72	3.50E-4	1.18	3.80E-4	0.78
Turku – Toijala	0.8	1.55E-3	0.85	3.20E-4	0.57	2.20E-4	0.37

*two adjacent 250 kN axle loads generate one cycle

4.4 Evaluation

The purpose of using the HCA model is to predict plastic deformation in cohesionless soils due to high cyclic loading. This model was developed based on a series of cyclic triaxial tests on sub-granular sand, and a list of material constants ($C_{N1}, C_{N2}, C_{N3}, C_e, C_p, C_Y$) for the tested sand were provided by Wichtmann et al., (2005). Instead of cyclic triaxial tests, the cyclic compression tests were used to demonstrate the accumulating plastic strain due to large number of cycles for Leca LWA materials. Therefore, some material constants (C_p, C_Y) were unable to acquire for the studied material, and consequently the values provided by Wichtmann et al., (2005) were used. Moreover, a suitable value of C_e was used for ensuring a reasonable accumulation rate because the range between e_{max} and e_{min} for Leca LWA materials are narrower than the tested sand. The range for Leca LWA materials falls between 0.50 and 0.45, while the range for the tested sand falls between 0.856 and 0.495. However, the value of C_e did not affect the value of f_e because e_{init} was assumed to be e_{max}, which equals to 0.50 for Leca LWA materials. Regardless of the value of C_e, the f_e has a value of 1.0. The above-mentioned factors are the causes of deviations for replicating the accumulation curve because Leca LWA and sand are eventually not the same material.

Minimum three series of cyclic triaxial tests are required for determining material constants (Wichtmann et al., 2010):

- C_e : a series with different initial densities under constant p^{av} and q^{ampl} (Figure 36b)
- C_p : a series with a variation of p^{av} under constant η^{av} and initial densities (Figure 36c)
- C_Y: a series with a variation of η^{av} under constant p^{av}, q^{ampl} and initial densities (Figure 36d)

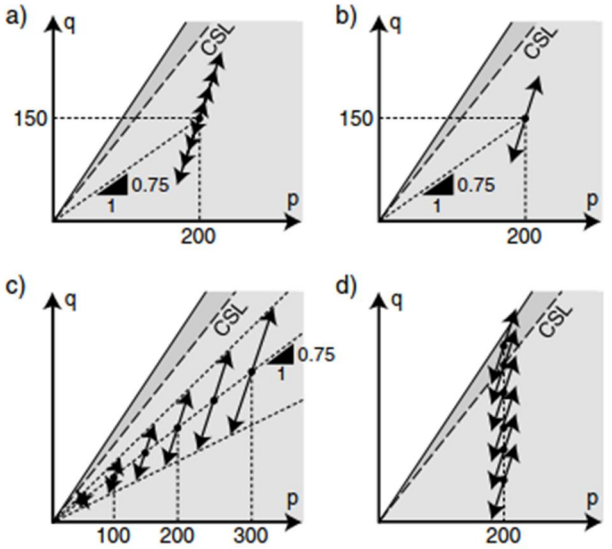

Figure 36. Potential stress paths in the cyclic triaxial tests for determining material constants (Wichtmann et al., 2010)

Watn et al., (2004) and Watn, (n.d.) reported that compaction can cause a reduction of 10-12% in volume for LWA materials and the maximum contact pressure of 50 kPa is

recommend if a caterpillar is used for compaction. The compaction shall be carried out every 0.6m in thickness at maximum or 0.4 m thick at maximum if a LWA layer is closed to structures. The pre-consolidation pressure (p') of 220 kPa in oedometer tests for Leca LWA materials was adopted as the pre-overburden pressure (POP) in the Plaxis simulation. It is assumed that Leca LWA reached the same state as in the cyclic compression tests.

As shown in Figure 34, the accumulation rate between using the Plaxis simulations and the HCA models are different, although they have similar magnitudes in terms of vertical strains. The accumulated curves computed by Plaxis are in a linear relation, while the curves reproduced by the HCA model are in a logarithmic relation. The volumetric creep strain ($\dot{\varepsilon}_v^c$) is given by Eq.(13) when using Plaxis SSC-model. Since the cyclic loading cause by moving trains does not exceed the plastic point, the repetitive loading and unloading remain on the recompression line. Thus, the value of p_p^{eq} is constant throughout the given time interval and consequently, the value of $\left(p^{eq}/p_p^{eq}\right)$ stays smaller than 1.0 all the time. Moreover, the value of μ^* is extremely small for Leca LWA materials, which has minimal effects in terms of changing the accumulation rate in time. Consequently, a linear relationship between vertical strain / deformation and time can be overserved in the Plaxis simulations. On the other hand, the value of $\left(p^{eq}/p_p^{eq}\right)$ in the beginning of time interval can be smaller, equal and larger than 1.0 for soft clay. During the consolidation process, the value of $\left(p^{eq}/p_p^{eq}\right)$ becomes smaller and smaller over time. Thus, a logarithmic relation between vertical strain / deformation and time can be overserved when using the parameters for soft soil. Additionally, the value of μ^* is relatively large which can influence the accumulation rate in time.

5 Analysis and result discussion

To verify sufficient bearing capacity at the top of subballast layers when using Leca LWA with different cover depths, Section 5.1 uses the Odemark method for calculating the bearing capacity at the top of the subballast layer. The calculations are based on subgrade classifications and extra subballast layer consisting three different Odemark E-moduli. Section 5.2 reports the results of embankment stability analyses using Plaxis. The simulations vary the thickness of the extra subballast layers and Leca LWA layers in order to determine the optimal location for Leca LWA in railway embankments. To identify the effect of cyclic loading on Leca LWA, Section 5.3 uses Plaxis to analyze the displacement induced by cyclic loading using Plaxis. The simulation varies the cover depth and thickness of Leca LWA layers. Additionally, the elastic displacement in the Leca LWA layers are calculated using three different subgrades, which are included to obtain baseline values for the magnitudes of the elastic displacement and the plastic displacement induced by cyclic loading in Leca LWA layers. Section 5.4 answers the research questions which are relevant to this chapter.

5.1 The bearing capacity at the top of the subballast layer

This section answers the research questions Q4 (Section 1.3).

Q4. What is the optimal location for Leca LWA in railway embankments?

The Odemark method is introduced in Section 2.3.2, and this method is used for calculating the bearing capacity at the top of the subballast layer. As mentioned in Section 2.5.4, subgrades can be classified from G to A based on their bearing capacities. Typically, softer subgrades, which have bearing capacity below 20 MPa (subgrade classification G, F and E), may require subgrade soil modification to reduce long-term settlement. In such situations, Leca LWA can be formed as part of the railway embankment and can also replace part of the subgrade.

Figure 37 presents the bearing capacity at the top of subballast layer with different thickness of Leca LWA layers. A 300-mm extra subballast layer with an Odemark E-modulus of 300 MPa is constructed above Leca LWA layers. The bearing capacity at the top of the subballast layer is increased by 10 MPa when the thickness of Leca LWA layers is increased from 1.0 m to 3.0 m on the soft subgrade with an Odemark E-modulus of 5 MPa (subgrade classification G). The difference in bearing capacity between these two thicknesses become smaller with increasing subgrade bearing capacities. It can be concluded that the thickness of Leca LWA layers has less influence on the bearing capacity at the top of the subballast layers. This can due to the total height of the embankment is relatively high. Since the thickness of Leca LWA layers do not affect the bearing capacity at the top of the subballast layer significantly, a 1.0-m thick Leca LWA layer will be adopted for the following two figures.

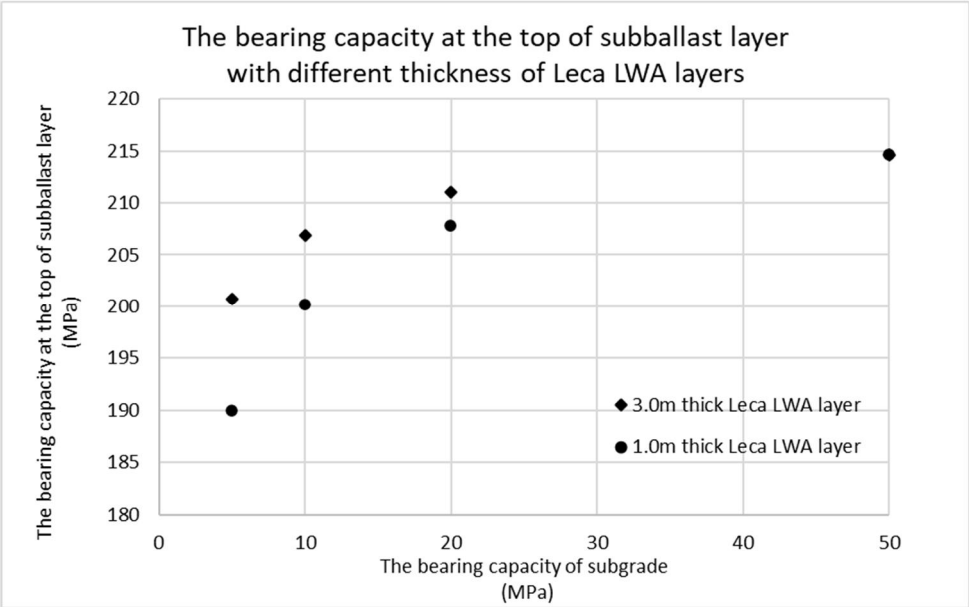

Figure 37. The bearing capacity on the top of subballast layer vs the thickness of 1.0m and 3.0m Leca LWA layers using the Odemark method (Extra subballast layer has on Odemark E-modulus of 300 MPa)

Figure 38 presents the minimum required thickness of extra subballast layer to fulfill 180 MPa bearing capacity at the top of subballast layer. Three Odemark E-moduli (300 MPa, 200 MPa and 150 MPa) are adopted for the extra subballast layer. The Leca LWA layers have a fixed thickness of 1.0 m. Overall, the result shows a logarithmic relation, that is, the minimum required thickness of an extra subballast layer only reduced slightly when the bearing capacity of subgrade is increased considerably. Nevertheless, an extra subballast layer is required to construct above a Leca LWA layer in order to provide sufficient bearing capacity at the top of subballast layer.

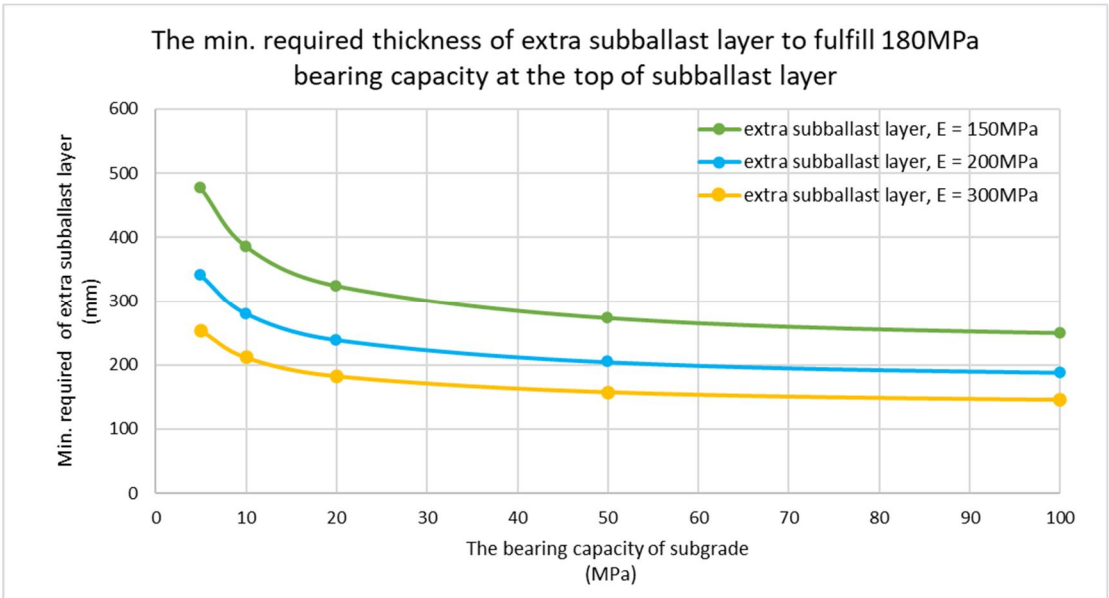

Figure 38. The min. required thickness of extra subballast layer vs. the bearing capacity of subgrade the Odemark method

Figure 39 presents the bearing capacity at the top of subballast layer as a function of extra subballast layer thickness. Three bearing capacities (20 MPa, 10 MPa and 5 MPa) are adopted for subgrades. The Leca LWA layers have a fixed thickness of 1.0 m. An Odemark E-modulus of 300 MPa is used for all cases and this modulus requires that the material of the extra subballast layer to be equivalent to the subballast layer, i.e., crushed rock. Figure 39 shows the values of bearing capacity with respect to various cover depths (various thickness of an extra subballast layer). The result shows that the bearing capacity at the top of the subballast layer do not grow linearly with increasing thickness of the extra subballast layer. Furthermore, the result suggests that a 300-mm thick extra subballast layer is optimal because the minimum required bearing capacity at the top of subballast layer (i.e., 180MPa) can be achieved regardless of the subgrade bearing capacity. The figure provides an answer to the research questions Q4.

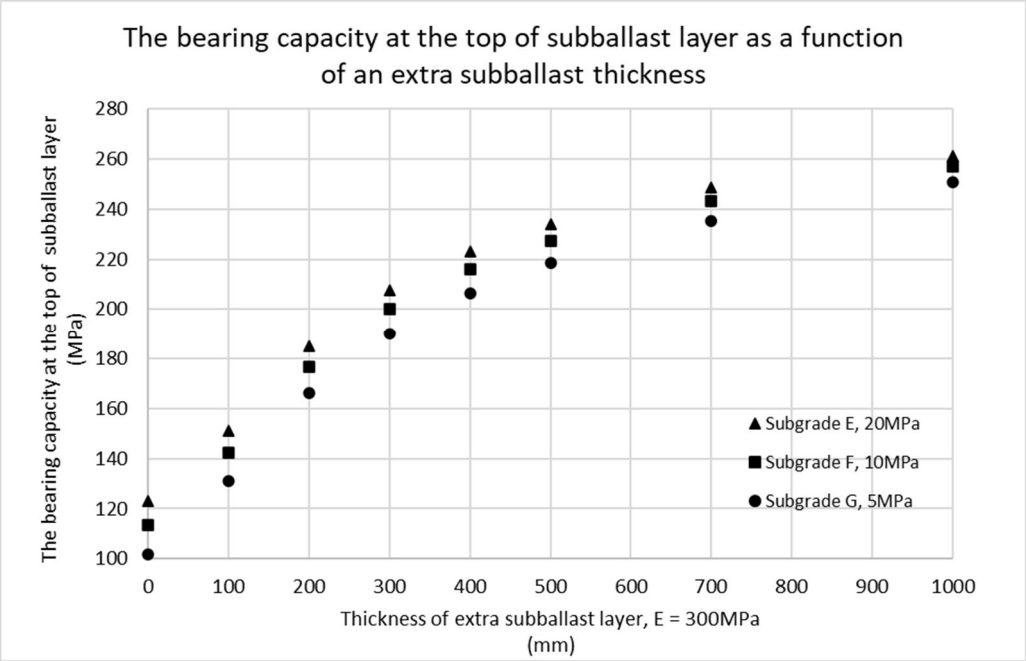

Figure 39. The bearing capacity of ballast layer vs. the thickness of extra subballast layer using the Odemark method

5.2 Embankment stability

This section answers the research question Q4 (Section 1.3).

Q4. What is the optimal location for Leca LWA in railway embankments?

From the perspective of embankment stability, the optimal location for Leca LWA can be determined by varying the thickness of the extra subballast layers and Leca LWA layers. Consequently, the factor of safety for every combination can be evaluated in order to conclude an optimal location for Leca LWA, which guarantee a relatively high factor of safety for railway embankments. Such stability problems can be analyzed by using Plaxis.

The typical cross section (one railway track) for calculating embankment stability is shown in Section 2.5.1. Table 18 summarizes all the variables which are simulated in this section, and an example of cross section which is modelled in Plaxis is shown as in Figure 40. Table 19 presents the HS-model parameters for substructure layers, while the MC-model parameters for subgrade are shown in Table 21.

Since the simulations vary the thickness of the extra subballast layers and Leca LWA layers (in total 52 analyses), Python scripts are written for drawing geometry, assigning soil materials, calculating staged construction, and finally retrieving the results (i.e., factor of safety) automatically. One example of Python scripts is attached in Appendix C.

The embankment stability is a symmetrical problem, therefore, only a half problem is modelled for simplification. One example is modelled for both full and half cases, the results are presented in Appendix D. Additionally, Leca LWA layers do not exposure to air in real situations as presented in Figure 40, instead, Leca LWA layers are typically covered by an another material (e.g., crushed rock or well-compacted sand). However, such layer does not affect the analysis results significantly. Consequently, this layer is not modelled for simplification.

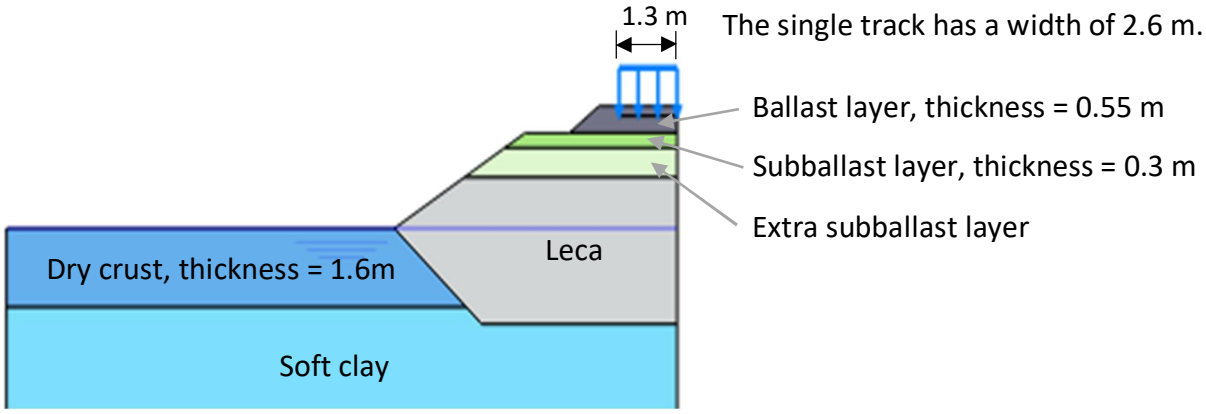

Figure 40. An example of cross section (one track) in Plaxis for embankment stability analysis

Because the extra subballast layers and Leca LWA layers are varying in thickness, the bottom of Leca LWA layers could be located in different layers. Figure 41 presents three scenarios based on their locations:

- Scenario 1 – the bottom of Leca was located at soft clay
- Scenario 2 – the bottom of Leca was located at dry crust
- Scenario 3 – the bottom of Leca was located right above the ground surface

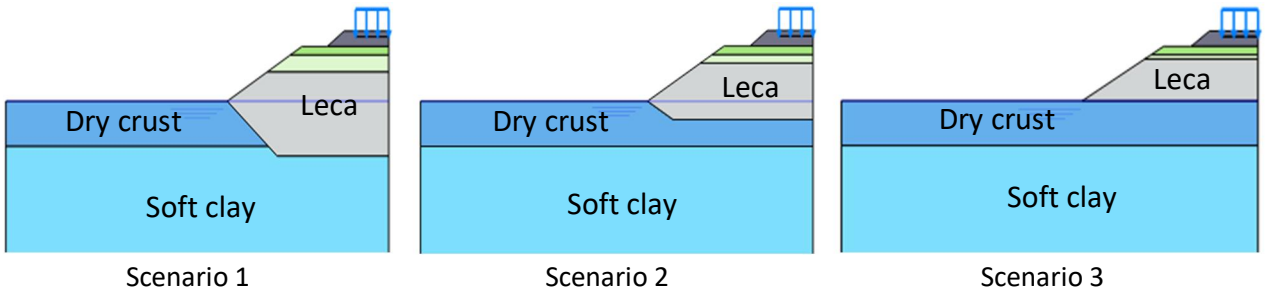

Figure 41. Three scenarios for embankment stability analysis in Plaxis

As for loads, which are modelled for analyzing 2D embankment stability, they can be referred to Table 4. The line loads of 103 kN/m and 119 kN/m were corresponding to the axle loads of 22.5 tons and 25 tons. Since the railway sleeper has a width of 2.6 m, the uniformly distributed load of 39.6 kN/m^2 and 45.8 kN/m^2 are modelled at the depth of 200 mm below the track in the Plaxis simulation.

The mesh size of 0.02 m is generated, and a water table is assigned to be located at the ground surface for all calculations. Three construction stages are involved for analyzing embankment stability. Firstly, an initial phase is active for all soil layers with the calculation type of gravity loading. Secondly, one uniformly distributed load is applied onto an embankment with the calculation type of plastic. Finally, the calculation type of safety is used to examine overall embankment stability for embankments.

Figure 42 shows the analysis results, i.e., factor of safety (FoS), graphically. All the calculations pass the minimum required FoS of 1.0. The legends in blue color represent the embankment height of 1.5 m, while the legends in orange color stands for the embankment height of 2.5 m. The circle and triangle symbols denote for the axle loads of 22.5 tons and 25 tons, respectively. Also, the lighter the legend color, the thinner the Leca LWA layer is.

As shown in Figure 42, the FoS is clearly improved when the thickness of the extra subballast layer increased from 0 to 0.3 m, as marked in grey color. However, the results show no clear indication whether an extra subballast layer helps further in increasing the embankment stability when the thickness of the extra subballast layer exceeds 0.3 m. This result also supports the same optimal location, which is beneath a 300-mm extra subballast layer, for Leca LWA as that of from bearing capacity calculations using the Odemark method (Section 5.1). These figures provide an answer to the research question Q4.

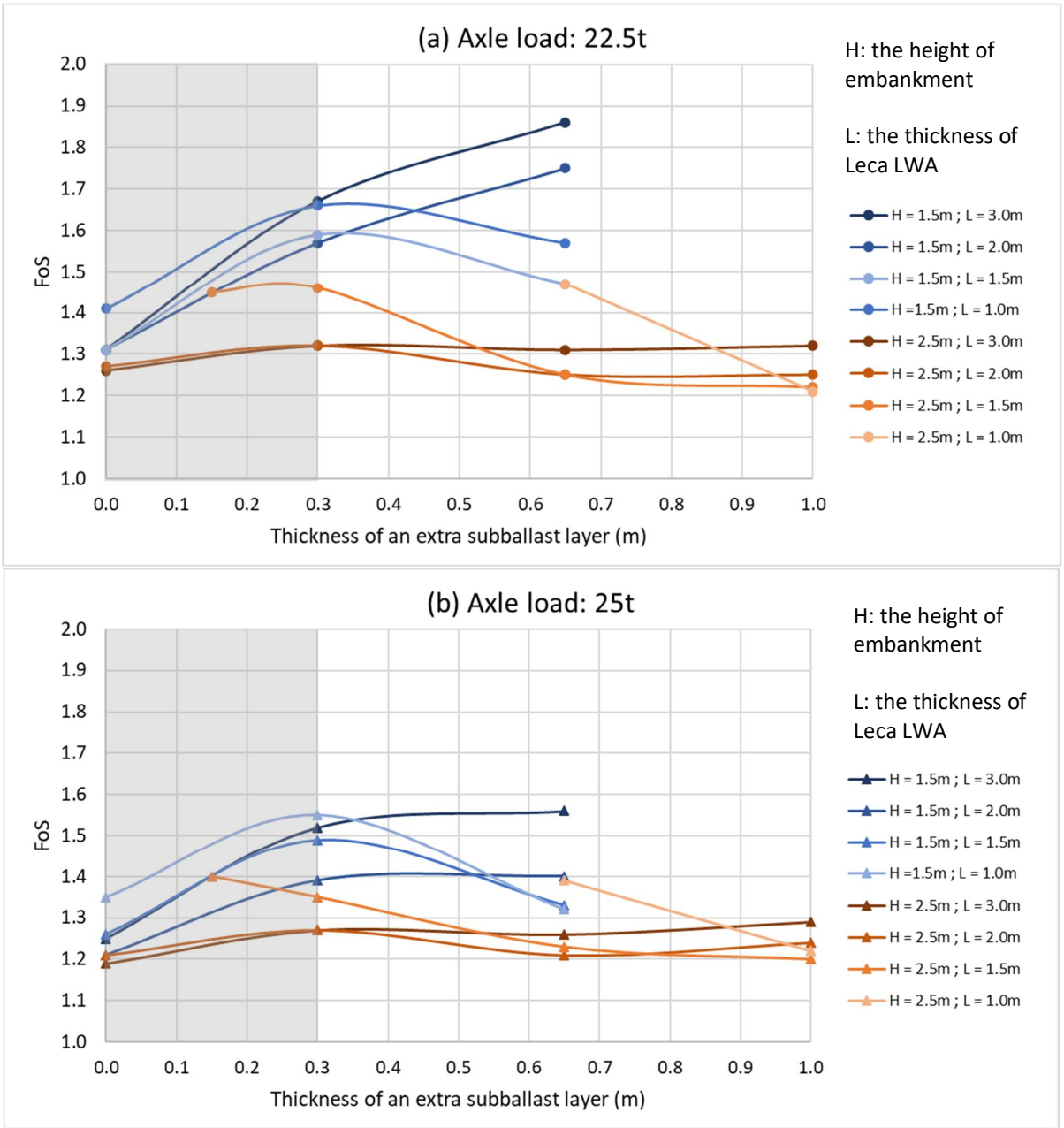

Figure 42. FoS vs. thickness of an extra subballast layer using Plaxis.

The analysis results, i.e., factor of safety (FoS), are numerically presented in Table 43 and Table 44 for the embankment height of 1.5 m and 2.5 m, respectively. These two tables show all the combination of different thickness of extra subballast and Leca LWA layers with respect to the axle loads of 22.5 tons and 25 tons.

Table 43. FoS results for embankment stability analyses (H = 1.5 m) using Plaxis

The height of embankment, H = 1.5 m					
Thickness of Leca	Thickness of extra subballast layer	Total thickness*	Scenario	Axle load 22.5t FoS	Axle load 25t FoS
L (m)	F (m)	T (m)	-	-	-
3	0	3.85	1	1.31	1.25
	0.3	4.15	1	1.67	1.52
	0.65	4.50	1	1.86	1.56
	1	4.85	1	N/A, F is below the ground surface	
2	0	2.85	2	1.31	1.21
	0.3	3.15	1	1.57	1.39
	0.65	3.50	1	1.75	1.40
	1	3.85	1	N/A, F is below the ground surface	
1.5	0	2.35	2	1.31	1.26
	0.3	2.65	2	1.59	1.49
	0.65	3.00	2	1.47	1.33
	1	3.35	1	N/A, F is below the ground surface	
1	0	1.85	2	1.41	1.35
	0.3	2.15	2	1.66	1.55
	0.65	2.50	2	1.57	1.32
	1	2.85	2	N/A, F is below the ground surface	

*The total thickness is a sum of the thickness of a ballast layer, a subballast layer, an extra subballast layer and a Leca LWA layer.

Table 44. FoS results for embankment stability analyses (H = 2.5 m) using Plaxis

The height of embankment, H = 2.5 m					
Thickness of Leca	Thickness of extra subballast layer	Total thickness*	Scenario	Axle load 22.5t FoS	Axle load 25t FoS
L (m)	F (m)	T (m)	-	-	-
3	0	3.85	2	1.26	1.19
	0.3	4.15	1	1.32	1.27
	0.65	4.50	1	1.31	1.26
	1	4.85	1	1.32	1.29
2	0	2.85	2	1.27	1.21
	0.3	3.15	2	1.32	1.27
	0.65	3.50	2	1.25	1.21
	1	3.85	2	1.25	1.24
1.5	0.15	2.50	3	1.45	1.40
	0.3	2.65	2	1.46	1.35
	0.65	3.00	2	1.25	1.23
	1	3.35	2	1.22	1.20
1	0.3	2.15	3	N/A, L≠1	
	0.65	2.50	3	1.47	1.39
	1	2.85	2	1.21	1.22

*The total thickness is a sum of the thickness of a ballast layer, a subballast layer, an extra subballast layer and a Leca LWA layer.

Depending on where the bottom of Leca LWA is located (refer to the scenarios in Figure 41), the analysis results can further be classified as shown in Figure 43. The scenarios without any extra subballast layer are excluded for clarity.

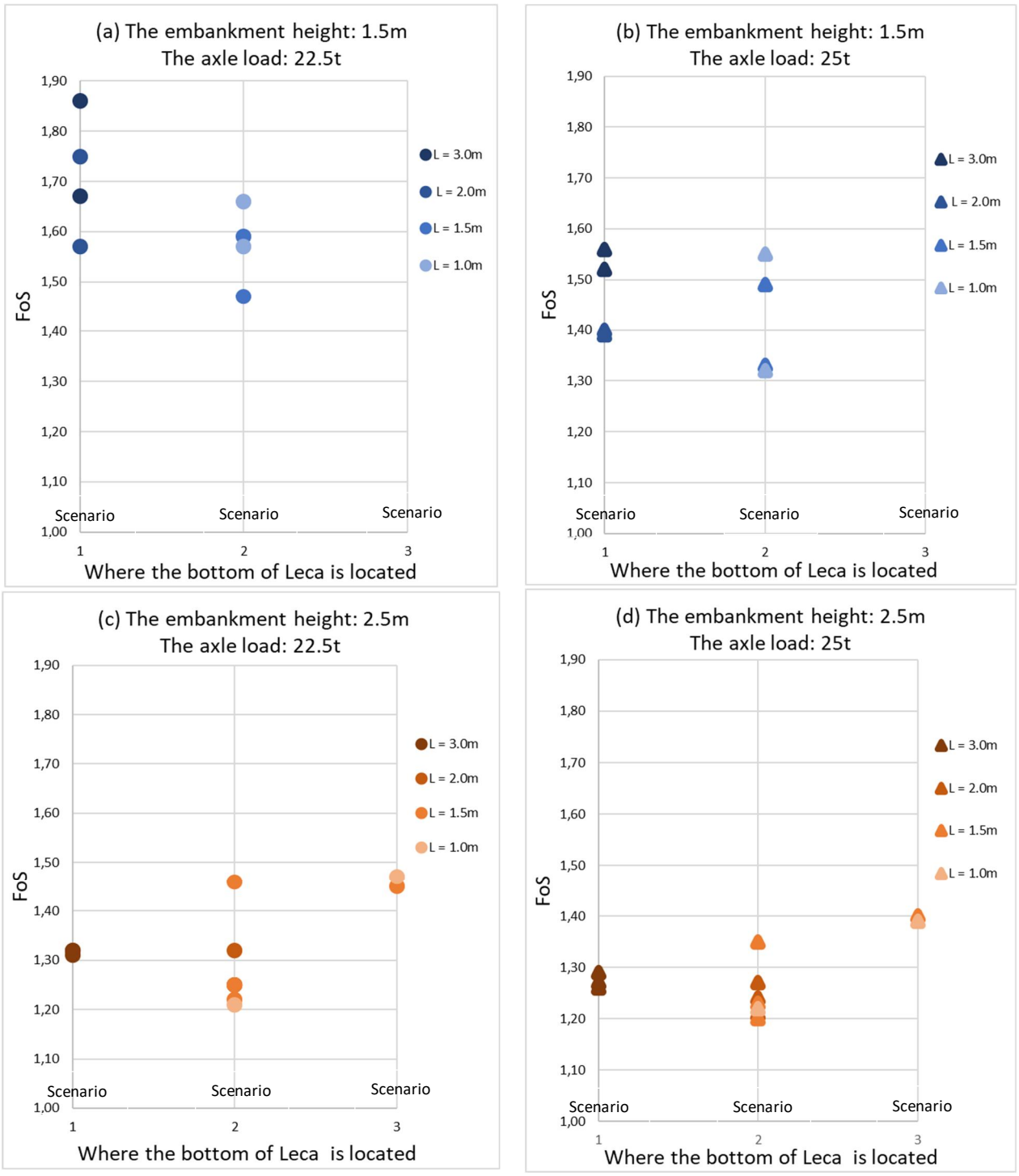

Figure 43. FoS results vs. the location of bottom Leca using Plaxis (Scenario 1 – the bottom of Leca was located at soft clay, Scenario 2 – the bottom of Leca was located at dry crust Scenario 3 – the bottom of Leca was located right above the ground surface)

The FoS results fell between 1.40 and 1.90, 1.30 and 1.60, 1.20 and 1.50, as well as 1.20 and 1.40 for Figure 43 (a), (b), (c) as well as (d), respectively. Figure 43 (a) has the highest

range of FoS among four cases, and this makes sense because the case (a) has the lower embankment height with the smaller axle load. The case (b) has a slightly higher range of FoS than the case (c). This may indicate that the 1.0 m increment in the embankment height has more negative effects compared to an increase of axle load from 22.5 tons to 25 tons. The case (d) has the lowest range of FoS among all cases due to the higher embankment height with the larger axle load. Figure 43 (a) and (b) reveal that using a thicker Leca LWA or replacing dry crust and part of soft clay by Leca LWA can improve embankment stability. However, this finding is not applicable for Figure 43 (c) and (d) when the embankment height is 2.5 m.

5.3 Displacement in Leca LWA layers

This section answers the research questions Q4 and Q5 (Section 1.3).

Q4. What is the optimal location for Leca LWA in railway embankments?
Q5. How does Leca LWA bear cyclic loading with different cover depths (suitable cover depths in railway embankment)?

The displacement occurs in Leca LWA layers including the plastic displacement induced by cyclic loading and the elastic displacement caused by static train load.

Section 4.3 presents the simulations of displacement induced by cyclic loading in Leca LWA layers. Using a 0.3-m thick extra subballast layer has been proven a positive impact in terms of bearing capacity (Section 5.1) and embankment stability (Section 5.2), therefore, such a layer is adopted in the model for analyzing displacement induced by cyclic loading in Leca LWA layer for Section 4.3.

To evaluate the effect of cyclic loading on Leca LWA with different cover depths, three thicknesses, 0 m, 0.3 m and 0.65 m, are adopted for the extra subballast layer. As for loads, which are modelled for computing displacement induced by cyclic loading, they can be referred to Table 5. The line loads (q_{vk}) of 80 kN/m and 88 kN/m with their additional load increment (Δq_{vk}) of 76kN/m and 84 kN/m are corresponding to the axle loads of 22.5 tons and 25 tons. Since the railway sleeper has a width of 2.6 m, the uniformly distributed loads of 75 kN/m^2 and 82.7 kN/m^2 are modelled at the depth of 200 mm below the track in the Plaxis. The applied uniformly distributed loads for the axle loads of 22.5 tons and 25 tons are calculated as in Eq.(42) and Eq.(43), which also includes the impulse factor (ϕ_v) of 1.25 when designing new tracks. The rest of conditions remain the same as the model used in Section 4.3, including a fixed 3.0-m thick Leca layer and the construction stages presented in Table 38.

$$q_{LM71-22.5\,t} = \frac{(q_{vk} + \Delta q_{vk})\,\phi_v}{L} = \frac{(80 + 76) \times 1.25}{2.6} = 75\ kN/m^2 \qquad (42)$$

$$q_{LM71-25\,t} = \frac{(q_{vk} + \Delta q_{vk})\,\phi_v}{L} = \frac{(88 + 84) \times 1.25}{2.6} = 82.7\ kN/m^2 \qquad (43)$$

The points on top, middle and bottom of Leca in the central line are selected for obtaining the displacement induced by cyclic loading in time. The plastic displacements at the top, middle and bottom points under three cover depths are summarized in Table 45 and Table 46 for the axle loads of 22.5 tons and 25 tons, respectively. The analysis results of the Plaxis simulations are attached in Appendix E. The chosen railway track sections and their corresponding estimated number of cycles per track per decade and time in the Plaxis simulations can be referred to Table 41.

Table 45. Displacement Induced by cyclic loading (axle load 22.5 t) for various Leca LWA cover depths using Plaxis

Axle load = 22.5 tons							
Railway track section	Estimated number of cycles* per track/ per decade	The thickness of extra subballast layer = 0 m		The thickness of extra subballast layer = 0.3 m		The thickness of extra subballast layer = 0.65 m	
		The selected points	Displ. induced by cyclic loading	The selected points	Displ. induced by cyclic loading**	The selected points	Displ. induced by cyclic loading
-	million	-	mm	-	mm	-	mm
Lahti – Kouvola	1.7	Top	2.00	Top	1.85	Top	1.65
		Middle	1.30	Middle	1.23	Middle	1.08
		Bottom	0.90	Bottom	0.82	Bottom	0.76
Seinäjoki – Pännäinen	1.6	Top	1.90	Top	1.72	Top	1.55
		Middle	1.23	Middle	1.18	Middle	1.01
		Bottom	0.85	Bottom	0.78	Bottom	0.71
Turku – Toijala	0.8	Top	0.98	Top	0.85	Top	0.76
		Middle	0.61	Middle	0.57	Middle	0.50
		Bottom	0.42	Bottom	0.35	Bottom	0.35

*two adjacent 250 kN axle loads generate one cycle Nurmikolu (2004)
**the values are the same as in Table 42.

Table 46. Displacement Induced by cyclic loading (axle load 25 t) for various Leca LWA cover depths using Plaxis

Axle load = 25 tons							
Railway track section	Estimated number of cycles* per track/ per decade	The thickness of extra subballast layer = 0 m		The thickness of extra subballast layer = 0.3 m		The thickness of extra subballast layer = 0.65 m	
		The selected points	Displ. induced by cyclic loading	The selected points	Displ. induced by cyclic loading	The selected points	Displ. induced by cyclic loading
-	million	-	mm	-	mm	-	mm
Lahti – Kouvola	1.7	Top	2.19	Top	2.02	Top	1.83
		Middle	1.43	Middle	1.37	Middle	1.21
		Bottom	0.97	Bottom	0.93	Bottom	0.84
Seinäjoki – Pännäinen	1.6	Top	2.06	Top	1.89	Top	1.71
		Middle	1.34	Middle	1.28	Middle	1.13
		Bottom	0.92	Bottom	0.86	Bottom	0.79
Turku – Toijala	0.8	Top	1.06	Top	0.95	Top	0.84
		Middle	0.64	Middle	0.63	Middle	0.55
		Bottom	0.46	Bottom	0.42	Bottom	0.38

*two adjacent 250 kN axle loads generate one cycle Nurmikolu (2004)

As seen in Table 45 and Table 46, when Leca LWA layers have a deeper cover depth, i.e., a thicker extra subballast layer, the displacement induced by cyclic loading reduced for all railway tracks. As shown in Table 45 (the axle load of 22.5 tons), the displacement on the top of Leca LWA for Lahti –Kouvola is reduced from 2 mm to 1.85 mm when the thickness of an extra subballast layer is increased by 0.3 m, and the displacement is further decreased to 1.65 mm when the thickness of an extra subballast layer is increased by 0.65 m. As seen in Table 46 (the axle load of 25 tons), the displacement on the top of Leca LWA for Lahti – Kouvola is reduced from 2.19 mm to 2.02 mm when the thickness of an extra subballast layer is increased by 0.3 m, and the displacement is further decreased to 1.83 mm when the thickness of an extra subballast layer is increased by 0.65 m. Nevertheless, these values are fairly small which can be almost neglected especially for the lower classification of railway substructures. In other words, Leca LWA materials can satisfactorily bear cyclic loading caused by moving trains regardless of the cover depth. Thus, these two tables provide an answer to the research questions Q4 and Q5.

Table 13 presents the maximum longitudinal slope in 2-9 years for different railway substructure classes. With the given limits, the plastic deformations at the top of Leca LWA layers for each railway track under the axle of 22.5 tons (Table 45) in a structural transitioning zone (e.g. per 10 m / 100 m in longitudinal direction) can be calculated in percentage. Then, the allowable displacements for other layers (i.e., ballast, subballast, extra subballast layers and subgrade) in percentage can be estimated by excluding the percentage taken by Leca LWA layers. Table 47 and Table 48 summarize the allowable displacement in a structural transitioning zone for other layers in percentage in longitudinal direction per 10 m and per 100 m, respectively. As shown in Table 47 and Table 48, Leca LWA only takes small percentage of allowable displacements, which gives more room for other layers for occurring plastic deformations.

Table 47. The allowable displacements (under the axle load of 22.5 t) in a structural transitioning zone for other substructure layers and subgrade in percentage per 10 m in longitudinal direction (RATO 3 Taulukko 2, 2018)

	2-9 years settlement	Lahti – Kouvola		Seinäjoki – Pännäinen		Turku – Toijala	
Railway substructure class	Max. longitudinal slope	Leca LWA layer	Allowance for other layers	Leca LWA layer	Allowance for other layers	Leca LWA layer	Allowance for other layers
	%	%	%	%	%	%	%
0	0.4	5	95	4	96	2	98
1	0.3	6	94	6	94	3	97
2	0.2	9	91	9	91	4	96
3	0.15	12	88	11	89	6	94
4	0.1	19	82	17	83	9	92

Table 48. The allowable displacements (under the axle load of 22.5 t) in a structural transitioning zone for other substructure layers and subgrade in percentage per 100 m in longitudinal direction (RATO 3 Taulukko 2, 2018)

	2-9 years settlement	Lahti – Kouvola		Seinäjoki – Pännäinen		Turku – Toijala	
Railway substruc-ture class	Max. longitudinal slope	Leca LWA layer	Allowance for other layers	Leca LWA layer	Allowance for other layers	Leca LWA layer	Allowance for other layers
	%	%	%	%	%	%	%
0	0.4	0.46	99.54	0.43	99.57	0.21	99.79
1	0.3	0.62	99.38	0.57	99.43	0.28	99.72
2	0.2	0.93	99.08	0.86	99.14	0.43	99.58
3	0.15	1.23	98.77	1.15	98.85	0.57	99.43
4	0.1	1.85	98.15	1.72	98.28	0.85	99.15

The geometry for computing elastic displacements caused by train loads is the same as the one used for calculating displacements induced by cyclic loading as shown in Table 37. The HS-model is adopted for all substructure layers with parameters presented in Table 19 and is used for two cohesionless subgrades (dense gravel and loose silt) with parameters presented in Table 23. The SS-model was adopted for cohesive subgrade (soft clay) with parameters presented in Table 22.

Three points on the top, middle and bottom of Leca at the central line, which are (0, -1.15), (0. -2.50) and (0, -4.15), are selected for computing displacement under static load. These points are the same as in Section 4.3.1, which computed displacements induced by cyclic loading in Leca LWA layers. One additional point, (0, -0.20) is included in this section in order to calculate displacements right below the applied load. Figure 44 presents the cross section for displacement analysis under the static train loads.

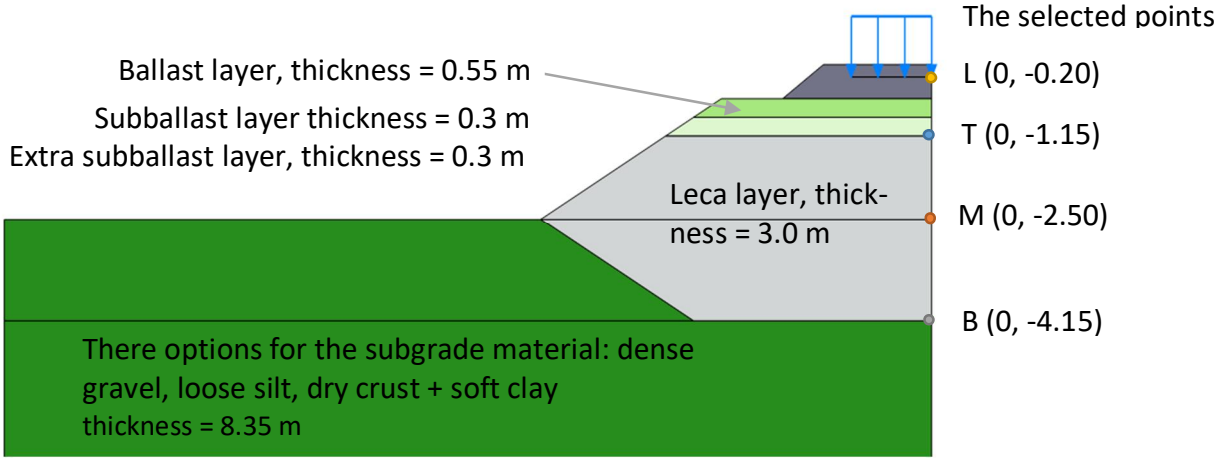

Figure 44. The cross section in Plaxis for displacement analysis under static train loads

As for loads, which are modelled for computing displacement induced by train load, they can be referred to Table 5. The line load (q_{vk}) of 80 kN/m with an additional load increment (Δq_{vk}) of 76 kN/m are corresponding to the axle loads of 22.5 tons. Since the railway sleeper has

a width of 2.6 m, the uniformly distributed loads of 75 kN/m^2 is modelled at the depth of 200 mm below the track. The calculation is shown in Eq.(42), which also includes the impulse factor (ϕ_v) of 1.25 for designing new tracks.

For cohesionless subgrades, the mesh size of 0.02 m is generated, and a water table is assigned to be located far below the ground surface for all calculations. A water table is assigned to be far away below the ground surface for all calculations. Eleven construction stages are involved as presented in Table 49 and Figure 45. For cohesive subgrade, twelve construction stages are involved as shown in Table 50.

Table 49. Staged construction for cohesionless subgrades using Plaxis

	Stage	Calculation type	Note
1	Initial phase	Plastic, gravity loading	-
2	Excavation	Plastic	
3	Place the lower Leca layer	Plastic	
4	Place the upper Leca layer	Plastic	
5	Build the whole embankment	Plastic	
6,8,10	Loading with 75kPa train load	Plastic	for generating resilient displace-ment
7,9,11	Unloading	Plastic	

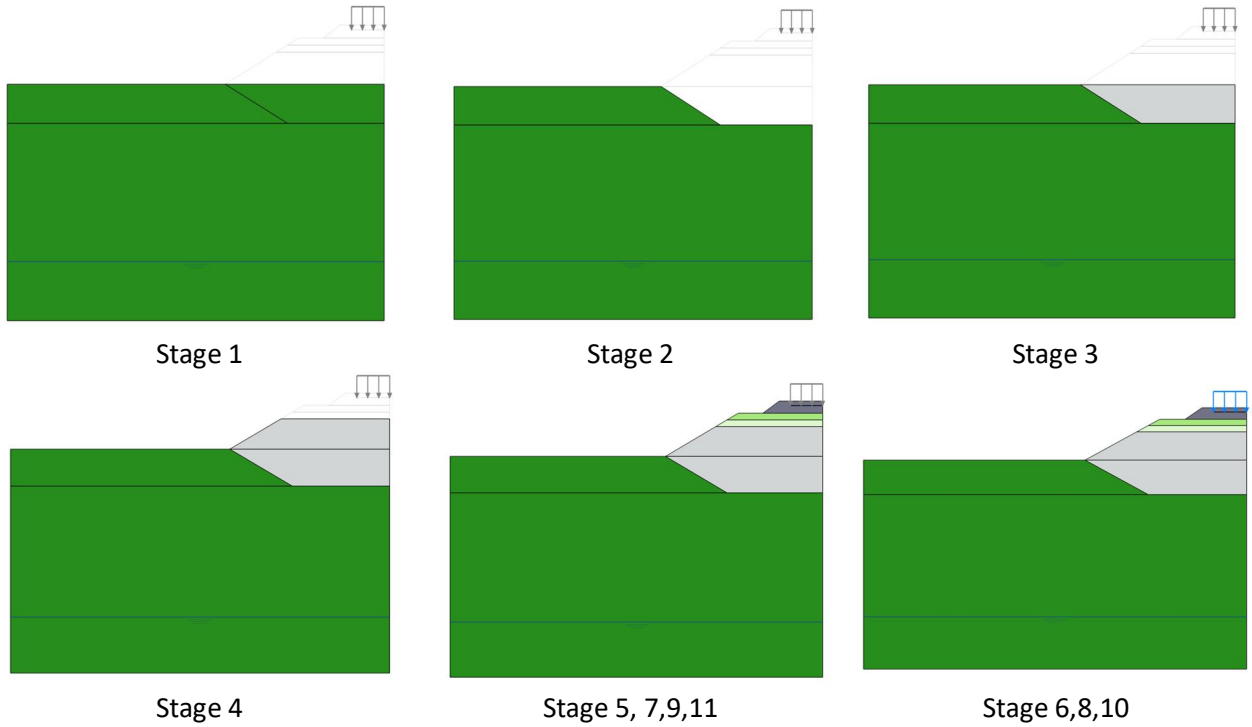

Figure 45. Pictures of staged construction for cohesionless subgrade

Table 50. Staged construction for cohesive subgrades using Plaxis

	Stage	Calculation type	Note
1	Initial phase	Plastic, gravity loading	-
2	Excavation, lower the ground water to a meter below the bottom of excavation level	Plastic	
3	Place the lower Leca layer	Plastic	
4	Place the upper Leca layer	Plastic	
5	Build the whole embankment	Plastic	
6	Consolidation with 20kPa load	Consolidation, t=100000d	
7,9,11	Loading with 75kPa train load	Consolidation, t=0.2d	for generating resilient displacement
8,10,12	Unloading	Consolidation, t=0.2d	

Table 51 summarizes the resilient displacement caused by static train loads. The results are separated as layers above, in and below Leca LWA layers based on three subgrades.

Table 51. Resilient displacement (the axle load of 22.5 t) for different layers based on various subgrades using Plaxis

Subgrade	Resilient displ. above Leca layers	Resilient displ. in Leca layers	Resilient displ. below Leca layers
	mm	mm	mm
Dense gravel	3.17	2.77	1.04
Loose silt	15.00	14.54	12.00
Dry crust + soft clay	16.92	16.81	14.59

The values in Table 51 may be overestimated for dense gravel and loose silt because the HS-model does not take small strain stiffness into account. The deformation of railway embankment is small, and it does not reach the failure such as in triaxial tests. Consequently, the values given by Table 51 is less realistic since the initial stiffness of Leca LWA materials should be much larger. As for the analysis using soft clay as the subgrade, the consolidation stages are unrealistic, for example, the consolidation time is too long in stage 6. Methods such as combining Leca LWA materials and stabilizing columns can be considered in real situations. Additionally, the problems are modelled in 2D, which assume an infinite length in plane. This leads to the overestimation of displacements because a train has an approximate length of 25 m. Regardless, the main purpose of this table is to show the magnitudes between the elastic displacement and the plastic displacement induced by cyclic loading in Leca LWA layers.

5.4 Summary

This thesis has found answers the following research questions.

Q4. What is the optimal location for Leca LWA in railway embankments?

The optimal location of Leca LWA in railway embankments can be determined by considering the bearing capacity at the top of subballast layer, the embankment stability and the effect of cyclic loading. Firstly, from the perspective of bearing capacity (Section 5.1), the optimal location for Leca LWA is to be beneath a 0.3-m thick extra subballast layer with the same or similar material as subballast layers (Figure 39). This works for all subgrades with various thickness of Leca LWA layers. Secondly, from the embankment stability point of view (Section 5.2), using an extra subballast layer can guarantee an improvement. However, no clear indication whether an extra subballast layer helps further in increasing the embankment stability when the thickness of extra subballast layer exceeds 0.3 m (Figure 42). Additionally, the height of a railway embankment and the designed axle load affect the optimal location for Leca LWA in a railway embankment. It appeared that a thicker Leca LWA can improve the embankment stability only when the height of embankment and the designed axle load are relatively low (e.g., Figure 43 (a)). No clear trend towards increasing embankment stability for relative higher embankments and heavier axle loads (e.g., Figure 43 (c) & (d)). Finally, from the perspective of cyclic loading (Section 5.3), Leca LWA can sufficiently bear such loadings regardless of the cover depth (Table 45 and Table 46). As such, it can be concluded that the optimal location for Leca LWA is to be beneath a 0.3-m thick extra subballast layer.

Q5. How does Leca LWA bear cyclic loading with different cover depths (suitable cover depths in railway embankment)?

Leca LWA can sufficiently bear cyclic loading regardless of the cover depth (Table 45 and Table 46) when the applied train axle load are 22.5 tons and 25 tons. Furthermore, Leca WA only takes small percentage of allowable displacements (Table 13), which gives more room for other layers for occurring plastic deformations (Table 47 and Table 48).

Q6. What parameters are required for design?

There are various methods available for designs, e.g., the limit equilibrium method and empirical methods, and each method may require different parameters. The answers here limit to the methods used in this thesis.

In terms of calculating the bearing capacity at the top of subballast layers, the Odemark E-moduli of each layer in railway substructures and subgrade are required. From the perspective of the embankment stability, the unit weight, friction angle, cohesion, and undrained shear strength for cohesive materials are the minimum requirements. Other parameters, such as secant stiffness, tangent stiffness, and unloading-reloading stiffness, are required for more advanced modelling in stability. When calculating the displacement induced by static load in cohesionless materials, the unit weight, friction angle, cohesion, secant stiffness, tangent stiffness, and unloading-reloading stiffness are required. When calculating the plastic displacement induced by static load in cohesive materials, the unit weight, friction angle, cohesion, compression index, swelling index, and pre-overburden pressure or over

consolidation ratio are required. Besides those parameters specified for cohesive materials, the creep index is required to estimate strain increment in Leca LWA due to cyclic loading.

Q8. Are all, of the required parameters defined for Leca LWA?

The Odemark E-modulus for Fin LWA 4-32 was defined by Pahkakangas et al., (2020). The unit weight, friction angle, and oedometer stiffness for various types of LWA were provided by Watn et al., (2004) and Høva et al., (2009). The secant and unloading-reloading stiffness were estimated using the correlation based on the oedometer stiffness provided by PLAXIS Material Manual, (2020). The compression index was interpreted by using the oedometer test results of Nor LWA 4-32. These tests did not perform unloading-reloading behavior, thus, the swelling index of the material was assumed to be the embankment between the first two load increments (Figure 19). The creep index is extremely small which did not affect the accumulation rate anymore. The pre-consolidation pressure was then estimated by using the Plaxis soil test based on these indices.

Q9. What additional laboratory analyses shall be performed in the future?

There are three potential laboratory tests could be performed in the future. Firstly, triaxial tests on Fin LWA 4-32 for more accurate secant and unloading-reloading stiffness for design when using an advanced Plaxis modelling such as the HS-model. Secondly, Oedometer tests on Fin LWA 4-32 with loading and unloading stages if Plaxis SSC-model is used to estimate the accumulation of plastic strain over time. Finally, minimum three series of cyclic triaxial tests on Fin LWA 4-32 are required if the HCA model is used to predict the accumulating plastic strain due to high cycle loads with relatively small strain amplitude. The proposed test series are summarized in Section 4.4.

The above-mentioned tests are applicable for other materials of interest such as Fin LWA 0-32.

6 Conclusion

This thesis has demonstrated the optimal location for Leca LWA is below a 300-mm thick extra subballast layer. Such a setting could significantly improve not only the bearing capacity at the top of the subballast layer but also the stability of railway embankments. When the thickness of the extra subballast layer exceeded 300 mm, no clear improvement was observed in these two aspects of railway geotechnical design. Regarding the effect of cyclic loading on Leca LWA, it was found that the material could sufficiently bear such loading regardless of the cover depth. However, these findings are limited to the cross section studied in this work, which consisted of a 550-mm thick ballast layer followed by a 300-mm thick subballast layer, with a maximum embankment height of 2.5 m, onto which was applied a maximum axle load of 25 tons. The suitable cover depth of 1150 mm, consisting of a 550-mm thick ballast, followed by a 300-mm thick subballast layer and a 300-mm thick extra subballast layer, is recommended to be constructed above a Leca LWA layer.

The displacement induced by cyclic loading was computed using the Plaxis SSC model, which accumulated the plastic strain over time. The analysis results were further used to validate the HCA model established by Wichtmann et al., (2005). This HCA model was used to replicate the results of cyclic compression tests on Leca LWA, which showed that the plastic strain accumulated due to the high number of cycle loads. This enabled the magnitude of plastic displacements under high-cycle train loads to be estimated by correlating the time provided by the Plaxis simulations and the number of cycles given by the HCA model. However, the method used for estimating the displacement induced by cyclic loading had limitations. Firstly, since a linear relation was discovered in the Plaxis simulations instead of a logarithmic relation as in the HCA model, the magnitude of accumulated plastic strain was underestimated or less accurate at the beginning of the time interval. Secondly, the HCA model was developed by using cyclic triaxial tests on sand, which was different from the provided cyclic compression tests on Leca LWA. This, in turn, caused challenges in replicating the accumulated strain curve. Lastly, it was assumed that Leca LWA layers experienced the same pre-consolidation pressure at the construction site (simulated by Plaxis) as in the provided oedometer test results.

This thesis evaluated the use of Leca LWA in railway embankments in terms of bearing capacity, embankment stability and cyclic loading, which could provide guidelines for geotechnical designers in effectively using Leca LWA as a railway embankment material. Additionally, this thesis has established the feasibility of using the HCA model and the Plaxis SSC model to simulate the accumulated plastic strain resulting from high-cycle loads caused by moving trains.

Based on these findings, this thesis recommends that future studies could use a higher number of cycles in cyclic compression experiments, as this could allow identifying the displacements induced by cyclic loading for even longer time periods. In this thesis, the manufacturer provided the cyclic compression tests for Fin LWA 4-32, consisting of two million cycles, which corresponded to the number of cycles that the railway track section between Lahti and Kouvola could experience over a 10-year period. However, since the service life of railway can span over a hundred year, it would be practical to test even higher numbers

of cycles. This, in turn, would enable railway operators to plan their maintenance schedules to upgrade the Leca LWA material over the decades. Secondly, the displacement induced by cyclic loading was simulated by assuming that the pre-consolidation pressure in construction sites could be reach as high as in the oedometer test. Therefore, it would be valuable if a test embankment containing Leca LWA layers could be set up to verify this assumption. Finally, to find the most cost-effective method for designing railway embankments, future studies could combine Leca LWA with reinforced geotextiles or other ground improvement methods, such as preloading and stabilizing columns, on different subgrade conditions.

Bibliography

Bane NORs technical regulations. (2021). Bane NORs. https://trv.banenor.no/wiki/Forside

BN1-59-4 Belastnings- og beregningsforudsætninger for sporbærende broer og jordkonstruktioner. (2010). Banedanmark. https://www.bane.dk/da/Leverandoer/Krav/Tekniske-normer-og-regler/Banenormer/Belastnings_-og-beregningsforudsaetninger-for-sporbaerende-broer-og-jordkonstruktioner

Bogusz, W., & Godlewski, T. (2019). Geotechnical design of railway embankments – requirements and challenges. In K. Wilde & M. Niedostatkiewicz (Eds.), *MATEC Web of Conferences* (p. 11002). EDP Sciences. https://doi.org/10.1051/matecconf/201926211002

Briggs, K., Loveridge, F., & Glendinning, S. (2017). Failures in transport infrastructure embankments. *Engineering Geology*, *219*, 107–117. https://doi.org/10.1016/j.enggeo.2016.07.016

Christiansen, T. (2018). *A Comparison of Railway Load Models for Geotechnical Analysis (Master's thesis)*. Norwegian University of Science and Technology, 10–24.

Do, T., Gunnvard, P., Mattsson, H., & Laue, J. (2021, April). Railway embankment behaviour due to increased axle loads - A numerical study. *IOP Conference Series: Earth and Environmental Science*, 012040. https://doi.org/10.1088/1755-1315/710/1/012040

EN 1991–2 : Eurocode 1: Actions on structures - Part 2: Traffic loads on bridges. (2003). The European Union, 66–122.

EN 1997–1: Eurocode 7: Geotechnical design - Part 1: General rules. (2004). The European Union, 128–140.

Eurokoodin soveltamisohje - Geotekninen suunnittelu - NCCI 7. (2017). Finnish Transport Infrastructure agency. https://julkaisut.vayla.fi/pdf8/lo_2017-13_ncci7_web.pdf

François, S., Karg, C., Haegeman, W., & Degrande, G. (2009). A numerical model for foundation settlements due to deformation accumulation in granular soils under repeated small amplitude dynamic loading. *International Journal for Numerical and Analytical Methods in Geomechanics*, n/a. https://doi.org/10.1002/nag.807

Høva, E., & Gylland, A. (2009). *Documentation of material properties for Leca aggregates*. SINTEF.

Kalliainen, A., & Kolisoja, P. (2017). *Pile supported embankment slabs under railway track line*. Finnish Transport Infrastructure Agency. https://julkaisut.vayla.fi/pdf8/lts_2017-28_pile_supported_web.pdf

Karstunen, M., Krenn, H., Wheeler, S. J., Koskinen, M., & Zentar, R. (2005). Effect of Anisotropy and Destructuration on the Behavior of Murro Test Embankment. *International Journal of Geomechanics*, *5*(2), 87–97. https://doi.org/10.1061/(asce)1532-3641(2005)5:2(87)

Koskinen, M., Vepsäläinen, P., & Lojander, M. (2002). *Modelling of An isotropic Behaviour of Clays Test Embankment in Murro, Seinäjoki, Finland*. Finnish Road Administration. https://www.doria.fi/handle/10024/139075

Li, D., Hyslip, J., Sussmann, T., & Chrismer, S. (2015). *Railway Geotechnics (Book)*. Railway Geotechnics CRC Press.

Liite 3 Kadun normaalipäällysrakenteet ja kantavuusvaatimukset kerroksittain (2015/1 asti Liite 01). (2020). InfraRYL.

Mansikkamäki, J. (2015). *Effective Stress Finite Element Stability Analysis of an Old Railway Embankment on Soft Clay (Doctoral dissertation)*. Tampere University of Technology.

Martinez Soto, F., Di Mino, G., & Acuto, F. (2017). *Effect of temperature and traffic on mix-design of bituminous asphalt for railway sub-ballast layer (Book)*. CRC Press.

Momoya, Y., Sekine, E., & Tatsuoka, F. (2005). Deformation characteristic of railway roadbed and subgrade under moving-wheel load. *Soils and Foundations*, *45*(4), 99–118. https://doi.org/10.3208/sandf.45.4_99

Nurmikolu, A. (2004). *Murskatun kalliokivlaineksen hienoneminen ja routivuus radan rakennekerroksissa*. Finnish Rail Administration.

Nurmikolu, A., & Silvast, M. (2013). Causes, effects and control of seasonal frost action in railways. *Sciences in Cold and Arid Regions*, *5*(4), 363–367. https://doi.org/10.3724/sp.j.1226.2013.00363

Pahkakangas, S., Dettenborn, T., Pöysti, M., & Jelonen, M. (2020). *Applications of Lightweight Aggregate Fill in Railway Construction*.

Penkereiden stabiliteetin laskentaohje. (2018). Finnish Transport Infrastructure Agency.

PLAXIS 2D-Material Models Manual. (2020). Bentley. https://communities.bentley.com/products/geotech-analysis/w/plaxis-soilvision-wiki/46137/manuals---plaxis

PLAXIS 2D-Reference Manual. (2020). Bentley. https://communities.bentley.com/products/geotech-analysis/w/plaxis-soilvision-wiki/46137/manuals---plaxis

PLAXIS 2D-Scientifics. (2020). Bentley. https://communities.bentley.com/products/geotech-analysis/w/plaxis-soilvision-wiki/46137/manuals---plaxis

Potts, D., & Zdravkovic, L. (1999). *Finite element analysis in geotechnical engineering (Book)*. ICE.

Pycko, S., & Maier, G. (1995). Shakedown theorems for some classes of nonassociative hardening elastic-plastic material models. *International Journal of Plasticity*, *11*(4), 367–395. https://doi.org/10.1016/s0749-6419(95)00004-6

Ratatekniset Määräykset Ja Ohjeet. (2004). Finnish Transport Infrastructure Agency.

Ratatekniset ohjeet (RATO) osa 3 Radan rakenne. (2018). Finnish Transport Infrastructure Agency.

Savolainen, L., Mansikkamäki, J., & Kalliainen, A. (2017). *2D Loads for Stability Calculations of Railway Embankments*. Finnish Transport Infrastructure Agency. https://julkaisut.vayla.fi/pdf8/lts_2017-56_2d_loads_web.pdf

Sivasithamparam, N., & Karstunen, M. (2015). *Evaluation of anisotropic creep model at embankment level*. International Conference on Geotechnical Engineering.

Suiker, A. S. J., & de Borst, R. (2003). A numerical model for the cyclic deterioration of railway tracks. *International Journal for Numerical Methods in Engineering*, *57*(4), 441–470. https://doi.org/10.1002/nme.683

Trafikverkets tekniska krav för geokonstruktioner TK Geo 13. (2014). Trafikverket. https://tekniskhandbok.goteborg.se/Arkiv/2016-

1/__site/Content/File/2BE_1_TK%20Geo%2013%20Trafikverkets%20tekniska%20krav%20f%C3%B6r%20geokonstruktioner_2015-12.pdf

Watn, A. (n.d.). *Lightweight aggregates for civil engineering. Technical solutions, mechanical properties, certification and quality control*. SINTEF.

Watn, A. (2004). *LWA for Roads and Railways Internordic research and development project*. SINTEF.

Wichtmann, T. (2005). *Explicit accumulation model for non-cohesive soils under cyclic loading (Doctoral dissertation)*. Ruhr-University Bochum.

Wichtmann, T., Niemunis, A., & Triantafyllidis, T. (2007). Strain accumulation in sand due to cyclic loading: Drained cyclic tests with triaxial extension. *Soil Dynamics and Earthquake Engineering*, *27*(1), 42–48. https://doi.org/10.1016/j.soildyn.2006.04.001

Wichtmann, T., Niemunis, A., & Triantafyllidis, T. (2009). On the determination of a set of material constants for a high-cycle accumulation model for non-cohesive soils. *International Journal for Numerical and Analytical Methods in Geomechanics*, *34*(4), 409–440. https://doi.org/10.1002/nag.821

Appendix A: Railway maintenance levels and action plans

Taulukko 13.3:1 Pää- ja sivuraiteiden kunnossapitotasot.

Kunnossa-pitotaso	Suurin nopeus V_{max} [km/h], sitä vastaava akselipaino P [kN] [1) 2)], raiteet	Kisko-paino vähintään	Ratapölkyt vähintään	Tukikerros vähintään
1AA	$V_{max} \leq 220$, $P \leq 185$	60E1	Betoni [3)]	Raidesepeli
1A	$V_{max} \leq 200$, $P \leq 185$	54E1	Betoni 1987 tai uudempi [3)]	Raidesepeli
	$V_{max} \leq 180$, $P \leq 185$	54E1	Betoni 1986 tai vanhempi [3)]	Raidesepeli
	$V_{max} \leq 160$, $P \leq 185$	54E1	Betoni /puu	Raidesepeli
	Sn 160 raiteenvaihtopaikat	60E1	Betoni [3)]	Raidesepeli
1	$V \leq 140$, $P \leq 185$	54E1	Betoni/puu	Raidesepeli
	Sn 140 raiteenvaihtopaikat			
2	$V \leq 120$	54E1	Betoni/puu	Raidesepeli
	Sn 110 raiteenvaihtopaikat			
3	$V \leq 110$	K43	Puu/betoni	Raidesepeli
4	$70 < V \leq 100$ pääraiteet	K43	Puu/betoni	Raidesora tai vastaava
	$70 < V \leq 100$ sivuraiteet			
	Sn 80 raiteenvaihtopaikat			
5	$50 < V \leq 70$ pääraiteet	K30	Puu	Raidesora tai vastaava
	$50 < V \leq 70$ sivuraiteet			
	Sn 35 raiteenvaihtopaikat			
6	$V \leq 50$ pääraiteet	K30	Puu	Raidesora tai vastaava
	$V \leq 50$ sivuraiteet			
	Kuormaus- ja seisontaraiteet			

1) Ei koske vetureita junassa.
2) Huomioitava RAMO 11 ”Radan päällysrakenne” mukaiset nopeus-/akselipainorajoitukset eri raiderakenteille.
3) Näissä saa olla enintään lyhyitä osuuksia mänty- tai kovapuuratapölkkyjä (RAMO 11 ”Radan päällysrakenne”) esimerkiksi silloilla tai vaihteissa.

Appendix A continues

Taulukko 13.3:2 Pää- ja sivuraiteiden tarkastustarve eri kunnossapitotasoilla.

Kunnossa-pitotaso	Raiteet	Mittaus tar-kastusvau-nulla kertaa / vuosi	Tarkastus liikku-vasta kalustosta kertaa / vuosi	Kävely-tarkastus kertaa / vuosi	Vaihde-tarkastus kertaa / vuosi
1AA		6 / v, väli ≤ 3 kuukautta	6 / v, tarkastusvau-nuajojen puoliväli-ssä	2–3 / v	4 / v
1A		6 / v, väli ≤ 3 kuukautta	6 / v, tarkastusvau-nuajojen puoliväli-ssä	2 / v	4 / v
1		3 / v	6 / v, tarkastusvau-nuajojen kolmas-osissa	1–2 / v	4 / v
2		2 / v	6 / v, väli ≤ 2 kuu-kautta	1–2 / v	2–4 / v
3		2 / v	6 / v, väli ≤ 2 kuu-kautta	1–2 / v	2–4 / v
4	Pääraiteet	2 / v	3 / v, vähintään 6 kuukauden välein veturista	1–2 / v	2–4 / v
	Sivuraiteet	1 / v	3 / v		
	Sn 80 raiteenvaihto paikat				
5	Pääraiteet	2 / v	2 / v, tarpeen mu-kaan, vähintään 6 kuukauden välein veturista	1–2 / v	1 / v
	Sivuraiteet	1 / 3 v	Mittaresiinalla tai vastaavalla 1 / v		
	Sn 35 raiteenvaihto paikat				
6	Pääraiteet	2 / v	2 / v, tarpeen mu-kaan, vähintään 6 kuukauden välein veturista	1–2 / v	1 / v
	Sivuraiteet	1 / 3 v	Mittaresiinalla tai vastaavalla 1 / v		
	Kuormaus- ja seisonta-raiteet	Sovitaan RHK:n kanssa			

Appendix B: Gross tons by railway track sections 2019

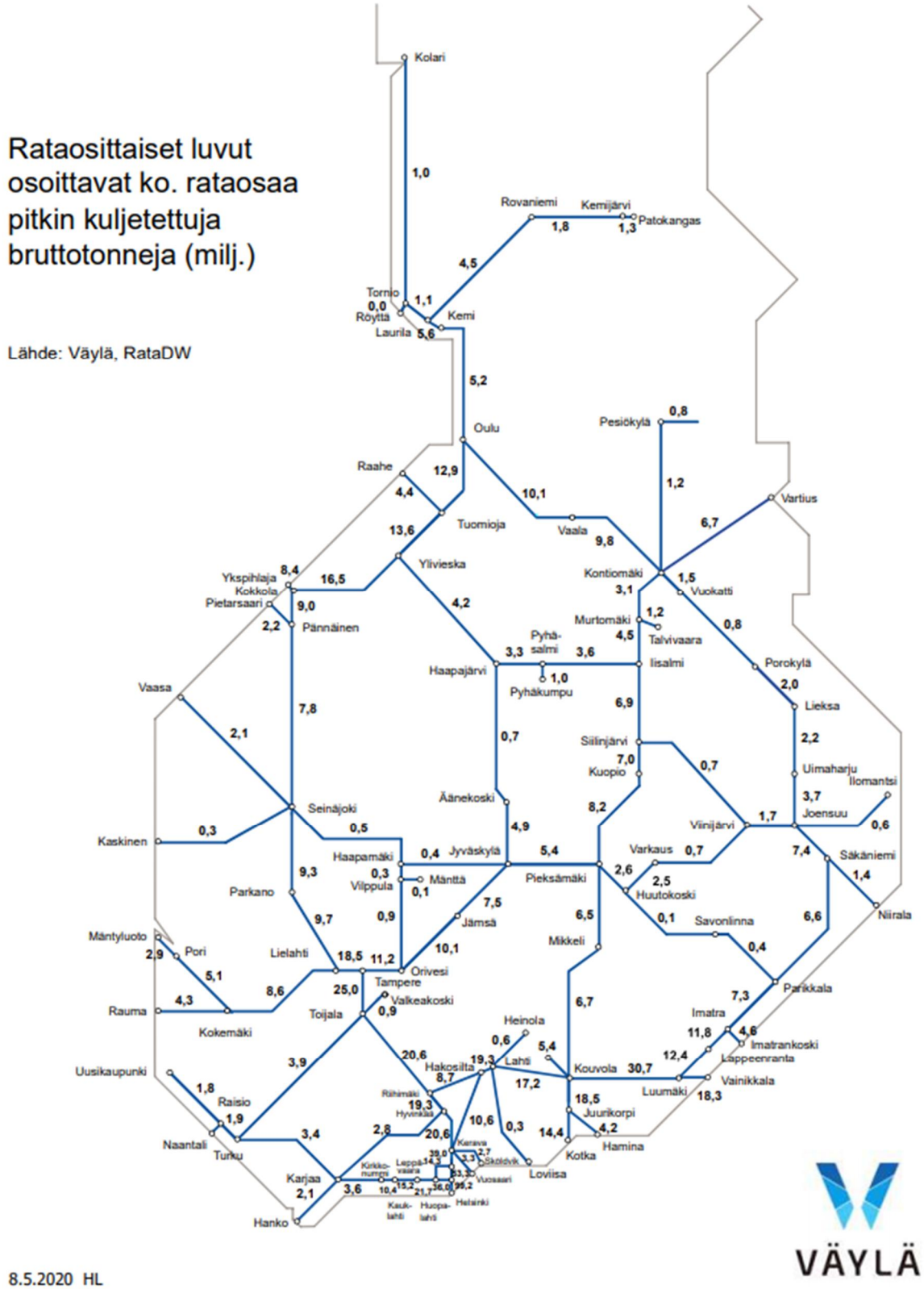

Appendix C: Python scripts

```
def make_geometry(H, F, L, slope, ballastlayer, subballastlayer, frostlayer, lecalayer, drycrustlayer, subsoillayer):
  # make geometry
  # determine polygon shape
  w_frost = F * slope
  w_leca_upper = (H - 0.85 - F) * slope
  w_leca_lower = (L - H + 0.85 + F) * slope_lower
  w_drycrust = 1.6 * slope_lower

  x_left = -3.85
  x_frost = x_left - w_frost
  x_leca_upper = x_frost - w_leca_upper
  x_leca_lower = x_leca_upper + w_leca_lower
  x_drycrust = x_leca_upper + w_drycrust

  # we make it in structure mode:
  g_i.gotostructures()
  # make polygons, start top right, counterclockwise

  # ballast
  ballast_points = []
  ballast_points.append([0, 0])
  ballast_points.append([-1.75, 0])
  ballast_points.append([-2.41, -0.55])
  ballast_points.append([0, -0.55])

  ballastpolygon, ballast = g_i.polygon(*ballast_points)

  # subballast
  subballast_points = []
  subballast_points.append([0, -0.55])
  subballast_points.append([-2.41, -0.55])
  subballast_points.append([-3.40, -0.55])
  subballast_points.append([-3.85, -0.85])
  subballast_points.append([0, -0.85])

  subballastpolygon, subballast = g_i.polygon(*subballast_points)

  # frost protection layer
  frost_points = []
  frost_points.append([0, -0.85])
  frost_points.append([-3.85, -0.85])
  frost_points.append([x_frost, -0.85 - F])
  frost_points.append([0, -0.85 - F])

  frostpolygon, frost = g_i.polygon(*frost_points)

  # leca layer
  leca_points = []
  leca_points.append([0, -0.85 - F])
  leca_points.append([x_frost, -0.85 - F])
  leca_points.append([x_leca_upper, -H])
  leca_points.append([x_drycrust, -H - 1.6])
  leca_points.append([x_leca_lower, -L - 0.85 - F])
  leca_points.append([0, -L - 0.85 - F])

  lecapolygon, leca = g_i.polygon(*leca_points)

  # dry crust
  drycrust_points = []
  drycrust_points.append([x_leca_upper, -H])
  drycrust_points.append([-15, -H])
  drycrust_points.append([-15, -H - 1.6])
  drycrust_points.append([x_drycrust, -H - 1.6])

  drycrustpolygon, drycrust = g_i.polygon(*drycrust_points)

  # subsoil
  subsoil_points = []
  subsoil_points.append([x_drycrust, -H - 1.6])
  subsoil_points.append([-15, -H - 1.6])
  subsoil_points.append([-15, -H - 10])
  subsoil_points.append([0, -H - 10])
  subsoil_points.append([0, -L - 0.85 - F])
  subsoil_points.append([x_leca_lower, -L - 0.85 - F])

  subsoilpolygon, subsoil = g_i.polygon(*subsoil_points)

  return ballastpolygon, subballastpolygon, frostpolygon, lecapolygon, drycrustpolygon, subsoilpolygon


def make_soilmaterial_1(soilinfo):
```

```
  soil_params = [("MaterialName", soil-
info["name"]),
          ("SoilModel", 3),
          ("drainageType", soilinfo["drain-
agetype"]),
          ("colour", soilinfo["colour"]),
          ("gammaUnsat", soilinfo["gam-
maunsat"]),
          ("gammaSat", soilinfo["gammasat"]),
          ("nu", soilinfo["nu"]),
          ("cref", soilinfo["cref"]),
          ("phi", soilinfo["phi"]),
          ("psi", soilinfo["psi"]),
          ("E50ref", soilinfo["E50ref"]),
          ("EoedRef", soilinfo["Eoedref"]),
          ("EurRef", soilinfo["Eurref"]),
          ("powerm", soilinfo["m"]),
          ("pref", soilinfo["pref"]),
          ("K0NC", soilinfo["K0NC"])]
  soil_material_1 = g_i.soilmat(*soil_params)

  return soil_material_1

def make_soilmaterial_2(soilinfo):

  soil_params = [("MaterialName", soil-
info["name"]),
          ("SoilModel", 2),
          ("drainageType", soilinfo["drain-
agetype"]),
          ("colour", soilinfo["colour"]),
          ("gammaUnsat", soilinfo["gam-
maunsat"]),
          ("gammaSat", soilinfo["gammasat"]),
          ("nu", soilinfo["nu"]),
          ("cref", soilinfo["cref"]),
          ("cinc", soilinfo["cinc"]),
          ("phi", soilinfo["phi"]),
          ("Gref", soilinfo["G"])]

  soil_material_2 = g_i.soilmat(*soil_params)
  return soil_material_2

def make_model(H, F, L, slope, ballastlayer, sub-
ballastlayer, frostlayer, lecalayer, drycrustlayer,
subsoillayer):
  # make geometry
  ballast_pg, subballast_pg, frost_pg, leca_pg,
drycrust_pg, subsoil_pg = make_geometry(H, F, L,
slope, ballastlayer, subballastlayer, frostlayer,
lecalayer, drycrustlayer, subsoillayer)

  # assign materials
  ballastmaterial = make_soilmaterial_1(bal-
lastlayer)
  ballast_pg.Soil.Material = ballastmaterial

  subballastmaterial = make_soilmaterial_1(sub-
ballastlayer)
  subballast_pg.Soil.Material = subballastmaterial

  frostmaterial = make_soilmaterial_1(frostlayer)
  frost_pg.Soil.Material = frostmaterial

  lecamaterial = make_soilmaterial_1(lecalayer)
  leca_pg.Soil.Material = lecamaterial

  drycrustmaterial = make_soil-
material_2(drycrustlayer)
  drycrust_pg.Soil.Material = drycrustmaterial

  subsoilmaterial = make_soilmaterial_2(subsoil-
layer)
  subsoil_pg.Soil.Material = subsoilmaterial

def meshcalculateread():
  # add line load

  g_i.gotostructures()

  load = g_i.lineload((-1.3,-0.2),(0,-0.2))
  g_i.Line_1.LineLoad.q_start = 39.6


  # mesh

  g_i.gotomesh()
  g_i.mesh(0.02)

  # set up ground water table
```

```
    g_i.gotoflow()
    Waterlevel = g_i.waterlevel((-15, -H),(0, -H))

    # set up calculation

    g_i.gotostages()

    # initial phase

    g_i.InitialPhase.DeformCalcType = "Gravity loading"
    g_i.activate(g_i.Soils, g_i.InitialPhase)

    # Add load

    Phase_1 = g_i.phase(g_i.InitialPhase)
    Phase_1.DeformCalcType = "Plastic"
    Phase_1.Identification = 'Add Load'
    g_i.activate(g_i.Line_1_1, g_i.Phase_1)

    # safety phase

    SafetyPhase = g_i.phase(g_i.Phase_1)
    SafetyPhase.DeformCalcType = "Safety"
    SafetyPhase.Identification ='Factor of Safety'



    # calculate
    g_i.calculate()

    # read result
    FoS = SafetyPhase.Reached.SumMsf.value

    return FoS

    pass

def determine_FactorOfSafety(H, F, L, slope, ballastlayer, subballastlayer, frostlayer, lecalayer, drycrustlayer, subsoillayer):
    s_i.new()
    # make the model
    make_model (H, F, L, slope, ballastlayer, subballastlayer, frostlayer, lecalayer, drycrustlayer, subsoillayer)

    # run calculation and retrieve results
    FoS = meshcalculateread()
    return FoS

#1st geometry (Leca is located at the subsoil)
# input parameters
slope = 1.5
slope_lower = 1
# height of embankent
H = 1.5
# thickness of frost protection layer (below sub-ballast)
F = 0.3    # to be controlled below in fs
# thickness of Leca
L = 3

ballastlayer = {"name": "ballast",
                "soilmodel": 3,
                "drainagetype": "drained",
                "colour": 8876915,
                "gammaunsat": 20,
                "gammasat" : 20,
                "cref": 10,
                "phi": 45,
                "psi": 10,
                "E50ref": 250000,
                "Eoedref": 210000,
                "Eurref": 500000,
                "nu": 0.2,
                "m": 0.5,
                "pref": 100,
                "K0NC": 0.3}
subballastlayer = {"name": "subballast",
                   "soilmodel": 3,
                   "drainagetype": "drained",
                   "colour": 8316838,
                   "gammaunsat": 20,
                   "gammasat" : 20,
                   "cref": 10,
                   "phi": 45,
                   "psi": 10,
                   "E50ref": 250000,
                   "Eoedref": 210000,
                   "Eurref": 500000,
                   "nu": 0.2,
                   "m": 0.5,
                   "pref": 100,
                   "K0NC": 0.3}
frostlayer = {"name": "frost",
```

```
        "soilmodel": 3,
        "drainagetype": "drained",
        "colour": 13629406,
        "gammaunsat": 20,
        "gammasat" : 20,
        "cref": 10,
        "phi": 45,
        "psi": 5,
        "E50ref": 160000,
        "Eoedref": 135000,
        "Eurref": 320000,
        "nu": 0.2,
        "m": 0.5,
        "pref": 100,
        "K0NC": 0.3}
lecalayer = {"name": "leca",
        "soilmodel": 3,
        "drainagetype": "drained",
        "colour": 14013906,
        "gammaunsat": 6,
        "gammasat" : 10,
        "cref": 1,
        "phi": 36,
        "psi": 0,
        "E50ref": 40000,
        "Eoedref": 40000,
        "Eurref": 120000,
        "nu": 0.2,
        "m": 0.5,
        "pref": 100,
        "K0NC": 0.4}
drycrustlayer = {"name": "dry crust",
        "soilmodel": 2,
        "drainagetype": 2,
        "colour": 15511397,
        "gammaunsat": 16.2,
        "gammasat" : 16.2,
        "cref": 30,
        "cinc": 0,
        "phi": 0,
        "nu": 0.35,
        "G": 4185}
subsoillayer = {"name": "soft clay",
        "soilmodel": 2,
        "drainagetype": 2,
        "colour": 16572285,
        "gammaunsat": 15,
        "gammasat" : 15,
        "cref": 6.11,
        "cinc": 1.77,
        "phi": 0,
        "nu": 0.35,
        "G": 741}


fs = [0.3, 0.6]
for f in fs:
  FoS = determine_FactorOfSafety(H, f, L, slope,
ballastlayer, subballastlayer, frostlayer, lecalayer,
drycrustlayer, subsoillayer)
  print("H={} F={} L={} FoS={:.2f}".format(H, f, L,
FoS))
```

Appendix D: Half and full cases for one railway cross section

The cross section consists of a 0.55-m thick ballast layer, followed by a 0.3-m thick sub-ballast layer, followed by a 0.3-m thick extra subballast layer, followed by a 3.0-m thick Leca LWA. The uniformly distributed load of 39.6 kN/m^2 was applied onto the railway embankment., which corresponds to the axle load of 22.5 tons.

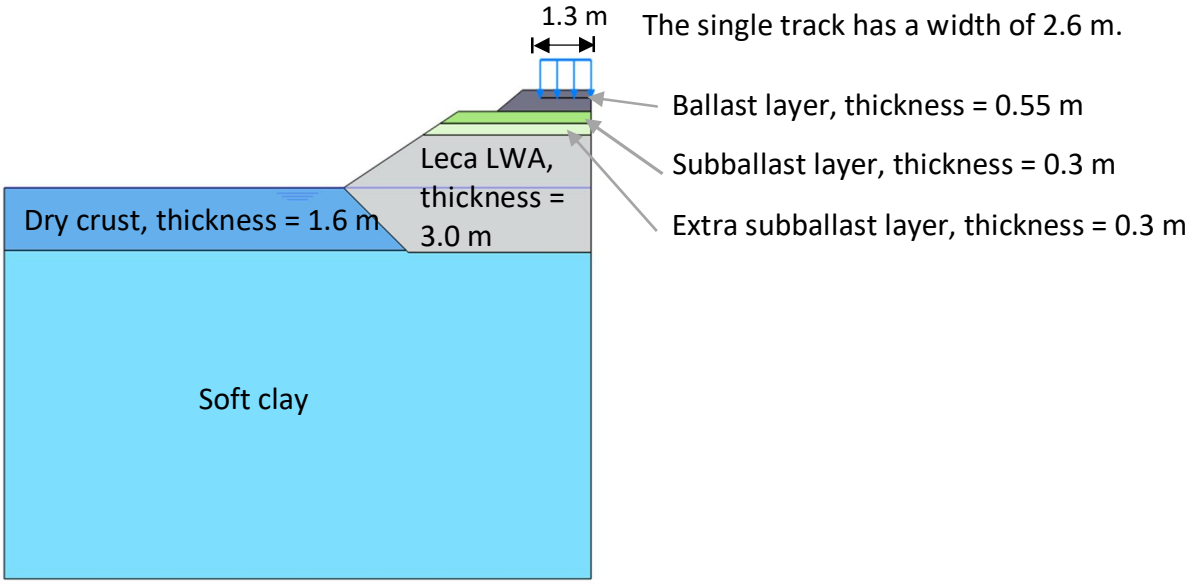

Cross section profile (a) Half case

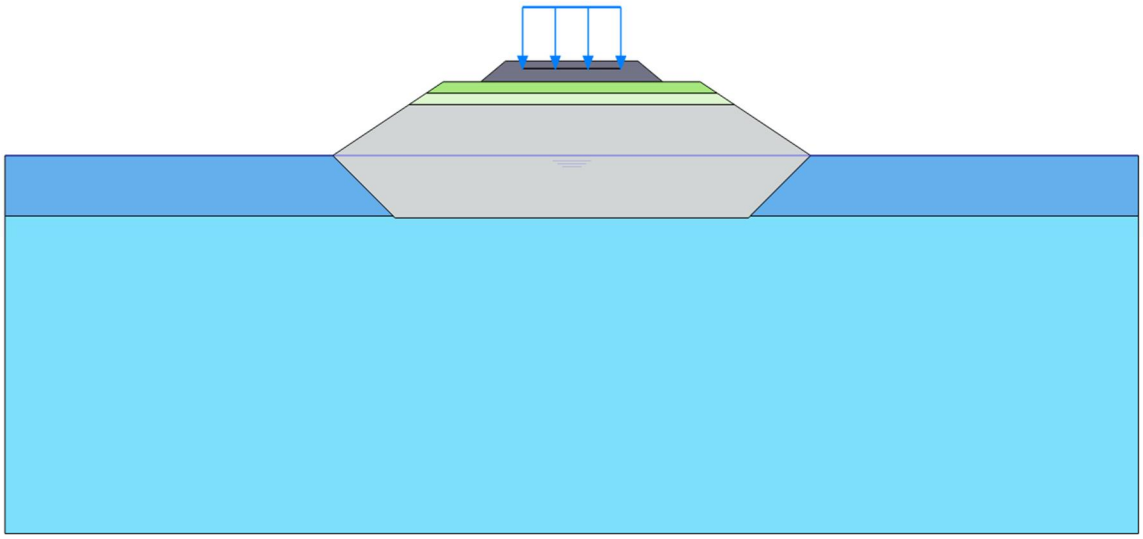

Cross section profile (b) Full case

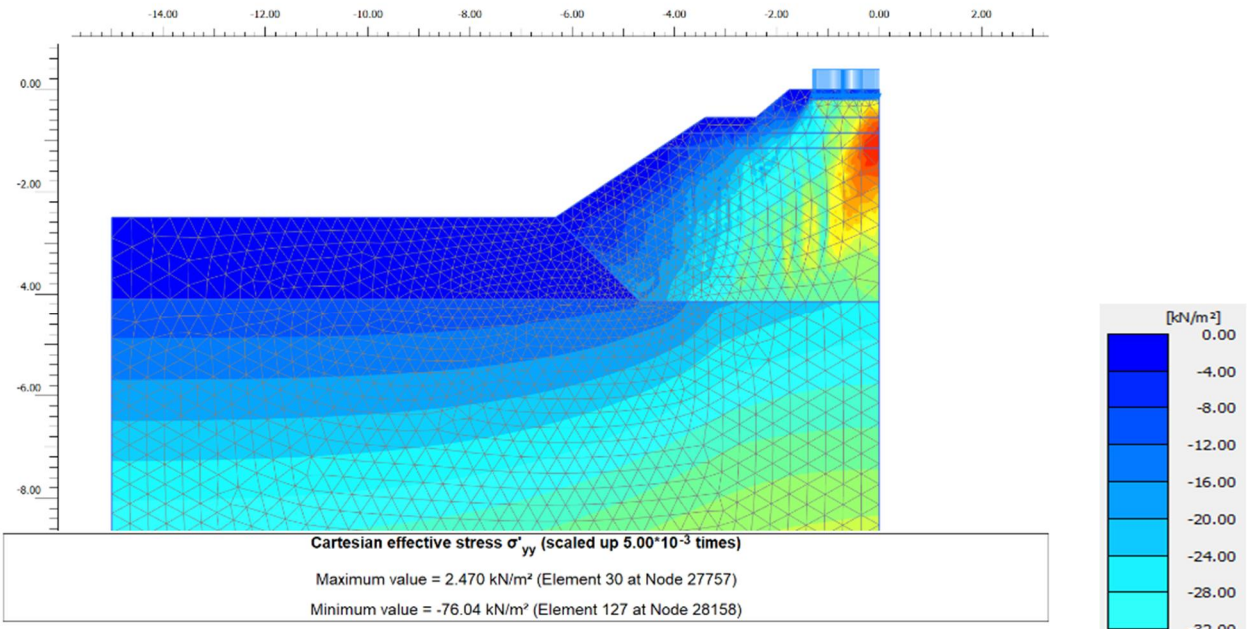

Distribution of vertical effective stress (a) Half case

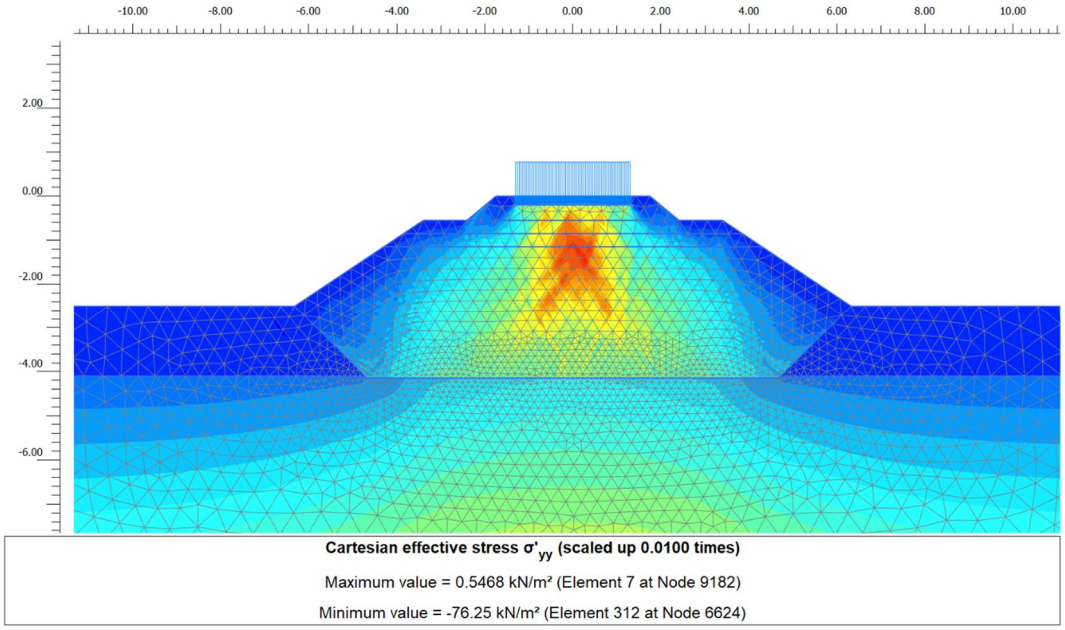

Distribution of vertical effective stress (b) Full case

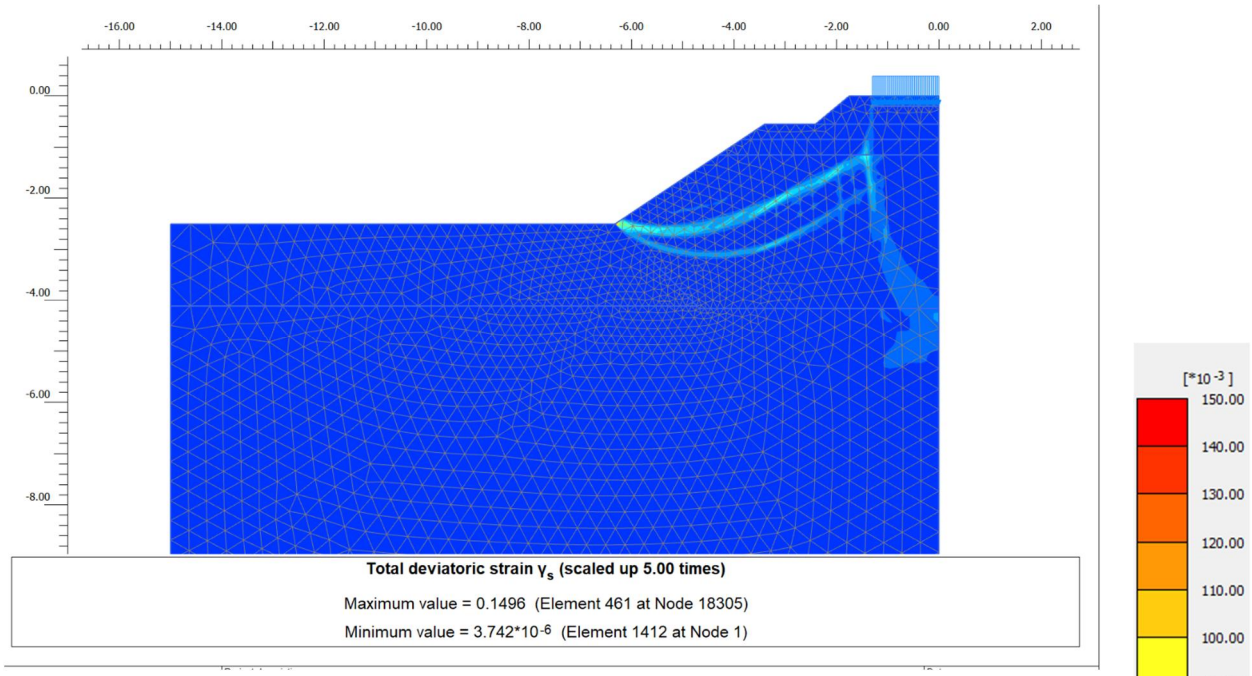

Total deviatoric strain (a) Half case, FoS = 1.32

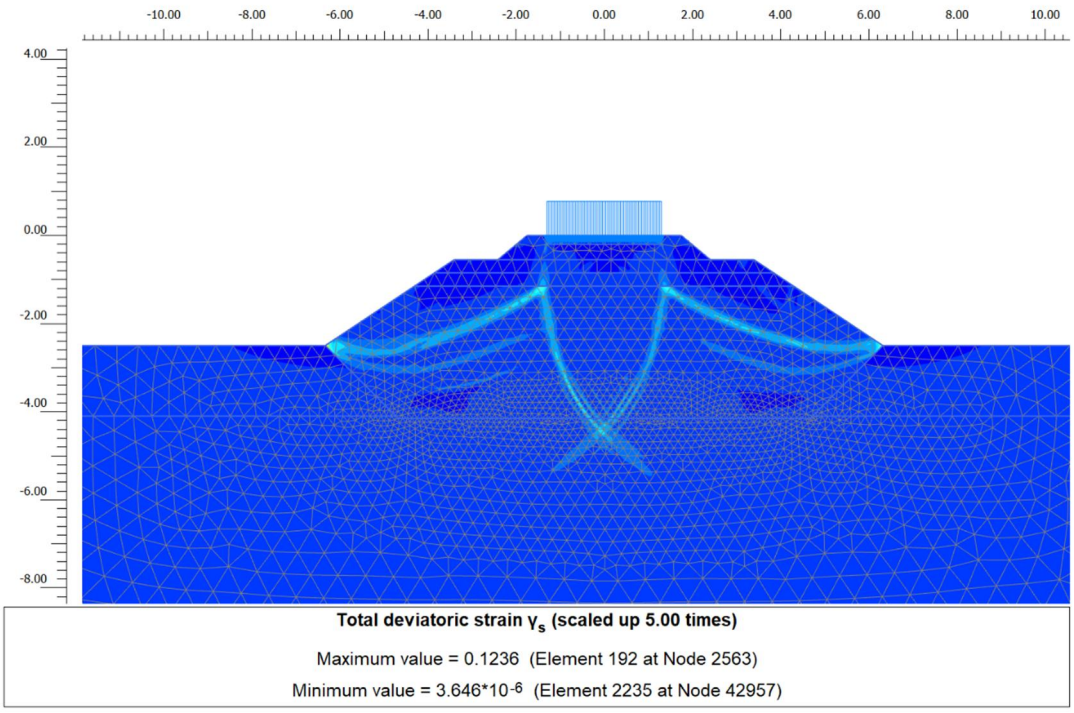

Total deviatoric strain (b) Full case, FoS = 1.31

Appendix E: Analysis results of the displacement induced by cyclic loading

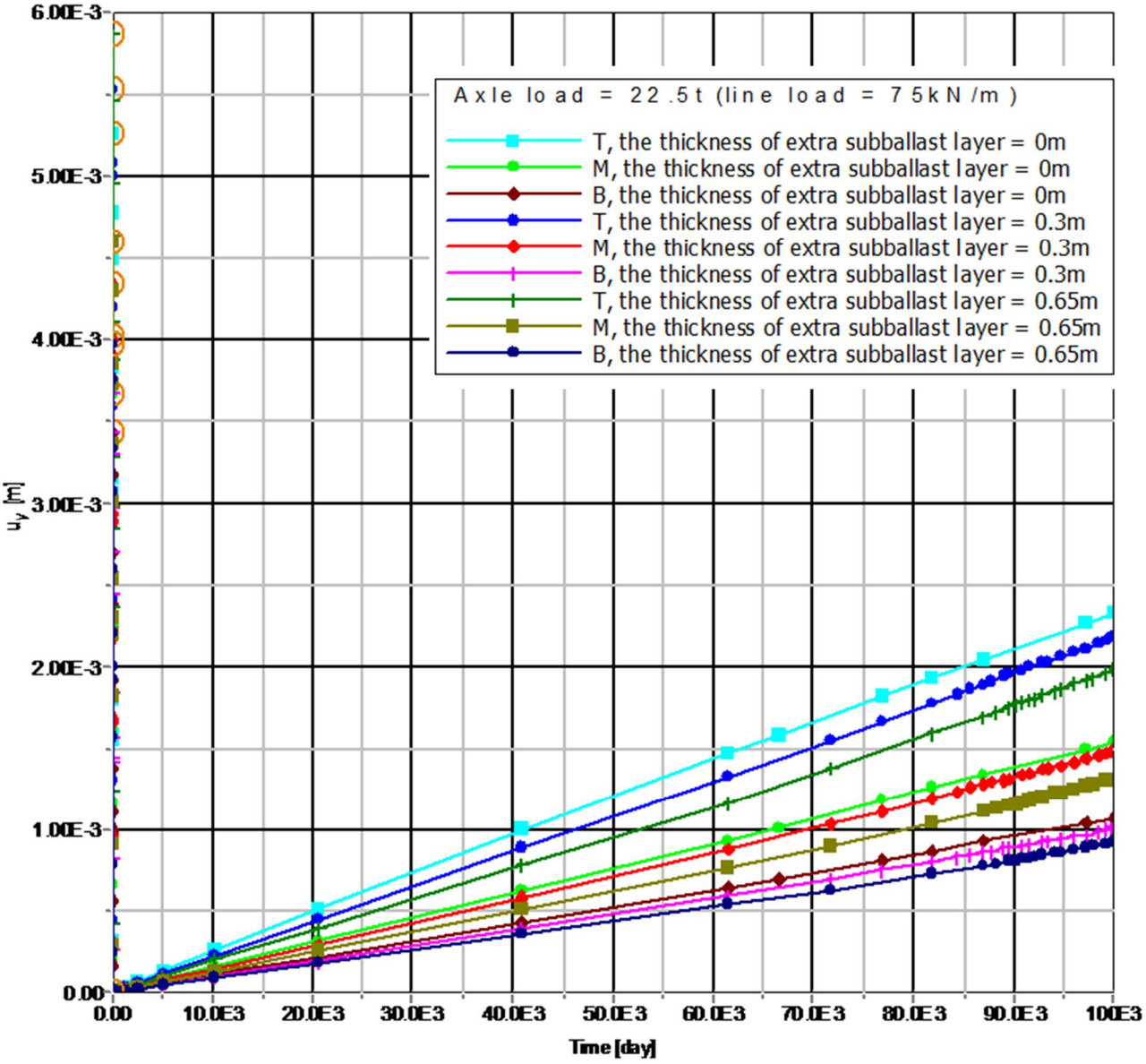

Appendix E contintues